Università degli Studi
dell'Aquila

Solitons and Nonlinear Optical Propagation in Ferroelectric and Near-Critical Paraelectric Photorefractive Crystals

by

Eugenio Del Re

tutor

Bruno Crosignani

Doctorate Thesis in Physics

Università dell'Aquila, Italy

December 1998

Research contained in this thesis is fruit of a long lasting collaboration amongst the Physics Department of Università dell'Aquila (Prof.Bruno Crosignani, Prof.Paolo Di Porto) and the Optics Communications Sector of Fondazione Ugo Bordoni (Prof.Benedetto Daino, Dr.Mario Tamburrini). Furthermore, most of this project would not have been possible without the combined effort of the Electrical Engineering Department of Princeton University (Prof.Mordechai Segev), the Applied Physics Department of the Hebrew University of Jerusalem (Prof.Aharon Agranat), and the Physics Department of Università di Roma "La Sapienza" (Prof.Antonio Degasperis). Funding was granted by the PhD program of Università dell'Aquila (MURST grant), and Fondazione Ugo Bordoni. Partial funding was granted by INFM, Princeton University, and the Hebrew University.

Table of Contents

Introduction

This thesis describes the theoretical and experimental investigation of a series of novel spatial optical phenomena mediated by intense beam self-action present in photorefractive nonlinear crystals. Emphasis is given to optical spatial solitons, the optical equivalent of a general nonlinear manifestation present in continuos dispersive media, characterized by a highly localized, robust, perturbation that propagates "indefinitely" without suffering distortion.

The first observation of centrosymmetric screening solitons, the theoretical prediction of diffusion-driven solitons, and the discovery of optical spontaneous solitons, along with other original results in the field of basic photorefraction, are discussed.

The recent discovery of soliton particles in photorefractive crystals has had far-reaching import in the field of nonlinear optics. The observation of multidimensional self-trapping, incoherent solitary waves, and other new physical phenomena, has spurned a rapid theoretical evolution from "standard" soliton physics to new fields, with peculiar concepts, still not fully grasped and understood. The photorefractive nonlinearity, in itself a complex, nonlocal, and anisotropic interaction, has, concurrently, paved the way for a more general and advanced investigation of condensed matter through optical soliton-like manifestations. Thus, although photorefractive solitons have become an independent field of research in nonlinear optics, they are far from being a well established subject, and this treatise fully reflects this reality. The reader will thus find that many phenomena described are not wholly understood; some are directly observed in an extremely complex light-matter interaction, others, stemming from an over-simplified theoretical description, have not yet found experimental confirmation. Theory and experiment are far from being in quantitative and qualitative accord. As it turns out, the results that are most important for actual applications in optical

wiring, optical interconnects, and all-optical elaboration, are still subject of intense debate.

Perhaps the most important contribution to nonlinear science of the present thesis is the gradual change of perspective that the observed phenomena support in the conceptual understanding of solitons. Photorefractive solitons were initially discovered in a peculiar type of crystal, SBN (Strontium-Barium-Niobate), a noncentrosymmetric ferroelectric with a strong electro-optic susceptibility. The initial observation concerned what is now known as photorefractive quasi-steady-state solitons in one transverse dimension. Self-trapping was observed only for a finite temporal window, and nonlinear propagation inevitably lead to instability and soliton decay. Successive studies demonstrated the existence of more stable particles, in both one and two transverse dimensions, known as screening solitons, that have attracted a great amount of interest and have been replicated in many different materials, and which are the main topic of Chapters 3, 4, 6, and 7. To date, they have been observed in ferroelectric SBN, BTO, BSO, $KNbO_3$, and $BaTiO_3$ through the standard screening nonlinearity, in $LiNbO_3$ through the so-called photovoltaic screening nonlinearity, in semiconductor InP, through a quasi-resonant equivalent screening interaction, and in slab photorefractive SBN waveguides. Such diverse systems support 1+1D self-trapping (one trapped dimension, and one propagation dimension), whereas both $KNbO_3$, and $BaTiO_3$ do not manifest circular-symmetric 2+1D solitons. On the contrary they seem to exhibit strong anisotropic effects, discussed in Chapter 4. Diversity in basic materials has demonstrated the overall generic qualities of the screening mechanism. A further diversification has been recently added: screening solitons in a ferroelectric sample of KLTN above the Curie temperature, that is, in the centrosymmetric paraelectric phase, as described in Chapter 6. Although in this case the screening mechanism is somewhat different, it is basically an extension of the physical system that gives rise to standard anisotropic screeners. Screening solitons inherit from integrable systems all the main characterizing qualities that classical soliton studies attribute to nonlinear self-trapped particles: a soliton existence curve, a nonlinear propagation equation, and a set of nonlinear interaction phenomena with almost complete analogy to classical integrable particles. They attract attention for two basic reasons. The first lies in the fact that they allow an accessible experimental investigation, given the strength of the photorefractive nonlinearity, of a multitude of novel physical phenomena, as

for example the higher dimensional characteristics of solitary wave interactions, and the recently observed “incoherent” solitons. The second reason lies in their possible application in bulk optical wiring circuits, such as reconfigurable directional couplers, optical steering, and nonlinear optical devices, such as parametric oscillators. The first realization of such a component is described in Chapter 3. Indeed recent studies have shown that most of the story still lies untold.

The screening nonlinearity, in its many ramifications and diversities, is but one of a multitude of different soliton supporting nonlinearities present in photorefractive materials. For example, in the centrosymmetric phase, close to the dielectric anomaly, the increased material polarizability allows the observation of self-focusing and self-trapping driven by charge diffusion, as opposed to the drift mechanism at the basis of screening solitons. The minimal photorefractive model in this case allows for an integrable nonlinear system that supports 1+1D and noncircular 2+1D solitons, that, in complete contrast to “traditional” solitons, are without existence curve. These particles, known as diffusion-driven solitons, are discussed in Chapter 8. Furthermore, apart from solitons, this nonlinearity, being anisotropic, supports nonlinear diffraction phenomena such as beam aspect ratio recovery and conservation.

Even more recently, studies have been carried out during the ferroelectric phase-transition: in this highly metastable configuration, new particles form, known as spontaneous optical solitons, in both one and two transverse dimensions, due to a highly nonperturbative, seeded, spontaneous thermodynamic crystal reaction, mediated, again, by charge diffusion fields. These solitons, to which Chapter 9 is dedicated, are insensitive to light parameters and actually form in a complex domain dynamic, in which the propagating field merely “seeds in” a macroscopic system fluctuation. They manifest hysteresis and have a set of interesting polarization dependent properties. Spontaneous solitons seem to be a quite natural and general manifestation of coupled propagation in critical systems.

These phenomena play against the classical view that solitons in Nature (at least in Optics) stem from nonlinear propagation that gives rise to a more or less approximate realization of one of the fundamental integrable systems to date known. Research discussed herein supports a perspective that envisages the soliton as a complex universal response to a strongly interacting wave-propagation system, in which the final trapped state is not a perturbation to the

initial linear regime, but rather represents a transition to a *qualitatively* different regime. The final system has peculiar "free" propagation entities, called solitons, that behave in a manner dictated by the properties of the entire collective entity. This new qualitative behavior, a direct consequence of collective like structuring due to strong interaction, manifests new and interesting dynamics of a somewhat general character, as the strong long range correlations wash out the peculiarities of the specific interaction.

The thesis is structured in chapters, each one adding a piece to the general conceptual perspective, remaining centered on a particular, almost self-standing argument. Most of the chapters report experimental achievements, although some contain novel theoretical approaches and predictions. As the investigation goes deeper into the nonlinear aspects of the crystal phase-transition, the material nonlinearities begin playing a crucial role and the subject acquires a complicated, but somewhat appealing interdisciplinary character. In the end, it is hard to distinguish amongst optical and purely material manifestations.

Chapter 1 addresses, in a general context, the subject of solitons in Nature and in particular in Optics.

Chapter 2 is dedicated to the basic physical mechanism on which most of the phenomena investigated is based: photorefraction. Apart from the standard linearized treatment of the model equations, a new nonperturbative iteration scheme, that in particular situations, allows a nonlinear analytical description of two beam coupling and nonlinear holographic effects, is described. This approach is tested in a series of experiments carried in a sample of $BaTiO_3$.

In **Chapter 3** photorefractive spatial solitons, from their discovery in 1992 to their diverse manifestation in various materials and configurations, is discussed, along with the realization of a soliton-based directional coupler in a sample of SBN.

In **Chapter 4**, experiments carried out in a sample of $BaTiO_3$ that have led to the observation of spatial screening solitons and anisotropic self-focusing, are described.

Chapter 5 is dedicated to near-transition electro-optics in centrosymmetric photorefractive samples.

In **Chapter 6**, the experimental observation of centrosymmetric screening solitons in near-transition KLTN is described, along with their theoretical interpretation.

In **Chapter 7,** phenomena somewhat connected to centrosymmetric screeners are briefly discussed: soliton instability, spatial multisolitons and phase-transitions effects connected to nonlinear material response.

In **Chapter 8,** diffusion-driven phenomena in a near-transition paraelectric are described. The theoretical prediction of diffusion-driven solitons, of diffusion driven self-trapping, and the experimental observation of spatial intensity independent self-focusing and beam aspect-ratio recovery observed in KLTN, are related.

Capter 9 is dedicated to the experimental discovery of optical spontaneous self-trapped particles (spontaneous solitons) in a thermodynamically metastable system: a ferroelectric undergoing a structural phase-transition.

Chapter

1

Nonlinearity, Solitons and Optical Spatial Solitary Waves

Introduction

In this Chapter wave propagation in nonlinear systems is considered, and the concept of a nonevolving, localized, noninteracting perturbation, the Soliton, is introduced. In particular, a "classical" approach to solitons and solitary waves, as isolated solutions of nonlinear integrable systems, is traced, and their interdisciplinary character is briefly hinted at. Finally the discussion is specialized to Optics, where different types of solitons have been observed, and in particular the basic characteristics of spatial solitary waves are discussed. In this context the so-called "linear" perspective is addressed.

Nonlinearity and "New" Objects

To speak of nonlinearity as an independent, peculiar, and *strange* field of Physics is a mystification. Nonlinear phenomena are yes interesting and attractive, because they appear to transcend our everyday intuition, but they are, at the same time, natural manifestations of a continuos system that evolves in a more or less nonperturbative manner, in which a small oscillation approach is insufficient. Nonlinear behavior is actually the *normal* evolution of systems. If we study a system close to a stable stationary configuration, we find that the most useful approach is to apply the basic fundamental laws to the single interacting elements and then approximate the dynamical behavior expanding the relevant quantities around the point of equilibrium. This generally allows the description of dynamics by means of more or less complicated *linear differential equations*. A natural consequence of this situation is the emergence of *new* relevant physical constructs : normal modes. These modes represent the eigenfunctions of the differential equations and, in a general propagation, are characterized by a (multidimensional) parameter K, the eigenvalue, known as *wave-vector*. The structure of the equation of evolution establishes a determined relationship between this wave-vector and the velocity of evolution of the solution in question

(dispersion relationship). Finally, the linearity of the system allows a generalized *superimposition* theorem to hold.

If we excite the continuos system with an initial localized perturbation, we find that the system evolves *spreading* its structure, due to the different velocities of its initial constituent modes. This phenomenon, known in Optics as diffraction (spatial localization) and dispersion (temporal localization), is in general peculiar to any linear (or more precisely linear-approximate) continuos system. When, on the contrary, the interactions in the system are such as to imply exchanges of momentum and energy comparable to the *binding* energy of the equilibrium potential, this description breaks down and more complex, nonlinear, phenomenology emerges. A general consequence is the appearance of coupling amongst the modes. Nonlinearity can channel energy from one mode to the other[1)]. This is for example the case of what might be called "classical" nonlinear optics, whose epitome is sometimes identified in second-harmonic-generation[2)] : the oscillating electrical field associated with an intense optical beam propagating in matter transmits to the charged particles of the medium an impulse that is comparable to their binding equilibrium energy. The resulting material polarization is strongly anharmonic, and the charges (electrons) begin oscillating both at the fundamental exciting optical frequency and at higher-harmonic frequencies. In particular the second harmonic oscillation, in special configurations, can give rise to a stable optical excitation at twice the initial frequency. The net effect is a transfer, by means of the anharmonic mediation of matter, of optical power from one free-space linear optical eigenmode to another, at twice the frequency. We might argue that in this case we are still in a near-linear small perturbation approximation, and this is indeed the case : if this were not so *the very use of the concept of linear mode would be misleading*. Strong nonlinearity, the general case, gives rise to more complicated situations. One broad observation is that as a system is brought far from its equilibrium by some interaction, its behavior will reflect the peculiar characteristics of the actual elemental parts. Are we therefore faced with an *unending diversification* of behavior ? The answer is yes, and no. If we attempt a close analysis of dynamics in terms of the initial linear particles (harmonic modes) we must introduce system dependent coupling terms, and not just at the lowest harmonic orders : strong interaction will inevitably involve a large amount of modes. In this case we are faced with the formidable task of a large dimensional nonlinear coupled system. We might call this approach a *reductionist perspective*. Investigation of interacting systems suggests a

different approach, as strong correlations have one main consequence : *they force the system to respond in a collective-like manner*.[3] This *locked* behavior makes the system acquire a new form of universality that can be investigated through the introduction of new, qualitatively different constituent *objects* with no linear analogue. These new collective structures are by all means *not* new fundamental physical entities : they are locked complexes of known elementary particles. As mentioned, these strong correlations *wash out* the peculiarities of the specific out-of-equilibrium system and allow for a universal, almost general, description of many diverse manifestations with few, simple and pseudo-linear laws. One of these new *basic* objects, perhaps the most attractive and conceptually useful, is the Soliton.

Solitons

A soliton is a highly localized perturbation that propagates in a continuos medium without suffering distortion or modification.[4] It is fruit of nonlinear interaction that exactly balances the tendency of a localized pulse to *spread* in a linear continuos medium. Solitons behave much like fundamental particles (although they are not) : they travel through matter leaving no scattered energy behind, and are characterized by a well-defined energy and direction, that, in some cases, is conserved in soliton-soliton collisions. Solitons arise in many undulatory systems, such as water waves, sound waves, and light waves. Although they have probably been observed many times in historical times (anomalous waves, huge shock waves, etc.), the first documented and conscious observation of a soliton, or solitary wave, was reported by Russell, a Scottish naval engineer, in 1844[1]. His first observation was supposedly a water wave in an irrigation canal, stimulated by the sudden halt of a horse-driven canal embarkation. The resultant wave propagated for many miles down the canal without spreading and without losing its initial energy, until Russell himself lost track of it in a series of canal diramations. Successive observations showed that the speed of the propagating wave was related to the amplitude of the perturbation : a signature of nonlinearity. An even more astounding discovery was that for other types of perturbation, more travelling pulses would form, each with the same solitary-like dispersionless evolution. These pulses would overtake and *pass through* each other without any perceptible exchange of energy or without loss of soliton-like characteristics. By the end of the

century Kortweg and de Vries found an analytical explanation to the observations : they formulated the problem of water wave propagation in a tight canal when the water displacement was small with respect to the actual depth of the canal. They were able to write explicitly the nonlinear propagation equation, now known as the KdV equation (Kortweg-de Vries), and find that this generally nonintegrable equation had actually isolated explicit integrable solutions in the form of localized non dispersing propagating pulses : Solitons. They were able to predict the observed anomalous relationship that tied pulse amplitude and speed of propagation and thereby interpret the phenomenology reported fifty years earlier by Russell. A second nonlinear propagation equation was investigated by Skyrme in 1958, known as the sine-Gordon equation, stemming from a simple periodic extension of the Klein-Gordon field equation: also this equation allowed for solitons (in the form of "kinks")[5]. In particular both these systems manifested a peculiar characteristic : when two solitons collided, they would not exchange any sort of energy nor would they in any way be affected by the interaction, apart from a peculiar *phase-shift* (this characteristic made Zabusky and Kruskal suggest the name of "soliton"). This fact highlights that the "new" physical entities, solitons, behave like classical particles apart from a "strange" phase interaction, signature of their complex nonlinear origin. A last fundamental nonlinear propagation equation supporting solitons, particularly important in Optics, was formulated by Hasegawa and Tappert in 1973, relevant to the propagation of an intense localised optical beam in an isotropic, weakly nonlinear, medium : the third order polarizability (known as optical Kerr effect) gives rise to what is known as the nonlinear Schroedinger Equation (NLSE). The isolated integrable solutions are so-called Kerr-solitons and their temporal realization, first observed in 1980 by Molenhauer, Stolen and Gordon, is presently used in high-throughput telecommunications links.

Multi-soliton structures, such as those observed initially by Russell, find in this context an elegant explanation : they represent higher-order soliton solutions, or multisoliton pulses, also analytically derivable from the initial nonlinear wave-equations.

Solitons in Physics

The rather marked theoretical successes in the study of solitons and solitary waves is considered one of the *silent*

revolutions in Physics[5]. The great achievements in this field, however, might be somewhat misleading : solitons exist in Nature in many more systems than those that can be more or less assimilated to the basic fundamental integrable nonlinear equations, whose main "universal" characteristics stem from the fact that they are realized in a quasi-linear regime. Integrability is indeed a sufficient condition to the existence of what might be called a generalized solitary wave function family, but recurring observations of solitons in nonintegrable systems have brought things into a more elaborated perspective, and one of the main examples of nonintegrable solitons is a crucial part of this treatise : *photorefractive screening solitons*.[6] Here I will not undertake a discussion on the actual terms : solitons, solitary waves, or other names. A soliton (or a solitary wave) is a more or less localized nonevolving propagating perturbation, and that's it.

In a more general context, theoretical investigation has extended the classical integrable-system techniques to the many diverse soliton-like situations that emerge in nonintegrable nonlinear propagation equations. In particular the so-called *inverse-scattering* method played a central role[1]. In many cases the final nonlinear propagation equation cannot be assimilated to an integrable soliton-supporting equation. An explicit formulation of the soliton pulse is not available, and numerical integration completes this last step. For these systems one main consideration holds : nonintegrable solitons behave in a very similar manner to *classical* KdV, sG, and NLSE pulses. This remarkable (although by all means not always true) observation leads us to believe that solitons are indeed not a derivation of a small set of very special equations. The first numerical discovery of a *nonclassical* soliton can be attributed to the first example of a molecular dynamics study: the Fermi-Pasta-Ulam 1955 calculation[1]. Without getting into the (very interesting) details of their work, the main qualitative observation that concerns us is that they studied the transfer of energy from one initially excited mode to higher harmonic modes in a one-dimensional chain of particles with a small cubic and quartic nonlinear interaction term (along with the linear nearest-neighbor elastic interaction). They indeed expected that the (small) nonlinear coupling would allow energy, initially contained in the excitation, to diffuse to other modes, and thus expected some sort of thermodynamic loss of coherence. They were surprised to observe that this was absolutely not the case : energy went into a number of different modes, but then began oscillating in a periodic and wholly determined way. They had essentially excited a new type of *coherent multi-wave* that

coexisted on a number of initial *linear* modes and that evolved conserving its structure (apart from periodical dynamics). Solitons have been investigated since then, to name a few, in plasma Physics, in hydrodynamics, in solid-state physics, and in other correlated fields, amongst which, of course, nonlinear optics.[5)]

A quick glance at the various fields in which solitons have been studied gives perhaps the main characterizing element of what is now known as soliton science : *interdisciplinarity*.

There is an ongoing discussion in recent times as to the importance of a reductionist perspective.[7)] In recent partisan articles, it was explicitly stated that Physical phenomena are *stratified*, and that going from one scale to another, qualitatively different concepts and laws are introduced. Thus, studies into the subatomic structure of matter cannot give insight into systems at different scales, and in particular, into everyday life. Apart from the intrinsic forcelessness of such a statement, one might ask how even such a stratification can possibly arise. One answer is that, in general, we investigate matter with approximate, linear concepts and tools. Stratification occurs exactly when these concepts break down (near, for example critical points, clusterization or molecularization). Thus we *leap* close to a different fixed point, in which the "linear" construct (for example, the soliton) might have nothing in common with the lower level constructs (free modes): a comparison between two "linear" systems in a completely nonlinear transition. Similar arguments apply to spontaneous phenomena in out-of-equilibrium systems, and, in particular, to spontaneous solitons in a metastable crystal here discussed in detail.[8)]

Optical Solitons

Optical solitons are localized (in time or space) pulses of light that do not diffract or disperse, when they travel in a particular host medium. They are attractive and interesting in many aspects. As far as applications are concerned, optical solitons find a natural collocation in modern and future telecommunication systems: Temporal solitons, that is, temporally localised pulses of light, are one of the backbone ingredients of future information links. Spatial solitons, that is, highly focused nondiffracting optical beams of light, are candidates for important applications in optical circuitry elements, parallel computing, and optical computer subassemblies, although no definite application has yet been implemented, apart from a laboratory realization of a

reconfigurable optical directional coupler and nonlinear switching.[9] From a fundamental point of view, optical solitons inherit all the intriguing aspects peculiar to general soliton-like phenomena. For light, furthermore, the continuos medium is intrinsically undulatory. This in fact opens up quite a number of fundamental questions, one among which is that of the localization of photon packets. What is the role and interplay between the quantum nature of light and nonlinearity ? Optical solitons, furthermore, give strong an sensitive insight into the state of the medium that supports them. This aspect is ever more important, the stronger the interaction between the medium and the beam. Near-transition solitons, as we shall see, are perhaps the most illuminating example of this aspect.[8)10)11)]

Solitons in Optics were first investigated in Kerr media.[4] These solitons stem from the first correction to linear medium polarizability in an isotropic system. Linear polarizability, for electromagnetic radiation at optical wavelengths, gives rise to a global dephasing of the propagating wave described by the medium's index of refraction. For intense optical fields, this "elastic" scattering is modified and corrected, to the lowest order, by a third order electronic susceptibility that gives rise to the so-called optical Kerr effect, which can effectively be described by an intensity-dependent index of refraction. Therefore, the velocity of propagation of optical radiation depends both on the optical wavelength and on the intensity of the field. In practice, a quite general way of interpreting this situation is by introducing the concept of self-interaction : the optical beam changes the host medium, and this, in turn, modifies the propagation of the beam. The net effect is that the beam changes itself during propagation. Optical propagation can be generally studied by means of a wave equation that involves the material polarization $\mathbf{P}$. Nonlinearity stems from the fact that $\mathbf{P}$ is itself a more or less complicated function of the propagating optical field $\mathbf{E}$. As long as $\mathbf{P} \cong \varepsilon \mathbf{E}$, that is, as long as there is a *linear* relationship amongst the propagating perturbation and the medium, the net effect is a change in index of refraction, with respect to free space propagation. When nonlinear terms are relevant, the resulting parabolic wave-equation describes nonlinearity. Temporal Kerr solitons are routinely generated, and are still subject of intense research. Generally speaking, they necessitate of extremely high optical powers and are thus only practically feasible in strongly confining structures. The Kerr nonlinearity also supports analogous spatial solitons, although they are extremely difficult to observe. This is mainly due to the fact that this particular interaction does not

allow for the formation of two-dimensional trapped particles, these being intrinsically unstable and leading to catastrophic self-focusing. Thus only solitons in one transverse dimension (1+1D solitons) can be observed, and to obtain these, the optical beam must illuminate an extended slab of light, limiting the local achievable intensity.

It is important to note that Kerr, or Kerr-like, interaction is of a quite general nature. As mentioned, this nonlinearity is actually the first nonlinear correction to any optical propagation in an isotropic medium. There are two other main types of optical solitons : quadratic solitons, and photorefractive solitons. These are supported by an indirect optical self-coupling, which is mediated by a secondary mechanism (only present in specific conditions). Quadratic optical solitons[4)] were initially discovered by Karanzin and Sukhorukov in the 1970s. These solitons cannot be interpreted as stemming from a modification of the medium's refractive index. They rely solely on strong interaction and energy exchange between two, or more, beams at different frequencies, mediated by nonlinear electronic polarizability: the net effect is a nonlinear polarization P that allows self-trapping of the components.

Photorefractive solitons were initially predicted by Segev, Crosignani, Yariv, and Fischer, and have ever since been observed in many different materials and configurations.[4)] They are one of the main subjects of this treatise and we shall leave their description to Chapter 3. We wish, however, to mention that the wording Photorefractive Solitons has come to refer to the main type of self-trapping to date investigated : screening solitons. Wholly different types of nonlinear self-interactions are actually supported by photorefraction. Such is for example the case of diffusion-driven self-trapping and nonlinear diffraction, and spontaneous solitons, to which are dedicated, respectively Chapters 8 and 9.[8)10)11)] These new types of solitons, although making use of the same basic ingredient, photorefraction,[12)] behave in a completely different manner with respect to standard screening particles. Furthermore, spontaneous solitons seem to reflect a general tendency of an out-of-equilibrium host to support soliton particles : a universal feature of propagation in a metastable host.

Spatial Optical Solitons

Limiting our scope to spatial effects, in the paraxial approximation, the relevant physical quantity for steady-state

investigation, the slowly-varying envelope $A(\mathbf{r}_\perp,z)$ of the optical field, obeys the so-called parabolic wave equation, as described in detail at the end of Chapter 2,[2)]

$$\left[\frac{\partial}{\partial z}+\frac{i}{2k}\nabla_\perp^{\,2}\right]\mathbf{A}=-\frac{ik}{n_1}\Delta n\mathbf{A} \qquad (1.1)$$

where k is the optical wave-vector, n_1 is the material index of refraction, and $\Delta n=\Delta n(\mathbf{P})$ is generally a tensorial function of the material polarization **P**. This last function is the source of nonlinearity of Eq.(1.1). The actual behavior of the optical field depends on the explicit form of Δn. Kerr effects can be generally described by an effective scalar $\Delta n=n_1+n_2 I$, where I is the optical intensity ($I=|\mathbf{A}|^2$). The screening photorefractive nonlinearity, on the other hand, can be approximately described, in most common configurations, by a scalar saturable nonlinearity $\Delta n= -1/(1+I/I_b)$, where I_b is a constant (background illumination). These nonlinearities have one major characteristic in common : they are **local**. What does this mean ? In a word, $\Delta n(\mathbf{r})$ in point **r** depends only on the value of the optical field in that same point. Apart from the actual simplifications that this fact implies to the investigation of Eq.(1.1), it intrinsically indicates that the nonlinearity does not introduce any additional (spatial) scales to the problem. In this case we can deduce from Eq.(1.1) a set of general necessary (but not sufficient) requirements for the formation of soliton-like particles.

The first question we can tackle is : how much nonlinearity ? This is indeed quite an important question in choice of material and optical source. The first term in Eq.(1.1) describes variations along the direction of propagation z. The second and third terms describe transverse spreading of the optical beam : diffraction. Thus, if diffraction is to be compensated by the nonlinear source term, the contribution to dynamics of the term to the RHS of Eq.(1.1) must be of the order of the diffractive terms. Diffraction depends on the ratio of the characteristic transverse length scale (size of the localized pulse) $l_{x,y}$ and the optical wavelength : $l_{x,y}/\lambda$. Imposing that the order of magnitude of the terms is the same, we obtain the following expression for Δn :

$$\Delta n\approx\left(\frac{\lambda}{l_{x,y}}\right)^2\frac{1}{2n(2\pi)^2} \qquad (1.2)$$

For example, for an optical beam at λ=0.5μm, in a material with n=1.5, with transverse Gaussian profile $I=I_0\exp(-r^2/\sigma^2)$, taking the characteristic transverse length scale to be $l_{x,y}=\sigma$=5μm , the trapping nonlinearity must be of the order of $\Delta n \approx 10^{-4}$. Clearly this is only a rough estimate, and a precise investigation of self-trapped solutions, given a local Δn, supply the "exact" value. This in turn implies conditions both on the actual shape of the soliton beam and on the quantities contained in Eq.(1.2). In particular, the value of Δn is generally related to some "free" parameter, such as, for example, peak intensity I_0 for Kerr solitons, or intensity ratio I_0/I_b for screening solitons. Thus given a value of $l_{x,y}$, there will be a set of values of this free parameter that allow diffraction compensation (like in Eq.(1.2)) : the set of these values is called generally the "soliton existence curve". Soliton formation is only possible on this curve in the system parameter space.

The above discussion fits in well with the so-called "linearist interpretation" of soliton formation. Some scientists working on optical spatial solitons believe that soliton formation can be viewed as linear propagation in a self-induced waveguide.[13] In fact, the above estimate is in accord with this view : to evaluate the amount of index change needed to linearly guide a beam, the exact same procedure can be followed. The main point is that this view distinguishes the soliton formation process (a definitely nonlinear process) from the final propagation process. Thus, for example, two-dimensional solitons have been analytically investigated in saturated Kerr-like nonlinearities and explicit beam profiles have been found along with the soliton existence curve. This approach is, albeit attractive and sometimes useful, wholly unfounded. In particular, it is based on a basic heuristic hypothesis : that the soliton actually forms. This is not always the case : a main characteristic of nonlinear interaction is actually in its nonpredictability, and in this the linear perspective seems a blatant oversimplification. This particular limitation is most of time admitted, and in itself does not create much confusion. A second, less advertised limitation, lies in the basic hypothesis that Δn is local, as supposed above. The linear view in fact completely fails when Δn is nonlocal and introduces a new length scale. An explicit example of this is treated directly in this treatise, in Chapter 8 : diffusion driven solitons. These solitons stem from a nonlinearity that is connected to the spatial diffusion of light generated charged particles and is thus inherently nonlocal (it contains a first derivative of the optical intensity). In this case, as will be discussed in detail in the mentioned Chapter, soliton

formation does not have a characteristic length scale, and the equivalent of condition Eq.(1.2) does not contain $l_{x,y}$. Thus these solitons do not have an existence curve, a circumstance wholly excluded by the linear approach to soliton formation.

REFERENCES:

[1] *Solitons: an introduction*, P.Drazin and R.Johnson (Cambridge University Press, Cambridge 1989)

[2] *Optical Electronics*, A.Yariv (Oxford University Press, New York 1991)

[3] *Exploring Complexity. An Introduction*, I.Prigogine and G.Nicolis (R.Piper GmbH & Co. KG, Monaco 1987)

[4] M. Segev and G. I. Stegeman, Physics Today, August 1998.

[5] A.Degasperis, Am.J.Phys. **66**, 486 (1998)

[6] B.Crosignani, P.Di Porto, M.Segev, G.Salamo, and A.Yariv, La Rivista del Nuovo Cimento **21**-6 (1998)

[7] For a very recent comment, see the letter by F.Rohrlich, Physics Today, November 1998.

[8] E.DelRe, M.Tamburrini, M.Segev, and A.Agranat, *Spontaneous self-trapping of optical beams in metastable paraelectric crystals*, submitted to Physical Review Letters (November 1998)

[9] S.Lan, E.DelRe, Z.Chen, M.Shih, and M.Segev, *Directional coupler using soliton-induced waveguiding*, to appear in Optics Letters (February 1999)

[10] B.Crosignani, E.DelRe, P.DiPorto, A.Degasperis, Opt.Lett. **23**, 912 (1998)

[11] B.Crosignani, A.Degasperis, E.DelRe, P.DiPorto, *Nonlinear optical diffraction effects and solitons due to anisotropic charge-diffusion based self-interaction*, to appear in Physical Review Letters (February 1999)

[12] *Introduction to photorefractive nonlinear optics*, P.Yeh (Wiley, New York 1993)

[13] For a recent example see A.Snyder and J.Mitchell, Opt.Lett. **22**, 16 (1997)

Chapter
2

Photorefraction

Introduction

Photorefraction is a basic process present in many diverse materials that is responsible for a wealth of physical phenomena observed in Optics. In particular, it is at the basis of almost all the phenomena described in this treatise, and this Chapter is dedicated to introducing the basic physical processes, and the general theoretical treatment. In particular, a simple linearization approach is described based on the pioneering work of what is known as the "Kiev Group". This approximation strategy, considered the main analytical approach to photorefractive phenomena, actually breaks down in most practical configurations. This is, for example, the case of two-wave-mixing (TWM). Thus, here is described a different, novel, approach to nonlinear description, based on an iteration scheme, first introduced and experimentally demonstrated by DelRe, Ciattoni, Crosignani, and Tamburrini in 1998 [1)], that allows a quite exhaustive description of a class of practical configurations, and, in particular, of a TWM holographic scheme. This new theoretical description is pitted against experiments carried out in a sample of photorefractive $BaTiO_3$, and good agreement is obtained. Finally, the general basic instrument used in the analysis of nonlinear optical wave propagation, the parabolic paraxial equation (already hinted at in Chapter 1), is briefly discussed.

Basic Phenomenology

Photorefraction is a process that occurs in materials that manifest some sort of photoconductivity and are at the same time electro-optic. It was initially discovered by Ashkin, Boyd, Dziedzic, Smith, Ballman, Levinstein, and Nassau (Bell Telephone Laboratories) in 1966[2)]. They observed an optically induced variation of the index of refraction in a sample of $LiNbO_3$ (Lithium Niobate) that strongly disturbed optical propagation, not allowing the use of these samples for their original purpose: second-harmonic generation. They referred to the process as "optical damage". Since then photorefraction has been observed in many diverse materials, $BaTiO_3$, KTN, KLTN, $KNbO_3$, BSO, BTO, BGO, $LiTaO_3$, SBN,

all ferroelectrics. In semiconductors, such as InP, GaAs, and in polymers and liquid crystals. It is characterized by "long" response times (reaction times vary generally from a few milliseconds to several seconds, depending on the optical intensity), and extremely intense changes of local crystal index of refraction induced by the incident light distribution. Furthermore, the index changes are reversible (or "erasable"). This extremely strong response makes photorefraction attractive for the experimental investigation of nonlinear optical processes, although their theoretical description is typically quite difficult, as discussed in what follows. Photorefraction, since its initial discovery, has been used to realize optical phase-conjugation, optical memory storage systems, mixing components, and real-time holographic schemes[3]. Initial studies made use of the strong material response to achieve what is generally referred to as a *light controlling light* process. More recent studies, especially those concerning photorefractive solitary waves, are centered on a physically more appealing case: *light controlling itself*.[4]

Physical Mechanism

In most cases photorefraction behaves in a manner that can be interpreted by a single physical model, known as the *band-transport* (or rarely *Kukhtarev*) model[5]. This simple, although highly nonlinear, picture clarifies a number of seemingly "strange" phenomena observed. For example, it has allowed the theoretical interpretation of photorefractive 1+1D screening solitons[6] and recently, diffusion-driven nonlinear diffraction in centrosymmetric crystals (discussed in the following Chapters). Apart from the introduction of more detailed charge-carrier mechanisms and other minor intricacies that do not fundamentally modify the basic physics, there is evidence that this model is not "complete" (of course no phenomenological model can ever be complete). For example, observed photorefractive two-dimensional (2+1D) spatial solitons, that, according to analysis and numerics based on the minimal model, do not exist in a circular-symmetric realization[7]. This peculiar aspect of photorefraction is addressed in Chapters 3 and 4. In what follows the "minimal" physical mechanism is described[8].

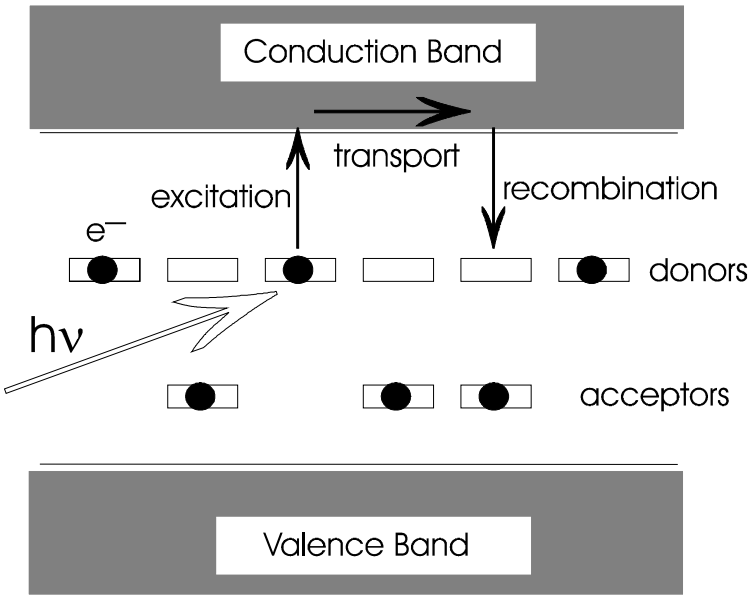

Fig.2.1: Schematic of the photorefractive band structure and charge separation mechanism.

With reference to the band scheme illustrated in Fig.2.1, consider a nonmagnetic dielectric (isolator) with a direct absorption at energies higher than visible wavelengths (typically a gap energy is $E_g \approx$ 3eV). For a visible beam the "perfect" crystal is *transparent*. Most actual samples are characterized by small amounts of spurious imperfections that are either voluntarily mixed into the initial design (standard doping), or are due to the inevitable presence of alien species in contact with the crystal growth area. In most cases these impurities do not influence perceptibly the overall structure of the crystal. Their presence engenders in-gap levels (as indicated in Fig.2.1) that we shall approximate with *two new levels*: one level describing *donor* impurities, and another, *acceptors*. Indicating the donor impurity concentration with N_d and the acceptor concentration with N_a, we shall furthermore assume that $N_d >> N_a$, an assumption generally valid for most ferroelectric materials (although in some samples of $BaTiO_3$ and $LiNbO_3$ the exact opposite is true; in these cases the entire discussion can be exactly repeated for mobile holes instead of conduction electrons).

In the absence of light, at thermodynamic equilibrium, all acceptor sites are occupied by electrons from ionized donors. In this configuration $N_d^+ = N_a$, where N_d^+ indicates the concentration of ionized donor sites, neglecting thermally excited electrons. Illuminating the sample with light of a given

optical wavelength λ ($hc/\lambda << E_g$) such that the photon energy allows direct ionization of donor sites, promotes electrons in the conduction band that are free to *drift* in an applied electric field (photoconductivity) or *diffuse* to regions of the crystal that are not equally illuminated. Photovoltaic effects, present in samples of $LiNbO_3$, will be discussed briefly in Chapter 3, and are here neglected (for the crystals used in this treatise, $BaTiO_3$, SBN, and KLTN, this in fact is a very good approximation). Once these electrons move into darker regions, they are retrapped by the ionized donors. The overall process is a highly random statistical response whose final effect is a light-induced charge separation and a resultant build-up of an internal electric field (responsible for the ceasing of the dynamic regime). Up to this point, the process is a simple impurity based photoconduction effect. Photorefraction is based furthermore on what is termed the *electro-optic effect*.[9)]

Some materials, especially those which are formed by interlaced, prevalently ionic, components, are susceptible to constant applied electrical fields. Such is the case, for example, for ferroelectrics (extensively discussed in Chapter 5). In these materials, the local ionic structure is slightly modified by the field and this change is directly reflected in the dielectric response at optical frequencies. The net effect, referred to as the **Pockel's Effect** (or Electro-Optic Effect), is a local constant-field induced change in the optical index of refraction n. The actual change in index depends on the direction of applied electrical field **E** , the crystal symmetry, and the polarization of the optical beam. The relevant physical quantity is the macroscopic local crystal polarization **P** , and the slight field-induced change in **P** (i.e.**P=P**(**E**)) generates a change in the index of refraction Δn that can be approximated by the expansion[9)]

$$\Delta\left[\frac{1}{n^2}\right]_{ij} = g_{ijkl}P_kP_l + l_{ijklmn}P_kP_lP_mP_n + \ldots \qquad (2.1)$$

where g_{ijkl} and l_{ijklmn} are material dependent constants, $\Delta[1/n^2]_{ij}$ is the high-frequency dielectric constant modulation for an input i-polarized component and an output j-polarized one, the polarization P is generally in the linear regime, i.e. $\mathbf{P}=\varepsilon_0(\varepsilon_r-1)\mathbf{E}$, $\varepsilon=\varepsilon_r\varepsilon_0$ being the dielectric constant, and generally only the first quadratic term gives rise to observable effects. Only terms with an even number of P components are present, since in its most general form, dielectrics are centrosymmetric. As discussed in Chapter 5, some dielectrics however, referred to

as *ferroelectrics*, in a certain temperature range, manifest strong spontaneous polarization P_s along a particular crystal axis (optical axis). Since, in general, $P_s >> P(E)$ for accessible values of external field E,

$$\Delta\left[\frac{1}{n^2}\right]_{ij} \cong g_{ijkl}(P_{spo\,k} + P_k)(P_{spo\,l} + P_l) \cong g_{ijkl}(P_{spo\,k}P_{spo\,l} + P_{spo\,k}P_l + P_{spo\,l}P_k) \quad (2.2)$$

The first term is the crystal birefringence. The second and third terms give

$$\Delta\left[\frac{1}{n^2}\right]_{ij} \cong r_{ijk}E_k\,, \quad (2.3)$$

which is the *linear electro-optic effect*, where $r_{ijk} \equiv r_{ijk\bar{1}} = 2g_{ijk\bar{1}}P_{spo\,\bar{1}}\varepsilon_0(\varepsilon_r - 1)$ and $\bar{1}$ is the optical axis. Thus ferroelectrics in the noncentrosymmetric phase exhibit a *linear* electro-optic response.

The photo-induced electric field **E**, generally referred to as the space-charge field, modifies, via the electro-optic effect, the local index of refraction. This modulation, in turn, modifies the propagation of the optical beam, giving rise to a typical nonlinear propagation. Note that nonlinearity here refers to the whole complex interaction process. In "classical" nonlinear Optics, nonlinearity is a term that generally refers to effects due to the nonlinear response to the oscillating optical field of the high frequency (electronic) polarizability. In photorefraction, given the generally low optical intensities used, these terms have a negligible effect and in fact light propagates "linearly" in the induced index pattern $n+\Delta n$. The process is however extremely nonlinear, as the propagating entity, through a mediated intermediate process, itself modifies its "linear" propagation. In practice this distinction is immaterial: the optical wave-propagation equation in both "classical" nonlinear optics and in photorefractive optics is nonlinear, as we shall see in further on.

Model

Photorefraction, as pictured above, is a mixture of simple basic processes. This simplicity is reflected in the relative

ease with which we can write down the basic equations and thus formulate the basic *minimal* model. The question as to how such a simple model can allow for many diverse phenomena (such as those for example contained in this treatise) is easily answered: solving the model produces a *highly nonlinear equation*.

The basic model, first formulated by the so-called Kiev group in 1977 [10)], is based on the assumption, almost universally supported by experimental evidence, that the basic process of charge photogeneration and recombination can be described by a simple probabilistic type rate equation. Clearly this treatment excludes *a priori* any direct effects due to optical coherence and thus eliminates any quantum photorefractive phenomenology: photons pass through the crystal, and some are absorbed, like bullets in a target, giving off free electrons. In the future it cannot be excluded that quantum effects based on a photorefractive process might prove interesting and observable, although to date no such evidence has been reported.

The rate equation assumes that the rate of variation in time of ionized donor sites is due to two processes: thermal and optical ionization, and charge recombination. The first process is taken to be proportional to the sum of the local optical intensity I(**r**, t) and the equivalent thermal intensity I_d (dark irradiance) and proportional to the nonionized donor sites available. Charge recombination is simply the product of the local density of free charges N and the available donor sites. The final rate equation is

$$\frac{\partial N_d^+}{\partial t} = s(I + I_d)(N_d - N_d^+) - \gamma N N_d^+ \qquad (2.4)$$

where s is the cross-section for photoexcitation and γ is the electron-ionized donor trap recombination rate. The photogenerated mobile charges must satisfy the continuity rate equation

$$\frac{\partial N}{\partial t} - \frac{\partial N_d^+}{\partial t} = \frac{1}{q}\nabla \cdot \mathbf{J} \qquad (2.5)$$

where –q is the electronic charge, and **J** is the local current density in the crystal. The engendered local electric field **E** is related to the charge density ρ through the Poisson equation

$$\nabla \cdot \mathbf{D} = \nabla \cdot \varepsilon \mathbf{E} = \rho \qquad (2.6)$$

where **D** is the displacement vector and ε is the dielectric constant (or tensor). The charge density ρ can be expressed in terms of charge concentrations

$$\rho = q(N_d^+ - N_a - N) . \tag{2.7}$$

Current density is due to charge drift and diffusion and is expressed by

$$\mathbf{J} = q\mu N\mathbf{E} + k_b T\mu\nabla \cdot N \tag{2.8}$$

where μ is the electron mobility, k_b is the Boltzmann constant, and T is the crystal temperature.

Equations (2.4)-(2.8) are highly nonlinear. Both equation (2.4) and equation (2.8) have a number of products of system variables. Treatments of this system generally introduce directly a first order linearization to highlight the main physical characteristic quantities, or scales. Since the linearization, hinted at in the next section, has definitely nothing to do with solitons, apart from the investigation of nonlinear TWM, we shall give a description starting directly from the nonlinear system. Interestingly, some basic texts on photorefraction seem to suggest that the quantities are somehow tied to the linearization procedure. This emphasis on the linearized approach may be at the basis of the very slow development of more advanced and powerful approaches in this field.

The process has two fundamental time scales. The first is the *charge lifetime* τ_e. Consider a single photon hitting the sample and ionizing a donor site: how much time will the photogenerated electron survive? Once the photon has been absorbed, the sample is characterized by a single asymmetry: the presence of the free electron. Statistically this electron will *not* diffuse of drift anywhere. It will just sit there. Thus, averaging on many single realizations, $\frac{\partial N_d^+}{\partial t} \approx \frac{\partial N}{\partial t}$ and from eq.(2.4) we immediately obtain that (assuming that $N_d^+ \approx N_a$ in the nonlinear term)

$$\tau_e \approx \frac{1}{\gamma N_a} . \tag{2.9}$$

The second characteristic time scale is the *dielectric relaxation time* τ_d. It is the time that a charge perturbation takes to disappear. Starting from eq.(2.5), we need to

evaluate the order of magnitude of the spatial divergence of **J**. Neglecting the diffusion term in eq.(2.8), we can estimate the value of **J** by estimating the order of magnitude of **E** through eq.(2.6). The final expression of τ_d is obtained from eq.(2.5) and gives

$$\tau_d \approx \frac{\varepsilon}{q\mu N} \tag{2.10}$$

where N of course is still a variable and must be estimated independently. If N is estimated as approximately $N \propto I$, we can qualitatively state that "steady-state is obtained in a time inversely proportional to the optical intensity." Having neglected the diffusion term in eq.(2.8) makes the estimate for τ_d independent of the characteristic length scale of the illuminating light Λ (separating the temporal scales from the spatial ones). This expression is valid when Λ is such as to make the effective diffusion term negligible (see below).

From the spatial point of view, the problem has *only one* spatial scale, Λ, determined by the input light distribution. The response, however, can be identified in a set of characteristic electric fields. The first field, the *diffusion field* E_d, can be evaluated through eq.(2.8). With no applied electric field, at steady-state, **J**=0, thus

$$E_d \approx \frac{k_b T}{q}\frac{1}{\Lambda}. \tag{2.11}$$

The second field is the *displacement field* E_m whose order of magnitude can be evaluated starting from eq.(2.4). Given a value of N_d^+, it will evolve (relax), in absence of external illumination, with a characteristic time scale $\tau \approx 1/\gamma N$. Neglecting N compared to N_d^+ in eq.(2.5) gives an estimate of the same scale $\tau \approx \Lambda N_d^+/\mu N E_m$, where E_m is the characteristic field (displacement) scale. Thus, equating these expressions

$$E_m \approx \frac{\gamma_r N_a}{\mu}\Lambda. \tag{2.12}$$

To interpret the physical meaning of E_m, we note that $E_m \mu \tau_e \approx \Lambda$. Thus the displacement field is such as to displace a single carrier the distance Λ during its lifetime τ_e.

The last characteristic field is the so-called *saturation field* E_q, and represents the maximum field that can be induced

through charge separation: the actual field present will be generally lower than this value. The order of magnitude of this quantity can be estimated directly from eq.(2.6) and eq.(2.7). From the first equation we obtain that $E_q \approx \rho\Lambda/\varepsilon$. The maximum value of ρ is obtained for $N \approx N_d^+$, and thus

$$E_q \approx \frac{qN_a}{\varepsilon}\Lambda . \qquad (2.13)$$

The quantities estimated in eqs.(2.9-2.13) are those initially introduced by the Kiev group in their linearized approach. Although they represent only a rough estimate of the physical scales, we shall *define* them quantitatively with these estimates (as is usually done in Literature).

The scales allow the introduction of an important quantity, the *Debye Length* L_{Db}, or, equivalently, the *Debye Field* E_{Db}. Consider a situation in which no external electric field is applied to the crystal. The maximum electric field attainable is E_{Db} (in analogy to plasma physics). In absence of external fields, an illumination with characteristic scale Λ will engender a diffusion field that is *at most* (always in a dimensional-type analysis) equal to E_q. Imposing $E_d=E_q$, we obtain the critical value of Λ ($=L_{Db}$)

$$L_{Db} = \left[\frac{k_b T\varepsilon}{q^2 N_a}\right]^{1/2} , \qquad (2.14)$$

and a corresponding Debye Field

$$E_{Db} = \frac{k_b T}{q}\frac{1}{\Lambda_{Db}} . \qquad (2.15)$$

All the quantities here introduced have an “exact” quantitative significance in the linearized approach. The above treatment, however, should make clear that these quantities are inherent to the minimal model in its full nonlinear complexity. The presence of these characteristic scales means that optical propagation in photorefractives will in general manifest *nonlocality*, both in space and in time, and this has important direct consequences on many phenomena. For example, temporal nonlocality has allowed the observation of so-called *incoherent spatial solitons*. Through an evaluation of spatial scales it will be shown (in Chapters 3 and 6) how this nonlocal system allows an approximate nonperturbative description of

spatial photorefractive soliton with a *local* nonlinearity (screening solitons).

Linearization

As mentioned, the system of equations (2.4)-(2.8) is highly nonlinear. One simple strategy, in attempting to tackle them analytically, is a straightforward linearization. Although the basic hypothesis of this approach are hardly ever met, it is by far the most commonly adopted, and few theoretical improvements have been achieved. One alternative method will be discussed in the next section, and there some previous attempts are recalled.

Here we summarize the linearized approach in the steady-state regime, that is, when the system has reached a temporal (albeit dynamic) equilibrium. In this case all the time derivatives in eqs.(2.4)-(2.8) are set to zero. This statement is actually valid for all the theoretical treatments in this treatise, leaving out some main issues: How is steady-state reached and in *how much* time? *Is* there a steady-state time-independent regime? What about *quasi-regimes*, in which the system keeps evolving, but in a qualitatively unimportant manner?

Linearization is obtained in a simplified one dimensional configuration, in which I changes only in one direction, say the x direction (1+1D case). Furthermore, I is taken to be a periodic sinusoidal function, $I = I_0 + \mathrm{Re}\{I_1 e^{-iKx}\}$, like that for example obtained making two plane waves, with wavevectors k_1 and k_2, interfere in the crystal ($K=|k_1-k_2|$) . Finally, it is assumed that the effect of this point dependent illumination is "small" compared to the overall configuration of the crystal. This is equivalent to assuming that the visibility of the interference fringes is very small, or, conversely, that the modulation depth $m=I_1/I_0$ of the interference pattern is much smaller than 1. This hypothesis implies that the system variables will depend on the x in the same way that I depends on x, and that the constant variable value V_0 will be much larger than the amplitude V_1 of the spatially modulated one (apart from the actual electric field variable E). Plugging the new variables

$$\begin{aligned} N &= N_0 + \mathrm{Re}\{N_1 e^{-i\vec{K}\cdot\vec{r}}\} \\ N_d^+ &= N_{d0}^+ + \mathrm{Re}\{N_{d1}^+ e^{-i\vec{K}\cdot\vec{r}}\} \\ J &= J_0 + \mathrm{Re}\{J_1 e^{-i\vec{K}\cdot\vec{r}}\} \\ E &= E_0 + \mathrm{Re}\{E_1 e^{-i\vec{K}\cdot\vec{r}}\} \end{aligned} \tag{2.16}$$

into eqs.(2.4)-(2.8), keeping only first order terms (linearizing), gives an electric field (in the complex representation)

$$E_1 = \frac{iK\frac{k_b T}{q} - E_0}{1 + \frac{K^2}{k_{Db}^2} + i\frac{qKE_0}{k_b T k_{Db}^2}} \frac{I_1}{I_0} = \frac{iE_d - E_0}{1 + \frac{E_d}{E_q} + i\frac{E_0}{E_q}} \frac{I_1}{I_0} \tag{2.17}$$

where $k_{Db}=L_{Db}^{-1}$ is the *Debye wavevector*, and E_0 is the externally applied electric field.

Equation (2.17) shows that when two waves interfere in a photorefractive crystal, they engender a periodic space-charge field that, through the Pockels Effect, can create a index of refraction grating. For crystals in the noncentrosymmetric phase, the linear electro-optic response will allow for an in-phase (with the initial light field) modulation, described by the real part of eq.(2.17) and an out-of-phase grating described by the imaginary part. This last grating allows the coherent transfer of optical power from one of the interfering waves to the other. The direction of amplification is determined by the direction of the ferroelectric optical axis. This process, known as two-wave-mixing (TWM), is of great importance both from the applicative point of view in phase-conjugation and real-time holographic schemes, and from the fundamental point of view, allowing a direct experimental verification of basic material models and approaches. Its theoretical and experimental investigation in a realistic experimental configuration is the subject of the next section of this Chapter, in which a novel approach to photorefraction is described.

Approach to Nonlinear Space-Charge Field Description in Photorefractive Crystals

To date, there are essentially three alternative approaches to the solution of the nonlinearized model equations (see, e.g.,

[2], [3], [11], [12]), all of which are not able to provide, in a straightforward manner, some of the essential relationships that tie external parameters, such as the external bias voltage and beam size and shape, to the space-charge field generated within the crystal (see linearization in the previous section). A first approach, particularly amenable to numerical implementation, is to solve the problem in Fourier space[13], keeping as many components as feasible (instead of only the first, as done above). A second approach, maybe the closest to what one may call a complete analytical solution, involves a partial linearization of the rate equation governing the effect, keeping all other nonlinearities[14]; however, this approach fails to provide a good description in the presence of an external bias voltage. A third approach is to consider the analytical problem solving for the ionized donor density instead of the space-charge field[15]. Although numerical simulations have provided useful results (see, e.g., [16] and [17]), no clear and concise full nonlinear analytical treatment is available.

Here, we describe a new alternative nonlinear approach and relative experiments concerning the 1+1D case of TWM geometry in which two spatially limited monochromatic coherent waves interact inside a the photorefractive (PR) crystal.

In the steady-state configuration the model is described by eqs.(2.4)-(2.8) annulling the time derivatives and adding the boundary condition

$$V = -\int_{-l/2}^{l/2} E dx, \tag{2.18}$$

where x is the transverse coordinate in which light modulation occurs, V is the applied external voltage in this direction, l the crystal size (along x). In obtaining a single differential equation, we neglect in eq.(2.7) N with respect to N_d^+ and N_a, this being valid in most situations of interest ($N<<N_a<<N_d$). Eq.(2.5) implies that J does not depend on x, and therefore assumes a constant value J_c, that is $J = J_c$. Eq.(2.6) can be used to express N_d^+ as a function of dE/dx. Inserting this relation into eq.(2.4), we are able to express N as a function of dE/dx. Finally, introducing the resulting expression for N in eq.(2.8), and using $J = J_c$, we obtain a differential equation for E alone which reads, without resorting to preliminary linearizations,

$$\frac{q\mu(\beta + sI)\left(N_d - \frac{\varepsilon}{q}\frac{d}{dx}E - N_a\right)}{\gamma\left(\frac{\varepsilon}{q}\frac{d}{dx}E + N_a\right)}E + \\ + \frac{d}{dx}\left[\frac{\mu k_b T(\beta + sI)\left(N_d - \frac{\varepsilon}{q}\frac{d}{dx}E - N_a\right)}{\gamma\left(\frac{\varepsilon}{q}\frac{d}{dx}E + N_a\right)}\right] = J_c$$

(2.19)

where $\beta = sI_d$. Once this equation is formally solved, the condition expressed in eq.(2.18) determines the value of the current J_c. Eq.(2.19) has been treated in a simplified approximation by Vachss et al.[18] , in which however TWM cannot be described. In order to deal with eq.(2.19), we first recast it in an appropriate dimensionless form by introducing the adimensional quantities

$$Y \equiv \frac{E}{E_{Db}},\ \xi \equiv k_{Db}x,\ Q \equiv 1 + \frac{I}{I_d},\ G \equiv \frac{J_c}{q\mu\beta_1 E_{Db}}$$

(2.20)

where $E_{Db} = (k_b T / q)k_{Db}$, k_{Db} is the Debye wave number defined by the expression $k_{Db}^{\ 2} = (q^2 N_a / (\varepsilon k_b T N_d))(N_d - N_a)$ (equivalent to the previous definition when $N_a << N_d$, as is generally the case), and $\beta_1 = \beta / \gamma$. After defining $\alpha = (N_d - N_a)/N_a$ and $\delta = \varepsilon k_{Db} E_{Db} / (qN_a)$, eq.(2.19) can be rewritten as

$$\frac{QY\left(\alpha - \delta\frac{d}{d\xi}Y\right)}{\left(1 + \delta\frac{d}{d\xi}Y\right)} + \frac{d}{d\xi}\left[Q\frac{\left(\alpha - \delta\frac{d}{d\xi}Y\right)}{\left(1 + \delta\frac{d}{d\xi}Y\right)}\right] = G \cdot$$

(2.21)

We consider the standard case $N_a << N_d$. This makes $\delta \cong 1$, $k_{Db}^{\ 2} \cong q^2 N_a / (\varepsilon k_b T)$, and $\alpha >> 1$. Furthermore, in order to proceed, we neglect $dY/d\xi$ with respect to α. This last approximation is warranted both by the fact that α is much

greater than 1 and by the fact that $dY/d\xi$ is small with respect to 1 in our approach, as we shall assume below. With these approximations, eq.(2.21) becomes

$$\frac{QY}{\left(1+\frac{d}{d\xi}Y\right)}+\frac{d}{d\xi}\left[\frac{Q}{\left(1+\frac{d}{d\xi}Y\right)}\right]=\frac{G}{\alpha}\equiv g\cdot \tag{2.22}$$

It should be noted here that taking $|dY/d\xi|$ <<1 implies some constraints also on ρ through eq.(2.6). It can be shown that, with these restraints, $N_d^+ \approx N_a$. This implies that although it is generally true that $N << N_a << N_d$, this does not directly authorize us to neglect N in eq.(2.7). An approximate condition for the simultaneous validity of the two approximations is that $N/N_a << N_a/N_d$, this condition being generally true for the light intensities normally used.

As briefly mentioned above, in a typical TWM setup (see fig.2.2), two coherent monochromatic beams $E_1(x,z,t)=A_1\exp(k_{1x}x+ik_{1z}z-i\omega t)$ and $E_2(x,z,t)=A_2\exp(k_{2x}x+ik_{2z}z-i\omega t)$ are made to interfere inside the PR crystal at a certain angle θ (symmetrically, $k_{1x}=-k_{2x}$) as shown, the resulting intensity pattern having the expression

$$I=I_0(1+m\cos[Kx]) \tag{2.23}$$

where $I_0=|A_1^2|+|A_2^2|=I_1+I_2$, $m=2|A_1A_2^*|/I_0$ is the modulation depth and $K=k_{1x}-k_{2x}=(4\pi/\lambda)n\,sin[\theta]$ is the transverse grating vector. Accordingly, the main scale of variation of I is associated with the grating vector K (apart from an eventually slowly varying beam-shape factor). We must now take into account the fact that to the dark irradiance $I_d=\beta/s$ previously introduced one has to add a background illumination I_b unavoidably present inside the crystal due to the experimental conditions (actually, the typical case is $I_d << I_b$). As a consequence, it is convenient to modify appropriately the normalization of I previously introduced, so that

$$\begin{aligned} \mathrm{Q} &= 1+\frac{\mathrm{I}_0}{\mathrm{I}_\mathrm{b}+\mathrm{I}_\mathrm{d}}(1+\mathrm{m}\cos[\chi\xi]) = 1+\mathrm{Q}_0(1+\mathrm{m}\cos[\chi\xi]) \\ &= (1+\mathrm{Q}_0)(1+\mathrm{m}_1\cos[\chi\xi]) \end{aligned} \tag{2.24}$$

where we have set $Q_0 = I_0/(I_b+I_d)$, $\chi = K/k_{Db}$ and $m_1 = m/(1+1/Q_0)$.

Returning to eq.(2.22) and solving for *Y*, one obtains

$$Y = -\frac{Q'}{Q}+\frac{g}{Q}+\frac{g}{Q}Y'+\frac{Y''}{1+Y'}, \tag{2.25}$$

where here the prime indicates a derivation with respect to ξ.

We consider eq.(2.25) under the following approximations

$$\begin{aligned} &i)\ |Y'| << 1\ , \\ &ii)\ |Y''| << \left|-\frac{Q'}{Q}+\frac{g}{Q}+\frac{g}{Q}Y'\right|\ . \end{aligned} \tag{2.26}$$

Conditions (2.26) imply that the "zero order" solution of eq.(2.25) is

$$Y^{(0)} = -\frac{Q'}{Q}+\frac{g}{Q} \equiv Y_d + Y_{dr}\,, \tag{2.27}$$

while a first correction in the drift regime ($|Q'/Q| << |g/Q|$) is given by the term $(g/Q)Y'$. In order to impose conditions (2.26), we can rewrite them consistently in the form

$$\begin{aligned} &i)\ \left|Y^{(0)'}\right| << 1\ , \\ &ii)\ \left|Y^{(0)''}\right| << \left|-\frac{Q'}{Q}+\frac{g}{Q}+\frac{g}{Q}Y^{(0)'}\right|\ . \end{aligned} \tag{2.28}$$

Eq.(2.27) is composed of two terms. The first is essentially the diffusion field, that we indicate with Y_d, the second is the drift term that we indicate with Y_{dr}. Making use of the expression for *Q* given in eq.(2.24), a sufficient condition for the validity of (2.28) can be proven to be [1)]

$$\varepsilon << 1 \ ,$$
$$\left|Y_{dr}\right| << \frac{1}{\varepsilon} \ , \tag{2.29}$$

where[1)]

$$\varepsilon = \begin{cases} \dfrac{\chi m_1}{1-m_1} & m_1 > \dfrac{1}{2} \\ \chi & m_1 < \dfrac{1}{2} \end{cases} . \tag{2.30}$$

We consider now the case when $m_1 / (1-m_1) \approx 1$. In the drift regime ($\left|Y_{dr}\right| >> \left|Y_d\right|$), conditions (2.29) imply that eq.(2.25) can be approximated to the zero order in ε by

$$Y = \frac{g}{Q} + o(\varepsilon) . \tag{2.31}$$

This solution describes the modulation of the crystal impedance due to the light intensity pattern *Q*. It completely neglects diffusion effects, and fails to describe TWM between the two writing beams introduced above since the field is in phase with the light distribution. Taking into account the terms of first order in ε we obtain iteratively the first order approximate solution

$$Y = -\frac{Q'}{Q} + \frac{g}{Q} - \left(\frac{g}{Q}\right)^2 \frac{Q'}{Q} + o(\varepsilon^2) . \tag{2.32}$$

This expression has, besides the zero order drift contribution Y_{dr}, the Y_d contribution and a *term that couples drift and diffusion* (proportional to the square of the applied voltage V, see eq.(2.33)). The first and last terms on the RHS describe possible TWM amongst the two beams. The last term describes the enhancement of TWM with increasing external voltage. Eq.(2.32) therefore appears to possess all the ingredients needed for a proper description of a quite general case (within the limitations imposed by the approximations used). In order to give a final form to eq.(2.32), we impose condition (2.18). The approximate expression for *g* we obtain, valid both for solutions eqs.(2.31) and (2.32), is[1)]

$$g = \left[\frac{-V}{lE_{Db}}\right] \frac{1}{\left(1-\dfrac{l_b}{l}\right) + \dfrac{l_b}{l} \dfrac{1}{(1+Q_0)\sqrt{1-m_1^{\ 2}}}} , \tag{2.33}$$

where l_b is approximately the transverse dimension of the region in which Q is sensibly larger than 1. Assuming $V<0$, and $(1+Q_0)\sqrt{1-m_1^2}>1$, eq.(2.33) becomes,

$$g=\left[\frac{-V}{lE_{Db}}\right](1+Q_0)\sqrt{1-m_1^2}=g_{\max}, \qquad \text{for } \frac{l_b}{l}=1, \tag{2.34}$$

and

$$g=\left[\frac{-V}{lE_{Db}}\right]=g_{\min}, \qquad \text{for } l_b=0. \tag{2.35}$$

Eq.(2.33) allows us to obtain the explicit solution from eq.(2.32). Condition (2.29) on Y_{dr} can be uniformly satisfied for all values of l_b by imposing

$$g_{\min} << \frac{1}{\varepsilon}\frac{1-m_1}{\sqrt{1-m_1^2}}. \tag{2.36}$$

For the diffusive regime, in which the constant current J_c is approximately zero ($g\cong 0$) and $|Y_{dr}| << |Y_d|$, conditions (2.29) imply that the lowest order solution in ε is

$$Y=-\frac{Q'}{Q}+o(\varepsilon^2). \tag{2.37}$$

The electric field worked out in ref.[14], valid for $l_b/l=1$, coincides with the expression given in eq.(2.27) supplemented by eq.(2.34). In our approach, this solution is of "intermediate" order in the drift regime, that is the diffusive term Y_d is, under conditions (2.29), of the same order of the first correction, the full expression being given by eq.(2.32) (along with eq.(2.34)). On the other hand, in the purely diffusive regime the two expressions coincide. Furthermore it is easy to show that for $m<<1$ the expression given by the standard approach (see, e.g., Ref.[3], Chap.3) coincides with eq.(2.32) to the first order in $\varepsilon\cong\chi$.

Comparison to Experiment:

In order to test some of the results found in the previous section and to give an example of the possible implementations of the novel approach, we have carried out a set of experiments on a sample of standard

noncentrosymmetric $BaTiO_3$. Primarily, two "innovative" results are tested. The first is the TWM and Bragg diffraction enhancement due to an external bias voltage in the high m configuration. The second is the dependence of the electric field on the (limited) size of the beams described by eqs.(2.32) and (2.33).

To relate the results obtained in the previous section to experiments, we recall that a static field *E* gives rise to a linear modulation of the index of refraction tensor given by (see eq.(2.3))

$$\Delta\left[\frac{1}{n^2}\right]_{ij} = r_{ijk} E_k , \tag{2.38}$$

r_{ijk} being the components of the electro-optic tensor. In our experimental configuration, as described below, eq.(2.38) reduces to the simple form (see, e.g., Ref.[3], Chap. 4)

$$\Delta n \cong -\frac{1}{2} r n^3 E \tag{2.39}$$

where *r* and *n* are the effective electro-optic coefficient and refractive-index, respectively. Besides, we recall that Bragg diffraction efficiency η_i of grating harmonic *i* (*i*=1,2,3...) is given by (see, e.g., Ref.[2])

$$\eta_i \cong \left[\frac{n^2 r k_R}{4\cos(\theta_i)} L E_{(i)}\right]^2 \tag{2.40}$$

where k_R is the wave number of the Bragg reflected light, *L* is the thickness of the crystal in the direction of propagation of the light, $E_{(i)}$ is the space-charge field spatial harmonic component of order *i* and θ_i is its Bragg-matching angle.

TWM coupling with higher harmonics in the index modulation, due to higher harmonics in *E* (*i*>1), is an extremely complicated issue (see, e.g., Ref.[2], Chap.7) and beyond the scope of this Chapter. Here, we analyze only coupling amongst the two writing beams, this being justified both by the fact that in our conditions TWM is generally small and that higher order components are a correction to the first harmonic. In these approximations, we will take the TWM energy coupling constant γ as proportional to the antisymmetric part of the first component $E_{(1)}^{a}$ of *E*, (see Ref.[3], Chap.4)

$$\gamma = \frac{\pi n^3 r}{\lambda \cos(\theta)} \left| E_{(1)}^{a} \right| . \tag{2.41}$$

Results for TWM are given in the form of amplified beam gain ratio

$$\frac{I_2(L)}{I_2(0)} = \frac{1+M}{1+Me^{-\gamma L}} e^{-\alpha' L} \ , \tag{2.42}$$

where $M=I_1(0)/I_2(0)$, α' is the material absorption constant, $I_1(0)$ and $I_2(0)$, respectively, the pump and amplified beam intensities before entering the crystal, and $I_2(L)$ the value of the amplified beam intensity at the exit face.

Experiment:

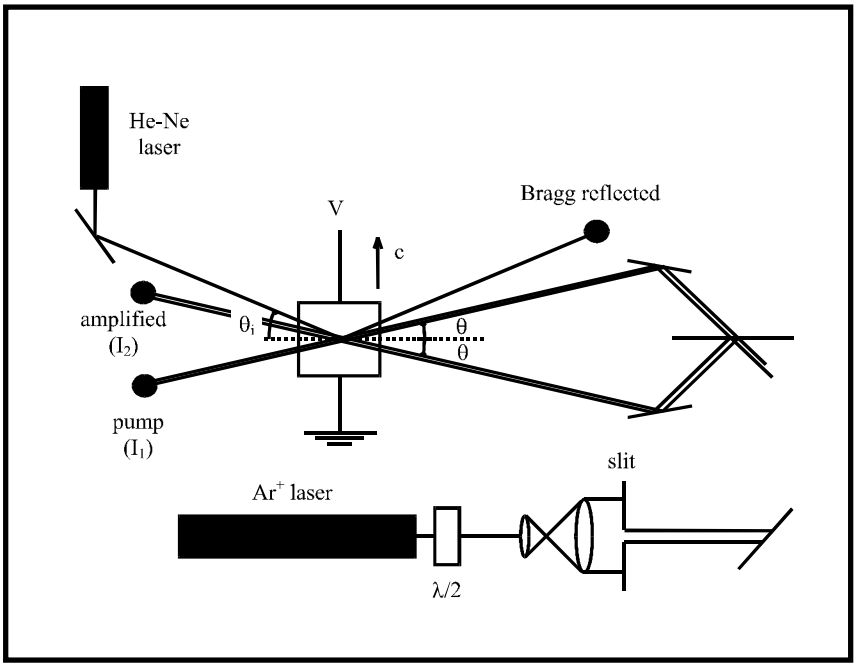

Fig.2.2: Basic experimental arrangement for measuring TWM, Bragg diffraction and TWM beam size dependence.

The setup is based on a typical TWM or two-wave holographic geometry and is schematically illustrated in fig.2.2. A single-mode Argon ion laser emits a λ=515nm vertically polarized beam. A $\lambda/2$ waveplate can be used to rotate the polarization of the beam making it parallel to the plane of the optical table (parallel to the plane of the figure).

The beam is expanded by means of a pair of lenses and an adjustable slit selects the central part of the beam, thus determining its transverse dimension (l_b). A beam-splitter separates this beam into two, generating the two interfering beams (E_1 and E_2), each of which is separately attenuated by a neutral density filter and made to impinge on a $BaTiO_3$ crystal, giving the possibility of controlling the value of m. The $4.8^{(a)}$ x $3.8^{(b)}$ x $4.7^{(c)}$ mm crystal is cut along its principal axes and is oriented so as to have its c-axis parallel to the plane of the page. The geometry is entirely symmetric, that is the two interfering beams give rise to a grating vector K parallel to the c axis. The angle among the two interfering beams outside the crystal is $2\theta_{ext} \cong 7.16°$ (corresponding to $2\theta \cong 2.98°$). The relevant electro-optic coefficients of the sample have the measured values of $r_{33} \cong 110$ pV/m and $r_{13} \cong 12$ pV/m whereas the absorption coefficient has a value of $\alpha \cong 2.9$ cm^{-1} at λ=515nm (single crystal face reflection was taken to be approximately 4%). By means of gold electrodes deposited on the c axis faces of the crystal, an external voltage source supplies the bias voltage V. The beam that experiences gain (E_2), due to the orientation of the crystal, is detected by a silicon photodiode, and the data sampled is transferred to a personal computer. The pump beam (E_1) is monitored via a second detector, and, finally, a (extraordinarily polarized) He-Ne laser beam operating at λ=632.8nm and at approximately 1mW power level, is directed by means of an adjustable steering system on the crystal so as to be Bragg matched with the various harmonics of the grating written by the two interfering beams. Bragg reflection is detected by a third silicon photodiode, and data is again transferred to the personal computer.

TWM Effects in the "holographic regime" (high m, χ<<1)

When attempting to write a hologram inside a PR crystal such as $BaTiO_3$, one is faced with the problem of beam coupling amongst the writing beams. Beam coupling, in basic holography, is an unwanted effect because in thick crystals it can alter considerably the value of the modulation depth m along the direction of propagation of the light and, hence, the overall diffraction efficiency of the volume hologram[20]. One way to limit this effect is to make the scale of variation of the light intensity K small, reducing, thereby, the diffusive out of phase component of the hologram grating and applying and external voltage. Because TWM is maximum approximately when $K \cong k_{Db}$, in a basic holographic setup $K << k_{Db}$ is chosen. Furthermore, in the case of $BaTiO_3$ (where $r_{13} << r_{33}$), one can write the hologram using ordinary polarized beams and read it

using an extraordinary beam. This enables one to limit drastically the effects of TWM, maintaining strong diffraction efficiencies in the read-out phase. If we were now to consider the expression given in eq.(2.27) (as is done for example in ref.[14]), it would seem that an external voltage would enhance diffraction efficiency without modifying TWM coupling. In effect, in this regime, where conditions (2.29) are satisfied, we should adopt eq.(2.32) from which it is apparent that enhancement via external voltage *does* enhance TWM coupling via the term that couples drift and diffusion mechanisms.

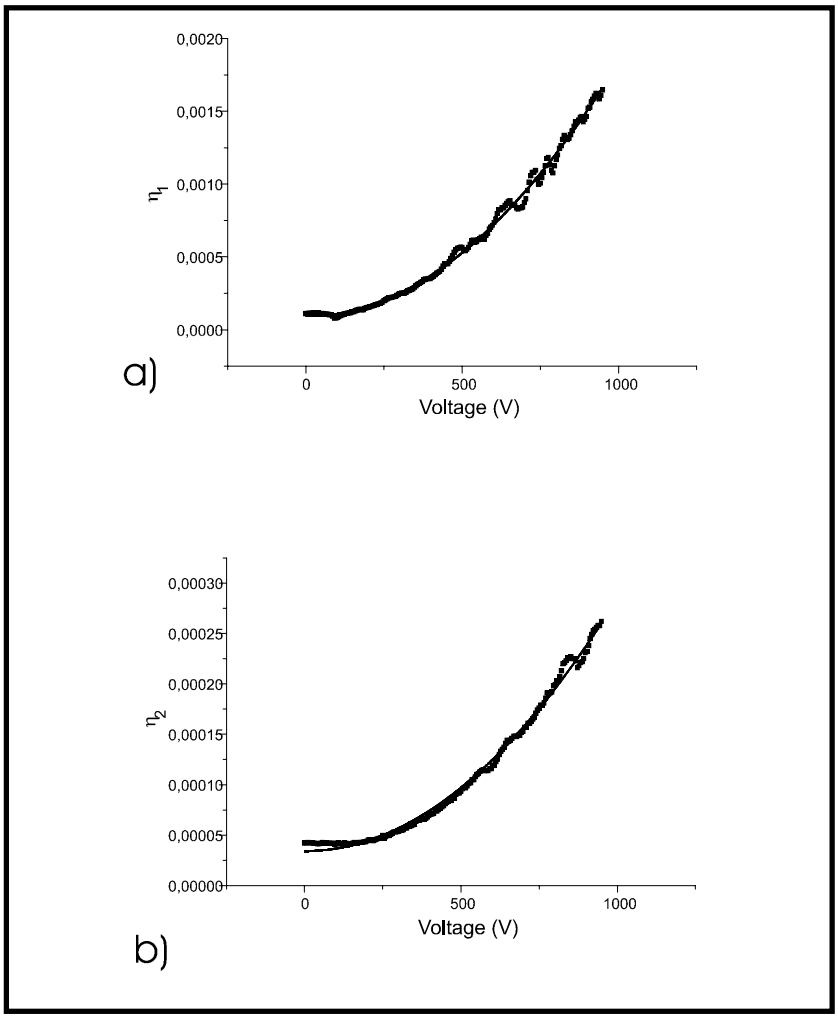

Fig.2.3: a) Values of first harmonic Bragg diffraction efficiency for an expected m_1=0.3 using He-Ne as a function of bias voltage. The fit is obtained taking the first harmonic of eq.(2.32) and using eq.(2.40). b) Measured values of second harmonic Bragg diffraction efficiency. The fit is obtained taking the second harmonic of eq.(2.32).

In figs.2.3a and 2.3b are reported, respectively, the experimental results of first and second harmonic Bragg diffraction enhancement of the He-Ne beam, with $m \cong 0.3$, $\chi \cong 0.1$, $K \cong 1.5 \times 10^6$ m^{-1} and $k_{Db} \cong 1.1 \times 10^7$ m^{-1}, as measured from low m diffusive TWM coupling angular dependence, and, finally, $l_b = l$. To the experimental plots we have superimposed the theoretical fit obtained by taking the first and second harmonics of eq.(2.32) and by using eq.(2.40), neglecting the third term on the RHS of eq.(2.32), of higher order in our approach as regards to Bragg diffraction efficiency (making the dependence of all diffraction orders quadratic in the external applied voltage). In this case, the smallness parameter is $\varepsilon \cong 0.4$. The data is obtained using ordinarily polarized writing beams and an extraordinarily polarized reading beam. As expected, no apparent TWM effects were observed. Curve fits were obtained varying two parameters, m and r_{33}, taking $m \cong 0.27$ and $r_{33} = 80$ pm/V. The value for r_{33} is lower than the value independently measured ($\cong$110 pm/V at 515nm, even though here the wavelength is 633 nm).

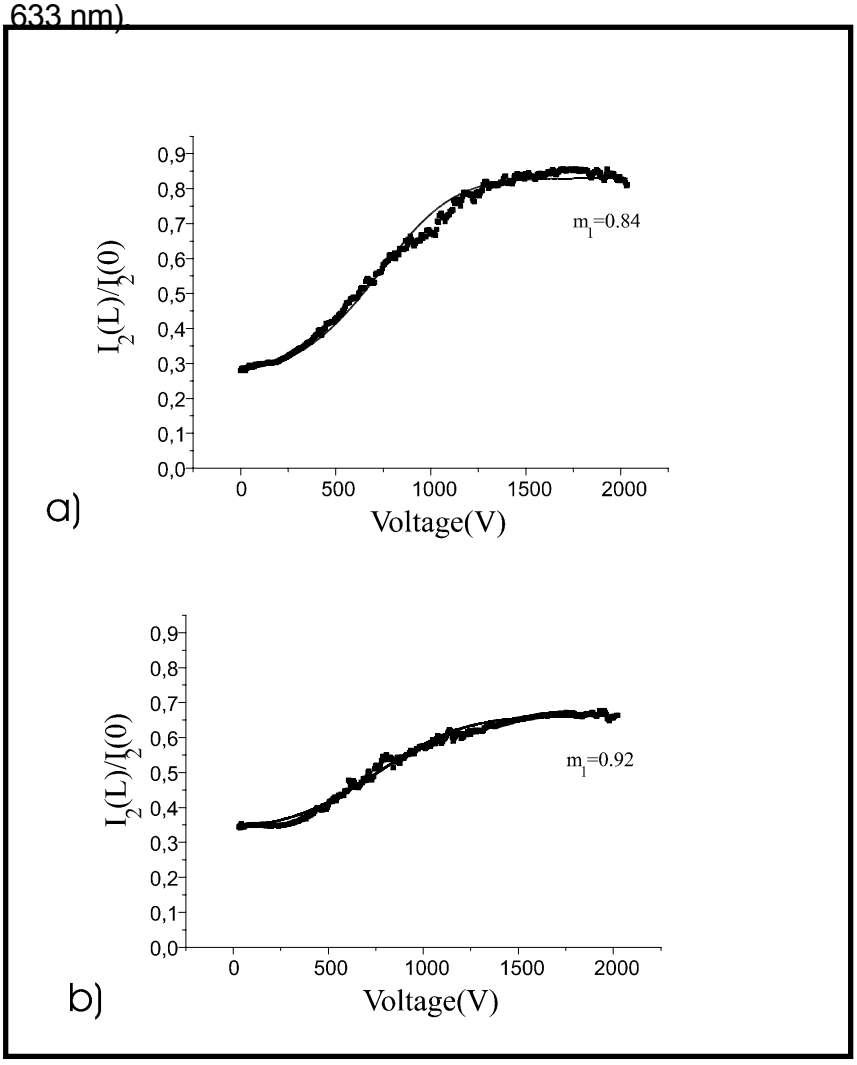

Fig.2.4: a) Measured values of TWM gain ratio of the amplified beam for m_1=0.84. Superimposed is the fitting curve obtained by taking the first harmonic of eq.(2.32) and using eq.(2.41). b) TWM gain ratio for m_1=0.92.

In order to assess the influence of TWM on diffraction efficiency we have performed the same experiment with extraordinary polarized writing beams, again with m≅0.3. Zero voltage first harmonic diffraction was measured obtaining $\eta_1 \cong 0.015$. This indicates a diminished diffraction with respect to the above case when TWM can be neglected ($\eta_1 \cong 0.020$). Expected diffraction in this case (using the expressions given in ref.[14]) is $\eta_1 \cong 0.017$.

In this same condition, but with extraordinary writing beams, TWM coupling is monitored for $m \cong 0.91$ and $m \cong 0.96$ and the results are shown, respectively in figs.2.4a and 2.4b, along with the theoretical fits obtained by taking the first harmonic of eq.(2.32) and using eq.(2.41). Fits were obtained letting the modulation depth m vary. The fitting values for m in the two curves were respectively m≅0.84 and m≅0.92. Apart from this discrepancy, these results cannot be explained (even qualitatively) relying solely on eq.(2.27). The gain ratio value at no applied voltage is determined by the material absorption (constant for both cases) and the zero voltage TWM due to the diffusion-driven space-charge field (relatively strong in $BaTiO_3$), which is dependent on m through eqs.(2.32), (2.41) and (2.42). Qualitatively a higher m corresponds to a higher zero applied voltage TWM gain.

Beam-size Effects.

One of the features of the approach described in the previous section is that it can take into account beams with finite dimension with respect to the crystal. One consequence of beam finiteness is contained in eq.(2.33), where it is apparent that the “effective” field in the illuminated area changes with the dimensions of this area. Intuitively this is quite obvious, in that a change in the size of the illuminated area modifies the overall resistivity of the crystal and therefore the value of the current density, thereby changing the effective field induced by an externally applied voltage. In fig.2.5 are reported the results of TWM coupling enhancement factor

$\sigma = g^2 / \left(V/lE_{Db}\right)^2$ (for $m \cong 0.2$) for various values of I_b/I. On this plot is also superimposed the theoretical fit of eq.(2.32) and eq.(2.33), in the same first harmonic TWM approximation used in the previous paragraph. The "quenching" of the effective field in the illuminated area is qualitatively evident. In order to fit the results we must take $Q_0 \cong 1.7$, although this value must be viewed as an "effective Q_0" since beam fanning effects, primarily responsible for the high value of I_b, generally depend on the size of the illuminated crystal region.

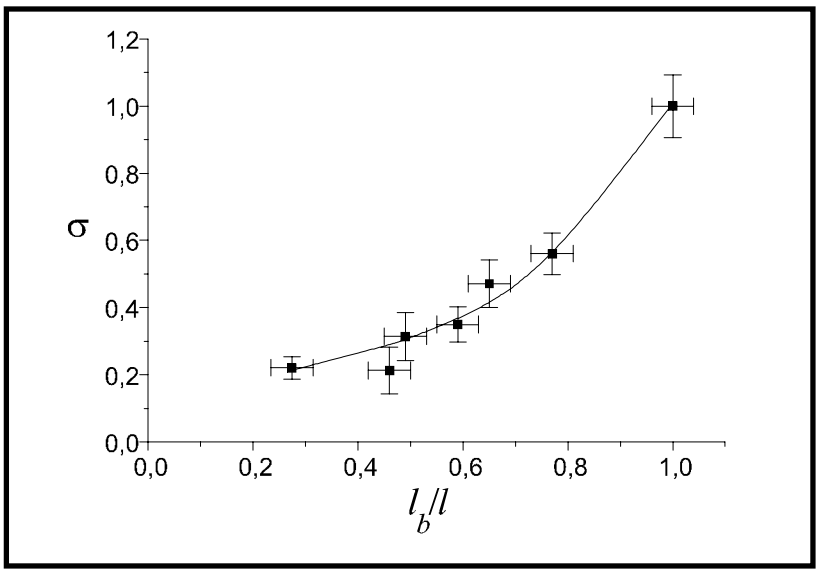

Fig.2.5: Measured values of $\sigma = g^2 / \left(V/lE_{Db}\right)^2$ for various values of I_b/I. The fitting curve is obtained for $m_1 \cong 0.2$ and $Q_0 \cong 1.7$. Higher than first harmonic beam coupling is neglected.

Parabolic Wave-Equation

Optical spatial solitons, in their present understanding, can be described by the so-called parabolic nonlinear dispersive wave-equation for the slowly varying amplitude introduced in Chapter 1. This is also true for photorefractive solitons. Here we discuss briefly the derivation of this equation.

Maxwell's equations in continuos media, in their macroscopic realization, for linear nonmagnetic media, form a linear set of equations that can be solved for single monochromatic components of the electric field $\mathbf{E}(\mathbf{r},t)=\mathbf{E}_\omega(\mathbf{r})e^{i\omega t}$+c.c. (temporal

Fourier terms). The resulting linear scalar differential equation is the so-called *Helmholtz equation*, given by

$$\nabla^2 \mathbf{E}_\omega + k^2 \mathbf{E}_\omega = 0 \tag{2.43}$$

where $k=n\omega/c$, n, the index of refraction, is

$$n(\omega, \mathbf{r}) = \left(\frac{\varepsilon(\omega, \mathbf{r})}{\varepsilon_0} \right)^{1/2}, \tag{2.44}$$

and ε_0 is the vacuum dielectric constant and ε is the medium's dielectric constant defined in the linear approximation

$$\mathbf{P}_\omega = (\varepsilon - \varepsilon_0)\mathbf{E}_\omega \tag{2.45}$$

and **P** is the induced linear polarization. Eq.2.43 is furthermore valid when n does not vary appreciably on the scale of the field wavelength $\lambda=2\pi c/\omega$.
Assuming that the index of refraction can be written in the form $n(\mathbf{r},\omega)=n_1(\omega)+\delta n(\mathbf{r},\omega)$ with $n_1(\omega)>>\delta n(\mathbf{r},\omega)$ and that the monochromatic component of the electric field, written in the form $\mathbf{E}_\omega(\mathbf{r})= \mathbf{A}_\omega(\mathbf{r}_\perp,z)e^{-ik(\omega)z}$ where $k(\omega)=n_1\omega/c$, has an envelope $\mathbf{A}_\omega$ that varies on a scale much larger that 1/k (slowly varying envelope), the Helmholtz equation takes on a simpler differential form, known as the *parabolic wave equation*, given by

$$\left[\frac{\partial}{\partial z} + \frac{i}{2k} \nabla_\perp^2 \right] \mathbf{A}_\omega = -\frac{ik}{n_1} \Delta n \mathbf{A}_\omega \tag{2.46}$$

where z is the *propagation variable*, and the second term on the LHS represents *diffraction*.
The parabolic wave equation in itself is *neither* linear *nor* nonlinear. All depends on the expression of Δn. If Δn is a given function *independent* of the optical field **A**, like for example in the case of a fabricated waveguide, propagation described by eq.(2.46) is linear. If, on the other hand, Δn is a function of **A**, eq.(2.46) describes nonlinear propagation.
Phenomena encountered in this treatise are described by eq.(2.46) where the optical field induces, through $I=|\mathbf{A}|^2$, an internal electric field E through eqs.(2.4-2.8) discussed in the previous section. This field modulates the crystal index of refraction through the electro-optic effect (eqs.(2.1-2.3)) leading to a $\Delta n=\Delta n(I)$, and in particular to *photorefractive nonlinear propagation*.

REFERENCES:

[1] E.DelRe, A.Ciattoni, B.Crosignani, and M.Tamburrini, J.Opt.Soc.Am.B 15, 1469 (1998).

[2] *The Physics and Applications of Photorefractive Materials*, L.Solymar, D.Webb, and A..Grunnet-Jepsen (Claredon Press, Oxford 1996)

[3] *Introduction to photorefractive nonlinear optics*, P.Yeh (Wiley, New York 1993)

[4] B.Crosignani, P.Di Porto, M.Segev, G.Salamo, and A.Yariv, La Rivista del Nuovo Cimento **21**-6 (1998)

[5] N.Kukhtarev, Sov.Tech.Phys.Lett. 2, 438 (1976)

[6] M.Segev, G.Valley, B.Crosignani, P.DiPorto, and A.Yariv, Phys.Rev.Lett. 73, 3211 (1994)

[7] M.Saffman, A.Zozulya, Opt.Lett. 23, 1579 (1998)

[8] More complicated models can be found in ref.2.

[9] *Optical Waves in Crystals*, A.Yariv and P.Yeh (Wiley, New York 1984)

[10] V.Vinetskii, N.Kukhtarev, V.Marhov, S.Odulov, and M.Soskin, Bull.Acad.Sci.USSR, Phys.Ser. 41, 135 (1977)

[11] See, for example, *Photorefractive Materials and Their Applications I*, Eds.P.Gunter amd J.Huignard (Springer, Berlin 1988)

[12] *Photorefractive Materials and Their Applications II*, Eds.P.Gunter amd J.Huignard (Springer, Berlin 1989)

[13] L.B.Au and L.Solymar, *Opt.Lett.* **13**, 660 (1988).

[14] M.G.Moharam, T.K.Gaylord, R.Magnusson, and L.Young, *J.Appl.Phys.* **50**, 5642 (1979)

[15] N.V.Kukhtarev, P.Buchhave, and S.F.Lyuksyutov, *Phys.Rev.A* **55**, 3133 (1997).

[16] Y.H.Lee and R.W.Hellwarth, *J.Appl.Phys.* **71**, 916 (1992).

[17] A.Bledowski, J.Otten, and K.H.Ringhofer, *Opt.Lett.* **16**, 672 (1991)

[18] F.Vachss and L.Hesselink, *J.Opt.Soc.Am.A* **5**, 690 (1988).

[19] Conditions (2.29) express in a compact form the limitations imposed by our resolving scheme. The first is quite restrictive. Apart from the possibility of relaxing it, at the cost of greater algebraic complexity, it has the advantage of being valid for all values of $0<m_1<1$. The condition on the drift field is related to the so-called saturation field and is easily verified in most doped crystals for standard applied voltages.

[20] J.H.Hong and R.Saxena, *Opt.Lett.* **16**, 180 (1991).

Chapter

3

Photorefractive Spatial Screening Solitons

Introduction

In this Chapter a brief description of the theoretical and experimental studies that have led to the discovery of spatial solitons in photorefractive crystals is undertaken, starting from the initial theoretical predictions of non-stationary self-trapped spatial pulses, known as "quasi-steady-state" solitons, to more startling effects observed in *stationary* screening solitons, such as incoherent solitons, and soliton spiralling. The main emphasis is, however, reserved to "standard" screening solitons, that have played the main role in the "minirevolution" in nonlinear science tied to photorefractive spatial nonlinear effects. For these, the presently accepted theoretical description, based on a nonperturbative approach to the band-transport model introduced in the previous Chapter, is summarized, for the 1+1D case. In the 2+1D configuration, the existence of circular symmetric screening solitons, an issue still subject to intense debate, is addressed. Finally, a first realization of an optical screening soliton directional coupler accomplished by Lan, DelRe, Chen, Shih, and Segev in 1998[1)], is described.

"Minirevolution"

We have mentioned that spatial photorefractive solitons have brought about a relevant change in nonlinear optics, and in general, in soliton science. Why? There are two main reasons. The first is connected to the optical intensities needed to obtain self-trapping. Before the discovery of spatial solitons in photorefractives, in near-resonant vapors, and in χ^2 materials, the only known nonlinearity supporting spatial particles was the optical Kerr effect. The intensities needed to obtain such solitons are typically higher than 1MW/cm^2. Such high power beams make spatial soliton investigation difficult and hardly amenable to applications. In photorefractives, on the other hand, intensity plays a *marginal role*, determining the overall duration of the transient dynamics of the observed phenomena. **Photorefractive solitons can be observed with intensities of a few μW** (corresponding to a few tens of mW input laser power in a typical setup). The second reason

is that photorefraction offers many diverse nonlinear mechanisms, and thus allows the observation of different and unexpected (possibly useful) phenomena. A main example is the observation of two-dimensional spatial self-trapping[2], not observable with Kerr-like nonlinearities (where higher dimensional confinement leads to catastrophic self-focusing).

Quasi-Steady-State Spatial Solitons

In 1992 Segev, Crosignani, Yariv, and Fischer[3] predicted that a continuum of spatial components of a spatially confined optical beam could gives rise to nondiffracting propagation in a photorefractive (noncentrosymmetric) crystal. The basic diffraction compensating process was based on a continuum of two-wave-coupling processes, similar to those described in Chapter 2. Limiting their analysis to the 1+1D case, they theorised that the mutual phase modulation of the single wave-couples could give rise to an effective guiding index of refraction modulation in presence of an externally applied electric field. The applied field makes the in-phase components of the generated gratings predominant as long as it is much greater than the expected diffusion field, responsible for two-wave-mixing and asymmetric beam breakup and fanning (see, for example, eq.2.17). The main predicted characteristics of these new soliton-like particles was that they are independent of beam peak intensity I_0, as long as dark irradiance could be neglected ($I_0 >> I_b$).

In 1993 experimenters[4] observed spatial self-trapping, in 1+1D, in a sample of biased SBN. They indeed observed intensity independent trapping, but *only for a limited temporal window*. For their particular configuration, solitons could be observed after approximately 20 ms, but after a "steady-state" of another 20 ms, the trapping would *disappear*, leading to standard diffracting propagation and fanning. Soliton decay was attributed to the insurgence of diffusion-driven fanning and to space-charge screening of the externally applied field. Thus, these solitons were termed "quasi-steady-state" solitons, and have been known as such ever since. They represent the first observation of a photorefractive optical spatial soliton.

Spatial Screening Solitons

In 1994 Segev, Valley, Crosignani, Di Porto, and Yariv[5] theoretically predicted the possibility of obtaining stable,

steady-state, photorefractive solitons induced by the optically modulated screening of an externally applied field. They discovered what is now known as the *screening soliton*, also referred to generically as "photorefractive" soliton. They were able to address the minimal photorefractive model with a nonperturbative approach that in the one-dimensional case predicts all the basic characteristics of screening solitons, thereafter observed in different materials, by different groups, and in many different configurations. The fundamental idea, to move from a *perturbative* approach based on the basic assumptions made in the so-called linearized formulation, discussed in the previous Chapter, to a *nonperturbative* (albeit approximate) approach, is to some extent the main theoretical achievement in photorefractive theory of this decade. Needless to say, a formulation based on a small modulation assumption could by no means hope to predict and describe the highly nonperturbative, highly modulated, configuration of a strongly confined and diffracting optical beam embedded in a weaker background illumination. In fact this is a typical example of what can be referred to as "new objects" induced by nonlinearity: screening solitons *could not exist* in terms of the basic concepts considered *fundamental* in the linearized approach based on small optical modulation.

The essential physical idea behind screening solitons can be summarized as follows: consider a photorefractive crystal cut along its principal axes and oriented so as to have its ferroelectric (for a noncentrosymmetric sample) c axis parallel to a given axis, say the x axis. Imagine launching a highly diffracting "slab of light" into the sample in an orthogonal direction, say z (propagation axis). The "slab" is a coherent monochromatic x-polarized beam that is strongly localized in the x direction, whereas it has no modulation in the remaining orthogonal y direction, and is focused onto the input face of the sample. As it propagates in the z direction, it diffracts according to standard linear propagation. Photorefraction leads simply to a slow (and sometimes very weak) beam fanning due to diffusion scattering. Furthermore, the sample is illuminated uniformly with a second, copropagating field polarized along the y axis. If a constant external field is applied to the sample in the x direction, the optically induced charges will drift in the field. The inhomogeneous illumination leads to an electron buildup in the immediate vicinity of the confined beam, on the positive electrode side. This local charge separation, whose origin can be intuitively visualized as deriving from a different electric conductance, higher in the more illuminated region, lower in the uniformly illuminated background region, leads to an effective *screening* of the

applied field. The electric field is lower in the illuminated region. If the particular crystal symmetry allows for a *negative* electro-optic response to a positive electric field ($r_{eff}>0$ in eq.2.3), the index of refraction will *drop* in the less illuminated regions more than in the illuminated ones. This index modulation is thus a "guiding" index structure that can lead to diffraction compensation. When the optically induced "lensing" is such as to exactly compensate diffraction, the beam will be guided in this self-induced wave-guide and lead to a spatial soliton particle. The background beam does not actually participate in the effect, it simply regulates the amount of screening obtained (by fixing the overall crystal conductivity). It is hardly affected by the insurgence of the soliton beam, since it is polarized along the y axis, and suffers generally negligible electro-optic modulation for an x directed electric field ($r_{xy}<<r_{xx}$).

The basic model was described in Chapter 2 and is essentially contained in eqs.(2.4)-(2.8). To this we need to add the nonlinear paraxial propagation equation 2.46 and the material response (eq.2.3). In this case, the optical intensity I is $I=|A|^2$, where A is the slowly varying amplitude of the propagating optical field. We limit the description to the 1+1D case (spatial transverse coordinate x), and steady-state conditions. Furthermore, we treat the scalar problem (corresponding to the typical experimental configuration), although "vector" screening solitons have been predicted[6]. The scalar configuration means that entering the crystal with a highly confined optical beam polarized in a particular plane, the polarization does not *evolve*. A necessary condition for this to happen in noncentrosymmetric crystals with strong birefringence, is to propagate along a principal axis of the crystal and with a polarization along another (orthogonal, of course) principal axis. This is, however, not a sufficient condition. In many ferroelectric (electro-optic) crystals the application of an external field drastically modifies the orientation of the principal axes (such as ADP). The peculiar symmetry of SBN (and $BaTiO_3$ for that matter) does not suffer from this effect, and the application of an electric field parallel to the optical axis (ferroelectric axis) does not change the orientation of the index ellipsoid. Thus, for an extraordinary confined beam (polarization along x axis), for an applied electric field along the x direction, and for a zero-cut sample of SBN-type ferroelectric with optical axis along the x axis (propagation is along the z axis), the linear electro-optic response is a scalar given by

$$\Delta n = \frac{1}{2} n^3 r_{eff} E \tag{3.1}$$

where the product of r_{eff} and E is taken to be negative (in the above expression, note the change of sign with respect to the convention adopted in eq.2.3), and r_{eff} is the effective electro-optic coefficient relative to the particular experimental configuration (typically $r_{eff}=r_{33}$). The actual sign of the index modulation (as described in Chapter 2) depends on the sign of r_{eff} and the orientation of the applied electric field with respect to the c axis. We assume that the end product is described by a *negative* index modulation to a *positive* field, as this is the case that supports photorefractive **bright** screening solitons (self-focusing case). Another class of soliton particles can be obtained with a positive modulation known as photorefractive **dark** screening solitons, but these will be mentioned briefly further on, and are not investigated in this treatise.

As mentioned, the model equations, when solved, must be corroborated by appropriate boundary conditions. In the case of screening solitons, we apply an external voltage V to the sample, and the electric field must satisfy the relation

$$V = -\int_{-l/2}^{l/2} dx E \tag{3.2}$$

where *l* is the length of the sample in the x direction (see eq.2.18).

Spatial solitons are localized non-evolving spatial profiles of the optical field. Therefore we look (self-consistently) for solutions of the form

$$A(x,z) = u(x) e^{i\Gamma z} (I_d + I_b)^{1/2} \tag{3.3}$$

where Γ is generally referred to as the propagation constant and I_b is the "artificial" background conductivity induced by the uniform background illumination. Typically, the dark conductivity can be neglected and $I_d \cong I_b$. We limit our analysis to real u(x). Since we will need to implement nonperturbative approximations to the basic band-transport model, we introduce dimensionless variables with the substitutions

$$\overline{N} = \frac{N}{N_d},\ \overline{E} = \frac{|E|}{V/l},\ \overline{N}_d^+ = \frac{N_d^+}{N_d},\ r = \frac{N_d}{N_a},$$
$$\overline{J} = \frac{|J|}{q\mu N_d V/l},\ \xi = \frac{x}{d} \qquad (3.4)$$

where d is the characteristic nonlinear length-scale defined by

$$d = \frac{l}{(-2kb)^{1/2}}, \qquad (3.5)$$

where k is the optical wavevector, $k=2\pi n/\lambda$, and

$$b = \frac{k}{n}\frac{n^3 r_{eff} V/l}{2}. \qquad (3.6)$$

The dimensionless equations are

$$N - a(1+|u|^2)\frac{(1-N_d^+)}{N_d^+} = 0,$$
$$J = NE + \varepsilon_2 N' = \text{const},$$
$$N_d^+ - 1/r - N - \varepsilon_1 E' = 0, \qquad (3.7)$$
$$l/d + \int_{-l/2d}^{l/2d} d\xi E = 0,$$
$$u'' = -\left[\frac{\Gamma}{b} + E\right]u,$$

where the prime stands for the derivative with respect to the variable ξ, and the dashed symbols have been simplified (suppressing the dash),

$$a = \frac{s(I_d + I_b)}{\gamma N_d},$$
$$\varepsilon_1 = \frac{V\varepsilon}{lqdN_d}, \qquad (3.8)$$
$$\varepsilon_2 = \frac{k_b T l}{qdV}.$$

For typical experimental configurations, $d\approx 1\mu m$, and ε_1, $\varepsilon_2 << 1$, whereas $r >> 1$. Taking the third equation of (3.7), neglecting

N and $\varepsilon_1 E'$ with respect to N_d^+ and 1/r, we obtain $N_d^+ \cong 1/r$. Substituting this expression into the first equation and remembering that r>>1, we get $N \cong -ar(1+u^2)$. Using this expression in the second equation, neglecting the $\varepsilon_2 N'$ term, we finally get

$$E = \frac{-\eta}{1+u^2}, \tag{3.9}$$

where η is determined by the boundary condition contained in the fourth equation of (3.7). It turns out that for bright solitons, in most configurations, $\eta \cong 1$.

Equation (3.9), through the electro-optic effect (see eq.(3.1)) gives a guiding saturated index pattern of the type $\Delta n \propto 1/(1+I/I_b)$. The most important characteristic of this nonlinearity lies in the fact that it is **local**. The problem itself is highly nonlocal, but the approximations, when they are valid, give us this very elegant end result.

It is worthwhile to translate the approximations that lead to the local screening nonlinearity in terms of the scales introduced in Chapter 2. From eqs.(2.13-2.15) we have that $\varepsilon_1 = \Lambda_{Db}(V/l)/(\alpha E_{Db})$ and $\varepsilon_2 = \Lambda_{Db} E_{Db}/(dV/l)$. $\varepsilon_1 << 1$ is generally validated by the fact that in most crystals $\alpha >> 1$. $\varepsilon_2 << 1$ implies that $\Lambda_{Db} << d$ and/or $E_{Db} << V/l$. Typically $\Lambda_{Db} \cong d$, thus the nonlocal system becomes local when the applied field is much larger than the maximum attainable diffusion field.

The nonlinear propagation equation (last equation of (3.7)) can be integrated through quadrature, and imposing the boundary conditions for *bright* solitons, $u_\infty = u'(\infty) = u''(\infty) = 0$, $u'(0) = 0$, and $u''(0)/u_0 < 0$, where $u(0) = u_0$, leads to the final nonlinear equation

$$\frac{d^2 u(\xi)}{d\xi^2} = -\left(\delta - \frac{1}{1+u(\xi)^2}\right) u(\xi), \tag{3.10}$$

where

$$\delta \equiv \frac{\Gamma}{b} = \frac{\ln\left[u_0^2 + 1\right]}{u_0^2}. \tag{3.11}$$

The quantity u_0^2 is referred to as the *intensity ratio* of the soliton, and represents the ratio of the soliton peak intensity and the background illumination.

Equation (3.10) is **nonintegrable**. Although it describes soliton particles, *it does not have explicit localised analytical solutions*. The fact that a saturable nonlinearity does not support "analytical" solitons is a well known circumstance, yet the question arises as to what these solitons look like, and for which physical parameter values they exist. Given an intensity ratio u_0^2, one can *numerically* solve the equation, and the resulting beam shapes are very similar to a Gaussian (but they are *not Gaussian*)[7]. Regarding the issue as to what are the parameters that lead to soliton formation, one can numerically construct what is known as the "soliton existence curve": for each value of intensity ratio u_0^2, the numerical solution has a well defined value of normalized soliton intensity full-width-half-maximum (FWHM) $\Delta\xi$. Thus, joining such existence points in the (u_0, $\Delta\xi$) phase space, one obtains the desired curve. For a given input beam width $\Delta\xi$, there is a given voltage V at which, for a given intensity ratio, self-trapping is predicted.

A very close approximation to a 1+1D screening soliton was first observed by Iturbe-Castillo et al. in 1994[8]. Subsequent studies have shown that the existence curve actually exists and qualitatively follows closely the predicted curve[9]. To date an immense amount of theoretical and experimental work has been carried on these "fully-understood" particles: from soliton-soliton interactions, to passive waveguiding.

In 1995 Shih et al. opened up an entirely *new* issue[2]: they launched a highly confined TEMoo laser beam directly in a sample of SBN in a configuration wholly similar to that allowing the observation of screening solitons, except for the *two-transverse dimension confinement*. To their "surprise", they observed *circular symmetric spatial steady-state solitons*. They had discovered 2+1D screening solitons. Higher dimensional solitons are a rarity in soliton science, as mentioned above. They represent an important and interesting physical phenomena, and are a major step towards the applicative development of soliton based optical bulk circuitry.

It does not take much physical insight to imagine that a highly anisotropic nonlinear interaction, such as that involved in 2+1D trapping, could hardly give rise to circular-symmetric self-trapping. Two main anisotropies are present: the tensorial nature of the electro-optic response (see e.q.2.3) and the fact that the external field is applied only along the x axis (whereas trapping occurs in both the x and y direction). To attempt to solve the full 3D nonlinear propagation

equations introduced in Chapter 2, is of course a formidable task, and only recently, in 1997, Crosignani et al.[10] have attempted an approximated analytical-numerical approach, although they did *not* reach a general conclusive result. Zozulya, Anderson, Mamaev and Saffmann have *repeatedly* reported that they could not numerically reproduce circular-symmetric solitons in the conditions in which they were actually observed[11]. Experimental evidence supporting the existence of circular-symmetric screening solitons has been recently reported by Del Re et al.[12] in a different screening-type nonlinearity, which will be amply discussed in Chapter 6. Some experiments, however, unveil a different story. Shih et al. in $KNbO_3$[13] and DelRe et al. in $BaTiO_3$[14] reported that these crystal support 1+1D screening solitons, but *do not allow circular symmetric spatial trapping*. They observed beam aspect ratio evolution, somewhat as predicted by numerics. The two situations, SBN, and $BaTiO_3$, for example, are in all identical regarding the general approach to spatial screening dynamics. A recent article on this matter by Zozulya et al. in 1998[15] is explicitly entitled *Circular Solitons Do Not Exist in Photorefractive Materials*. What is going on? What is wrong with the numerics, what is wrong with experiments?

In a recent paper by Gatz and Herrmann in 1998 [16] , the full 3D propagation problem was tackled and numerically the propagation solutions were found. When the nonlocal processes at work in photorefraction (diffusion) had a negligible effect, indeed non circular-symmetric trapping should be observed, in agreement with Zozulya et al.. *However*, when these effects *were* included, they "quenched" the deformations and effectively allowed a quasi-soliton circular-symmetric propagation. The work by Zozulya et al. *neglects* these nonlocal terms (essentially connected to charge diffusion and displacement). What remains to be seen is whether experiments agree with this new model: that is, whether in $BaTiO_3$ and $KNbO_3$ the nonlocal terms can be neglected, whereas in SBN and KLTN they cannot. If this is indeed the case, the "mystery" is altogether solved. The screening mechanism, in itself based on a local nonlinear interaction, does *not* support 2+1D circular symmetric solitons. These exist when diffusion, coupled to screening processes, "quenches" the inherent anisotropy of the system ("Nonlocal Screening Solitons"). Nonlocality seems "triggered" by the increased dimensionality of the process, whereas it does not play a crucial role in the 1+1D configuration.

Related Phenomena

Some photorefractive crystals manifest what is called the photovoltaic effect. Free electrons photoexcited from donor sites to conduction have an initial kinetic energy prevalently in a particular direction with respect to the crystal axes. This is, for example, the case of $LiNbO_3$, where photoexcited holes give rise to a net current, called the *photovoltaic current*, along the c axis of the crystal. This effect, coupled to "normal" photorefraction, can support dark screening solitons[17], where the external field is substituted by the equivalent effective photovoltaic field, and the interaction is equivalent to a saturated defocusing nonlinearity supporting nondiffracting propagation of a confined non-illuminated region in an otherwise uniform plane wave.

Screening solitons suffer one main disadvantage in possible applications to optical communications: they are slow. Typical experimental configurations necessitate of at least a few seconds to obtain a given steady-state soliton, although actual times differ greatly as a function of temperature, crystal sample, and intensity ratio. The observation of screening solitons in semiconductors has opened up a possible avenue to speeding up these response times, given the higher charge mobilities in these crystals. Chauvet et al. observed in 1996 1+1D spatial screening solitons in a bulk sample of InP doped with Fe[18]. Later on, the same group obtained successfully 2+1D self-trapping in GaAs[19]. A different approach was undertaken by Kos, Salamo, and Segev in 1998[20] : they observed the formation of self-trapped particles in under 90ns with the use of high intensity picosecond pulses. In this case speed is realized at the direct expense of local optical intensity.

Recent experiments with screening solitons show how this nonlinearity can be of central importance in the study of more exotic and hereto unobserved physical nonlinear phenomena. In this respect, one of the most interesting behaviors of soliton particles is their interaction. Screening solitons have been made to interact in their 2+1D realizations, and 3D *soliton spiraling* has been actually observed[21]. A second, fundamental, discovery is the observation of incoherent self-trapping. Can a spatially and temporally incoherent wave form a soliton, a coherent entity by definition? It can. Incoherent solitons have been observed by Mitchell and Segev, and are still subject to intense investigation, especially from the theoretical point of view[22].

A Soliton-Based Directional Coupler

Photorefraction is a wavelength dependent process since donor impurities are photoactive only for beams of wavelength λ such as to allows a direct donor ionization ($\hbar\omega=hc/\lambda>E_D$, the donor gap energy). Therefore, if a soliton is formed at a photoactive wavelength λ_s, another beam a longer wavelength λ_g will propagate in the crystal in a wholly linear manner. It will, in particular, "feel" the index pattern supporting the soliton. Since this pattern is essentially a waveguide (if the induced nonlinearity supporting the soliton is approximately local), this nonactive beam will be *linearly guided by the soliton beam*.

To close this Chapter on screening photorefractive solitons, we mention the first complex realization of a basic component in a bulk crystal using such soliton induced waveguides: a tunable directional coupler, accomplished in an experimental trial by Lan, DelRe, Chen, Shih, and Segev in 1998[1)] .

Loosely defined, as discussed in previous sections, optical spatial solitons are narrow beams that propagate without diffraction even when they are focused down to small spots.[23)] Intuitively, a spatial soliton forms when the intensity of a beam modifies the refractive index (via an optical nonlinearity) in such a way that a waveguide is created, and the beam becomes a guided mode of that waveguide and thus self-traps.[24)] These soliton-induced waveguides can be used to guide other "probe" beams. Typically, a probe beam is much weaker than the soliton that has induced the waveguide, and the soliton controls the probe beam.[25)] Such soliton-induced waveguides are much more flexible as compared to fabricated waveguides: one can change all the waveguide properties by changing the soliton. This kind of reconfigurable waveguides can be used in many applications in beam control and optical steering systems.[26)]

Among the various types of spatial solitons that have been found thus far, photorefractive solitons appear to be rather unique, at least as far as far as soliton-induced waveguiding in concerned.[27,28)] First, photorefractive solitons form at μWatt and lower optical power levels. Second, as mentioned, the photorefractive effects are wavelength-sensitive, which means that a soliton formed by a low power beam can guide an intense beam of a less photosensitive (typically longer) wavelength. Another advantage is that photorefractive solitons are stable in both (1+1) D and (2+1) D, which enables

3D waveguiding structures, e.g., optical “fibers” induced in the volume of a bulk medium. Finally, photorefractive solitons are “fixable”, that is, it is possible to impress the waveguide structure into the crystalline lattice so that it remains permanently,[29] yet it is always possible to erase and over-write this “impression” by electrically re-poling the crystal or by bringing its temperature near a crystalline phase transition.

One important application of waveguides / integrated optics / optical fiber networks is directional couplers. A directional coupler typically consists of two waveguides at close proximity, which couple to one another by evanescent fields. In principle, in a directional coupler consisting of two completely identical waveguides, as much as 100% of the energy can transfer from one waveguide to the other after a given propagation distance. This section is dedicated to the description of the experimental demonstration of a directional coupler utilizing two photorefractive soliton-induced waveguides. Two identical parallel solitons are used to form a coupler and the mutual coupling as a function of the separation between the solitons is studied.

In light of the benefits of utilizing solitons in directional coupling applications, one needs to keep in mind that actually realizing such a “device” poses one basic challenge: When two solitons propagate at a close proximity, they interact, that is, they may attract, repel or transfer energy to one another, depending on their relative phase.[23] The propagation direction of the solitons is directly affected by the interaction, and the solitons bend their trajectories. Thus, propagating two mutually-coherent parallel solitons at close proximity is inherently impossible. However, the phase-sensitive interaction between solitons can be reduced considerably if the solitons are mutually-incoherent. This means that, while each soliton is a coherent entity in itself, the relative phase between the solitons varies much faster than the response time of the nonlinear medium.[30] The “force” between two such mutually-incoherent solitons is considerably weaker than the coherent force between the same solitons separated by the same distance. In this way, almost-parallel mutually-incoherent solitons are launched at the closest proximity possible that still permits parallelism.

However, it is obvious that the wave functions of the solitons have very little overlap. Therefore, if we use the parallel soliton-induced waveguides to guide probe beams of the same wavelength as that of the solitons that have formed the waveguides, the directional coupling is weak. This means that full energy transfer from one waveguide to another will take a

large distance, at which the soliton-like state will actually have evolved. To get higher coupling efficiency, we have to use longer wavelengths, for which, the confinement of the (lowest) guided modes is relatively low, so that the overlap integral of these modes is much higher, and results in efficient directional coupling. In the experiment, the wavelength of the probe beam is roughly twice the wavelength of the solitons.

An SBN:75 crystal is used. The optical beams propagate a distance of 4.5mm along a crystalline ***a***-axis, and the external voltage is applied along the ***c***-axis. Thus we employ the r_{33}=330pm/V (λ= 488nm) electro-optical coefficient. Two ***e***-polarized 488-nm laser beams generate two (1+1)-D solitons, by using cylindrical lenses, and a broad ***o***-polarized beam acts as the background illumination. A Ti:Sapphire laser is used to generate a 980-nm probe beam to test the coupling between the two waveguides. The probe beam is also extraordinarily polarized so as to allow the use of the large r_{33} coefficient.

Initially, a single soliton is generated and used to test the guidance of the induced waveguide. The beam is focused (with a cylindrical lens) to a FWHM of 13μm along ***c***-axis while it is kept uniform along ***a***-axis at the input surface of the crystal. After 4.5mm propagation, it diffracts to 34μm at the output surface. The soliton forms when a voltage of 800V is applied and attains the same FWHM as at the input. Then a 24μm FWHM probe beam is launched into the induced waveguide. A wider input beam is used because for the same waveguide, the confinement of the lowest guided mode for the longer wavelength of the probe is weaker. When the voltage is on, the probe beam is guided well.

The directional coupler is generated by launching another identical soliton alongside the first one. As discussed above, this soliton is made incoherent with the first soliton so that the interaction between them is so weak that the trajectories are almost fully parallel. The peak-to-peak separation between the two solitons is 30μm. Since the intensities and the widths of the two beams are identical, both solitons form when we apply a voltage of 800V, as shown in Fig.3.1a.

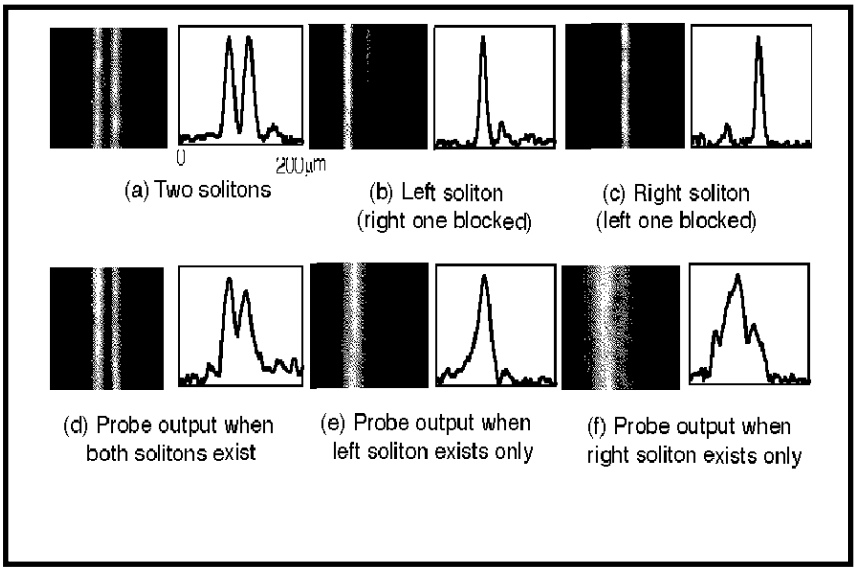

Fig.3.1: Coupling (see text).

Then a probe beam is launched into the first soliton only and the beam output is monitored. It was found that a large portion of the energy coupled from the original waveguide into the other one. The coupling efficiency (the fraction of transferred energy via directional coupling) is about 45%. To show further evidence of this directional coupling, the second soliton is blocked and the output probe beam is again monitored immediately after, before the crystal can respond. As shown in Fig.3.1b, it is found that there is only very little energy from the left soliton coupled into the other soliton via incoherent soliton interaction. When only the first soliton is present (when we wait a time longer than the response time of the crystal, so that the waveguide induced by the second soliton has vanished), and a probe beam is launched into the first soliton, the probe is guided well by the single waveguide (Fig.3.1c). For comparison (Fig.3.1d), the first soliton is blocked and the probe beam is launched into where it had been: when the second soliton is "on", the probe beam is not guided (it diffracts, Fig.3.1e), because the waveguide that had supported it has vanished, but part of the energy is trapped by the waveguide induced by the adjacent right soliton. All of these results show that the co-existence of two solitons works as a directional coupler, and the probe beam is coupled from one soliton-induced waveguide into the other.

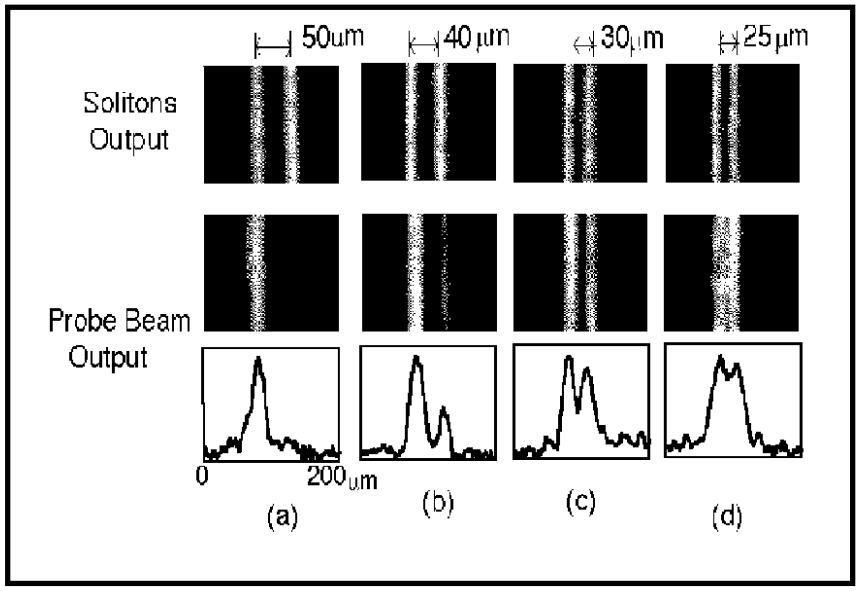

Fig.3.2: Directional Coupling (see text).

In order to study the relationship between the directional coupling and the separation between the solitons, the position of the second soliton was varied and the coupling as a function of soliton separation was monitored (Fig.3.2). When the two solitons are 50μm apart, no coupling is observed (Fig.3.2a). When the separation is 40μm, roughly 20% of the probe beam is coupled from the first waveguide into the second one (Fig.3.2b). When the separation is 30μm, the coupling increases to 45% (Fig.3.2c). When the separation is 25μm, the output probe beams almost fully merge. This is because the lowest guided modes for the 980-nm beam in the two waveguides overlap with one another and are almost indistinguishable. Therefore, clear coupling from one waveguide to another can not be obtained. It can be expected that for probe beams at telecommunication wavelengths (λ=1300-1550 nm), the coupling efficiency will be almost unity.

REFERENCES:

[1] S.Lan, E.DelRe, Z.Chen, M.Shih, and M.Segev, *Directional coupler using soliton-induced waveguiding*, to appear in Optics Letters (February 1999)

[2] M.Shih, M.Segev, G.Valley, G.Salamo, B.Crosignani, and P.DiPorto, Electron.Lett. 31, 826 (1995)

[3] M.Segev, B.Crosignani, A..Yariv, and B.Fischer, Phys.Rev.Lett. 68, 923 (1992)

[4] G.Duree et al. Phys.Rev.Lett. 71, 533 (1993)

[5] M.Segev, G.Valley, B.Crosignani, P.DiPorto, and A.Yariv, Phys.Rev.Lett. 73, 3211 (1995)

[6] M.Segev, G.Valley, S.Singh, M.Carvalho, and D.Christodoulides, Opt.Lett. 20, 1764 (1995)

[7] M.Segev, M.Shih, and G.Valley, J.Opt.Soc.Am.B 13, 706 (1996)

[8] Iturbe-Castillo et al., Appl.Phys.Lett. 64, 408 (1994)

[9] K.Kos et al. Phys.Rev.E 53, R4330 (1996)

[10] B.Crosignani et al., J.Opt.Soc.Am.B 14, 3078 (1997)

[11] A.Zozulya et al., Europhys.Lett. 36, 419 (1996)

[12] E.DelRe et al., Appl.Phys.Lett. 73, 16 (1998)

[13] S.Lan, M.Shih, and M.Segev, Opt.Lett. 22, 1467 (1997)

[14] E.DelRe, G.Egidi, M.Tamburrini, and M.Segev, *Bright photorefractive screening solitons in tilted $BaTiO_3$*, submitted to Applied Physics Letters (June 1998)

[15] M.Saffman and A.Zozulya, Opt.Lett. 23, 1579 (1998)

[16] S.Gatz and J.Herrmann, Opt.Lett. 23, 1176 (1998)

[17] G.Valley et al., Phys.Rev. A 50, R4457 (1994)

[18] M.Chavet et al., Opt.Lett. 21, 1333 (1996)

[19] M.Chavet et al., Appl.Phys.Lett. 70, 2499 (1996)

[20] K.Kos, G.Salamo, and M.Segev, Opt.Lett. 23, 1001 (1998)

[21] M.Shih, M.Segev, and G.Salamo, Phys.Rev.Lett. 78, 2551 (1997)

[22] M.Mitchell and M.Segev, Nature 387, 880 (1997)

[23] M. Segev and G. I. Stegeman, Physics Today, August 1998.

[24] A. W. Snyder, D. J. Mitchell, L. Polodian and F. Ladouceur, Opt. Lett. **16**, 21 (1991).

[25] R. De La Fuente, A. Barthelemy and C. Froehly, Opt. Lett. **16**, 793 (1991); B. Luther-Davies and Y. Xiaoping, Opt. Lett. **17**, 496 (1992).

[26] P. V. Mamyshev, A. Villeneuve, G. I. Stegeman and J. S. Aitchison, Elect. Lett. **30**, 726 (1994).

[27] M. Morin, G. Duree, G. Salamo and M. Segev, Opt. Lett. **20**, 2066 (1995).

[28] M. Shih, M. Segev and G. Salamo, Opt. Lett. **21**, 931 (1996); M. Shih, Z. Chen, M. Mitchell and M. Segev, J. Opt. Soc. Am. B **14**, 3091 (1997)

[29] M. Klotz, H. Meng, M. Segev, and S. R. Montgomery, *Fixing the photorefractive soliton,* to be published (accepted), Opt. Lett., 1998

[30] Note the distinction from ***incoherent solitons***, which are partially spatially incoherent [M. Mitchell, Z. Chen, M. Shih and M. Segev, Phys. Rev. Lett. **77**, 490 (1996)], or spatially and temporally incoherent [M. Mitchell and M. Segev, Nature (London) **387**, 880 (1997)], entities.

Chapter
4

Screening Spatial Solitons in Ferroelectric $BaTiO_3$ and Nonlinear Anisotropic Self-Focusing

Introduction

In the previous Chapter screening solitons were introduced. This Chapter is dedicated to the description of experiments carried out by DelRe, Tamburrini, and Segev[1] in a sample of photorefractive $BaTiO_3$. The observation of 1+1D spatial soliton particles supported by the screening nonlinearity is outlined along with comparison to 1+1D theory (summarized in the previous Chapter). In the 2+1D case, a peculiar beam aspect ratio evolution, a signature of strong nonlinear anisotropy, is observed, in contrast to experiments carried out in SBN and KLTN (described in Chapter 3 and 6, respectively). Finally, the tensorial (vector) properties of screening self-trapping are experimentally investigated by implementing a tilted configuration, and results are partially described by a simple scalar phenomenological model.

$BaTiO_3$ and Screening Solitons

Among the family of photorefractive crystals commonly used in nonlinear applications, $BaTiO_3$ occupies a place of honor: it manifests an extremely strong electro-optic response ($r_{42}\approx$600-1600pV/m) and can be easily grown in many different configurations. It has allowed extremely efficient phase-conjugation and, in general, *is* the material of choice for wave-mixing experiments[2]. It is a perovskite that manifests a 4mm symmetry from approximately 4°C to its ferroelectric phase-transition at approximately 120°C. Regarding spatial soliton studies, $BaTiO_3$ has been traditionally considered a material of *second choice*, since in the typical screening soliton configuration it does not make use of the off-diagonal r_{42}, but rather makes use of $r_{33}\cong$100pm/V , smaller than the corresponding coefficient in SBN ($r_{33}\cong$330pm/V) . *Why search for screening solitons in $BaTiO_3$?* First of all, $BaTiO_3$ is a commonly used material, thus its growth has become part of the well-known techniques of crystal growing companies: it is less expensive and of higher quality than other less common crystals. The second motivation is that in a *standard* configuration it is less

appealing than SBN, *but* in a more elaborated tilted configuration, such as the one we will describe in this Chapter, the off-diagonal r_{42} coefficient can be activated, and unobserved *tensorial effects* can be investigated (experimentally, for the moment). Actually, "vector" solitons, the vectorial counterpart of scalar screening particles illustrated in the previous Chapter, have been predicted, in a different configuration, in 1995 by Segev et al.[3]. The third, unexpected, motivation is that, surprisingly, $BaTiO_3$ *does not support 2+1D circular-symmetric self-trapping*. As will be discussed in what follows, 2+1D screening solitons were not observed, in direct contrast with observations in SBN and KLTN. This discovery might allow, in the near future, a more profound understanding of the basic processes that support 2+1D screening solitons. In particular, these observations can be compared directly to analogous results obtained in photorefractive $KNbO_3$[4], where asymmetric self-focusing was also observed. These two crystals seem to behave in a very similar manner; not only, they seem to respond in a manner very similar to numerical predictions of nonlinear focusing in a local screening model[5], suggesting that nonlocal effects in these sample have a negligible influence whereas they *cannot* be neglected in SBN and KLTN.

Experiment

Experiments are carried out in the standard configuration for observing 1D bright screening solitons, described in detail in Chapter 6, using an Ir-doped zero-cut n-type $BaTiO_3$ crystal made by Deltronic Crystal Industries. Initially, on-axis soliton propagation is examined by cylindrically focusing a 514 nm laser beam and launching it along a crystalline a-axis (||z) and having it polarized parallel to the c-axis (extraordinary polarization, ||x), as shown in Fig. 4.1a. We apply an external voltage V on the c-faces of the crystal. In addition, we launch a second, ordinarily polarized (||y) uniform beam co-propagating with the soliton-forming beam, that serves as the background beam[6]. The screening mechanism that establishes a non-uniform space charge field which gives rise to solitons is described in Chapter 3. For 1D steady-state self-trapping, in the configuration of Fig. 4.1a, all the light-matter interaction variables depend only on the transverse coordinate x. In this condition, bright screening solitons satisfy eq.(3.10) in Chapter 3, that is

$$\frac{d^2u(\xi)}{d\xi^2} = -\left(\frac{\ln(1+u_0^2)}{u_0^2} - \frac{1}{1+u(\xi)^2}\right)u(\xi) \tag{4.1}$$

where we recall that $u(\xi)$ is the soliton amplitude normalized to the square root of the background illumination, $\xi = x/d$ the transverse coordinate normalized to the quantity $d = (-2kb)^{-1/2}$ with $b = \left(k/n_b\right)\left[\left(1/2\right)n_b{}^3 r_{eff}\, V/l\right]$, where $k = 2\pi n_b/\lambda$, λ is the wavelength and *l* the width of the crystal between the electrodes, n_b is the background refractive index and r_{eff} the effective electro-optic coefficient. The solutions of Eq. (4.1) give a set of parameter values compatible with soliton formation, which are cast in the form of a soliton "existence curve" of $\Delta\xi$ intensity full-width-half-maximum (FWHM) as a function of $u_0 \equiv u(0)$. For a given value of u_0 only one value of $\Delta\xi$ can give rise to self-trapping.

A 4.7 X 2.9 X 4.8 mm (x X y X z of Fig. 4.1a) $BaTiO_3$ crystal is used, which at λ=515nm has $n_b \cong 2.4$ and electrooptic coefficients of r_{13}= 12pm/V, r_{33}= 110pm/V, r_{42}= 660pm/V.

1+1D Particles

(1+1) D solitons are generated in the standard "on-axis" configuration of Fig. 4.1a .

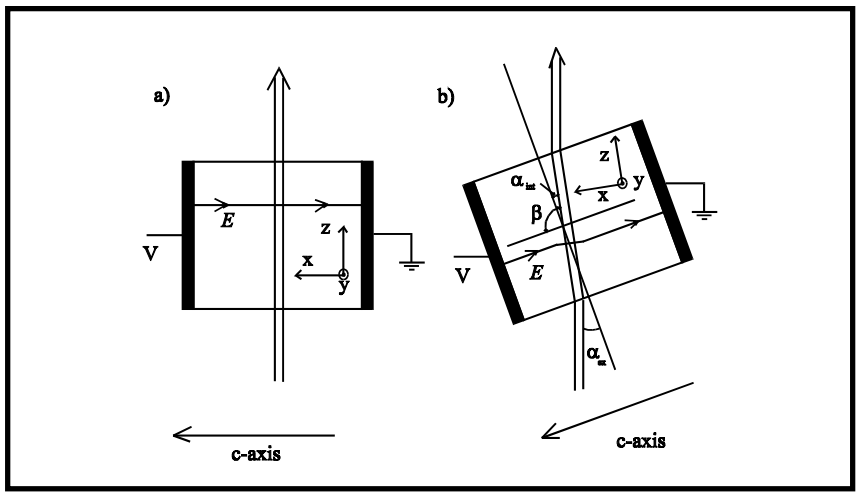

Fig.4.1: Soliton propagation in (a) the standard on-axis crystalline configuration and (b) in an off-axis configuration.

Typical experimental results are shown in Fig. 4.2, with u_0=2.7. A 12-μm FWHM input beam (left) diffracts in the absence of nonlinearity (V=0) to FWHM of 39 μm (middle), as expected from linear Gaussian beam propagation. When a voltage of V=1.15 kV is applied, at the exit facet a beam FWHM equal to the input (right) is observed.

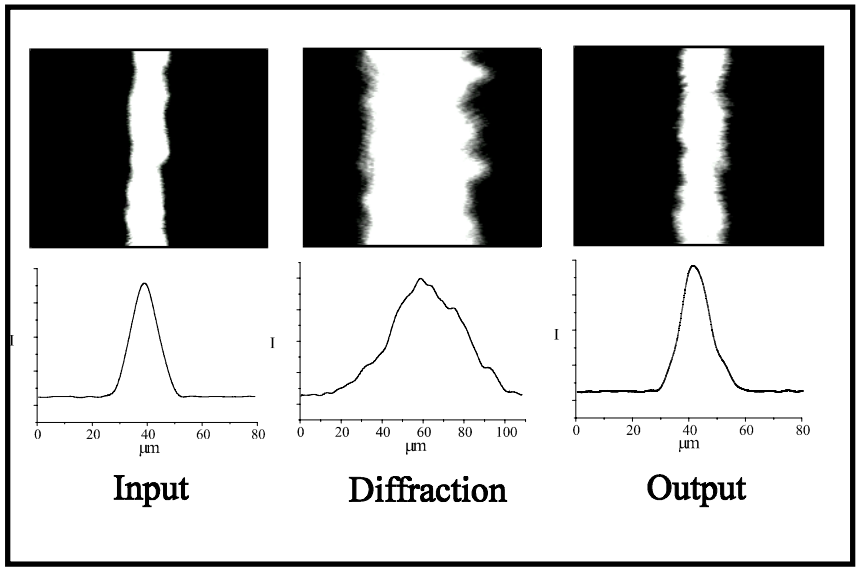

Fig.4.2: Photographs and profiles of the 12 μm FWHM input beam (left), regularly diffracting 39 μm FWHM output beam (middle) and soliton output (right) with V=1.15kV and u_0=2.7.

In Fig. 4.3 three experimental parameter conditions in which soliton formation has been observed are shown, as compared to the theoretical soliton existence curve. In this case of on-axis propagation $r_{eff}=r_{33}$ because the polarization is solely extraordinary and the space charge field is in the c-direction only.

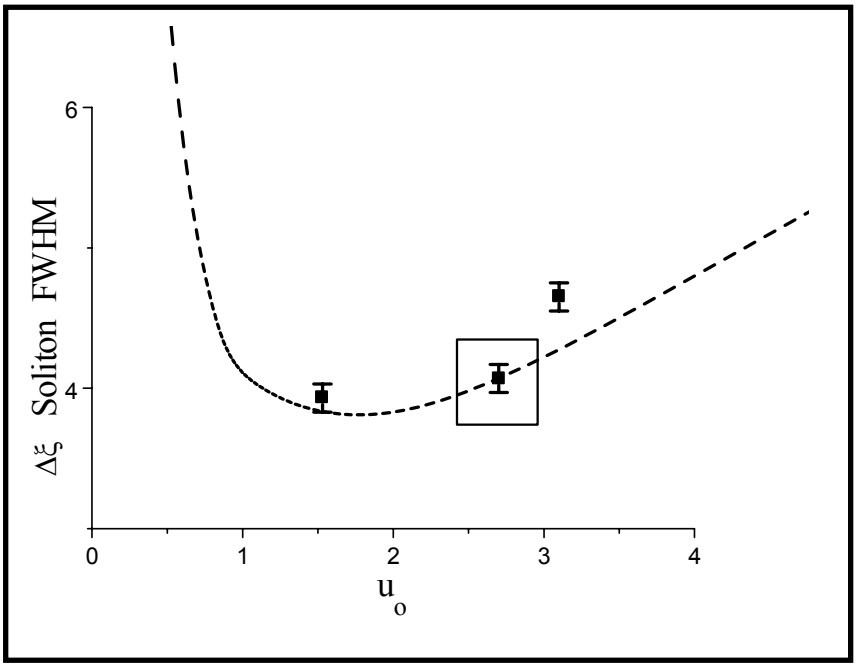

Fig.4.3: Theoretical soliton existence curve and experimental existence points (normalized units).

Tilted Configuration

The effect of crystal rotation on soliton formation is studied adopting the modified configuration illustrated in Fig. 4.1b. The crystal is rotated of an external angle α_{ex} keeping the c-axis in the plane of the figure, thus the beam propagates at an angle $\beta=\pi/2+\alpha_{int}$ ($\alpha_{int} \cong Arc\,\mathrm{sen}(\mathrm{sen}(\alpha_{ex})/n_b)$) with the c-axis. **The theoretical description in this case would need a more elaborate treatment, as now the external electric field is not orthogonal to the direction of propagation anymore** (in fact, theoretically, this becomes a 2D boundary condition problem). However, one of the main results on the formation of screening solitons that remains valid even in a full 3D case, is that the local density of electrons in the conduction band N is proportional to the local optical intensity I(**r**) plus the dark (or the background) irradiance I_{dark}[7]. This implies that the illuminated region is more conductive and therefore locally the electric field is both diminished in value (screening effect) *and* distorted (as schematically shown in Fig. 4.1b), so as to be approximately *orthogonal* to the direction of propagation in the regions involved in the confinement and where it has a nonvanishing value. Thus, it would seem qualitatively plausible that the simplified 1D theory should apply also in the tilted configuration, at least for small enough rotation angles α_{int}. With this assumption, we

expect to observe self-trapping for values of V obtained from the above described existence curve, while employing the relative effective electro-optic coefficient r_{eff} ***as calculated for two-wave-mixing***[8]. The value of r_{eff} as a function of the rotation angle α_{int} for a zero-cut sample of $BaTiO_3$ as determined from the crystal symmetry and α_{int}, is

$$r_{eff} = r_{13}\cos(\alpha_{int})\sin^2(\alpha_{int}) + r_{42}\sin(|\alpha_{int}|)\sin(2\alpha_{int}) + \\ + r_{33}\cos(\alpha_{int})\cos^2(\alpha_{int}) \quad . \tag{4.2}$$

A series of experiments in the tilted configuration have been therefore performed. Up to a maximum experimentally available angle of $\alpha_{int}^{max} \cong 12°$, self-trapping results are obtained that look practically identical to those shown in Fig. 4.2, for the same experimental parameters, while varying the angle and adjusting the voltage. The working hypothesis implies that *all observations refer to one single point in parameter space*, highlighted in Fig. 4.3. In Fig. 4.4 are plotted the experimental values of V as a function of α_{int}, along with the "theoretical curve" obtained by substituting directly Eq. (4.2) into 1D theoretically-predicted existence curve[7].

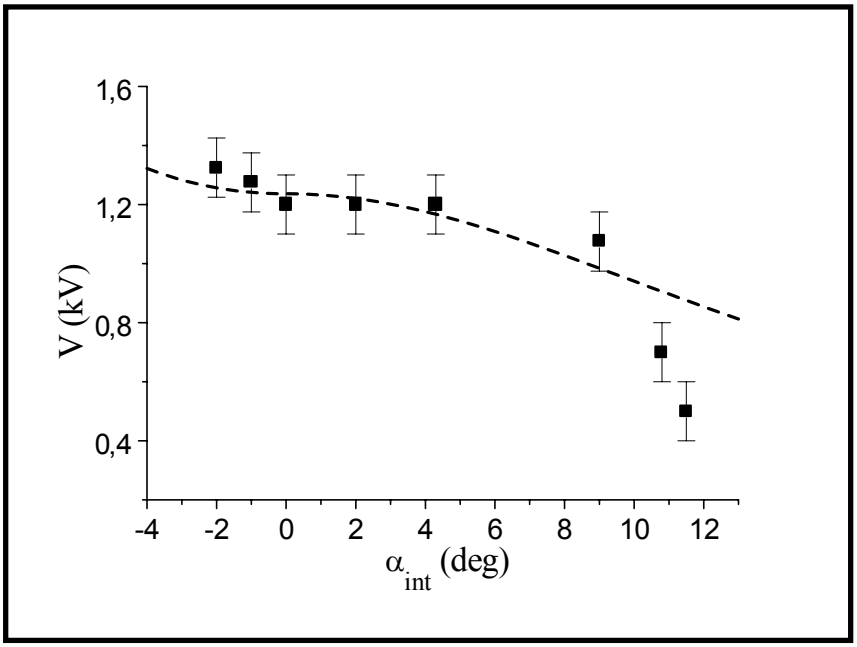

Fig.4.4: Experimental values of V for the tilted crystal configuration and the simplified scalar 1D model (dashed curve).

Good qualitative agreement for angles up to $\alpha_{int} \cong 9°$ suggests that 1D theory in this range is still valid in the tilted configuration. For the maximum available angle (determined by the dimensions of the sample) $\alpha_{int}^{max} \cong 12°$, for the conditions listed above, self-trapping is obtained with a field of ≅1 kV/cm, as compared to the untilted ≅2.5 kV/cm.

This experiment shows that in photorefractive crystals with very large electrooptic coefficients of the type $r_{i,j,k}$ where $i \neq j$ (e.g., $r_{42}=r_{51}$ in $BaTiO_3$), one can obtain solitons at *lower voltages* or, alternatively, *narrower solitons*, by employing off-axis propagation. It is also apparent from Fig. 4.4 that at large angles (>10^o) this "scalar approximation" that utilizes r_{eff} **fails**. Instead, one needs to solve a tensorial 2D boundary value problem and actually compute the separate contributions from both space charge field components to the refractive index.

Anisotropic Self-Focusing

Finally a circular input beam is launched (by substituting the cylindrical lens with a spherical one) in order to observe 2D

screening self-focusing effects. While strong 2D *self-focusing* is observed, the output beam is always *elliptical*. Typical results are shown in Fig. 4.5, for u_0=2.4, with a 11 μm FWHM input beam (left), which diffracts to approximately 44 μm in the absence of nonlinearity (middle). For V=1.9 kV, the output beam has a vertical (||y) width of 19 μm and a horizontal (||x) width of 12 μm. Thus, the beam self-focuses in an *astigmatic* manner. As mentioned earlier, a similar result has been recently observed with $KNbO_3$. This distinguishes $BaTiO_3$ and $KNbO_3$, both of which seems to support elliptically-shaped self-trapped beams, from SBN and from KLTN, in both of which circular solitons are easily observed (Chapter 6).

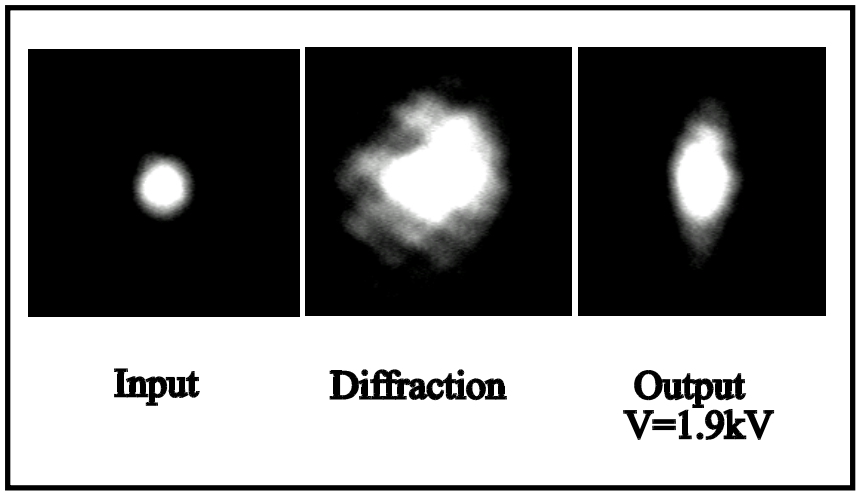

Fig.4.5: Photographs and profiles of the 11 μm FWHM circular input beam (left), regularly diffracting 44 μm FWHM output beam (middle) and astigmatic 12 μm x 19 μm self-focused beam (right) with V=1.9kV and a u_0=2.4.

REFERENCES:

[1] E.DelRe, M.Tamburrini, and M.Segev, *Bright photorefractive screening solitons in tilted $BaTiO_3$*, submitted to Applied Physics Letters (June 1998)

[2] *Introduction to photorefractive nonlinear optics*, P.Yeh (Wiley, New York 1993)

[3] M.Segev et al. Opt.Lett. 20, 1764 (1998)

[4] S.Lan, M.Shih, and M.Segev, Opt.Lett. 22, 1467 (1997)

[5] A.Zozulya et al., Europhys.Lett. 36, 419 (1996)

[6] M.Segev, M.Shih, and G.Valley, J.Opt.Soc.Am.B 13, 706 (1996)

[7] M. Segev, G. C. Valley, B. Crosignani, P. DiPorto and A. Yariv, Phys. Rev. Lett. **73**, 3211 (1994); D. N. Christodoulides and M. I. Carvalho, J. Opt. Soc. Am. B**12**, 1628, (1995): M. Segev, M. Shih and G. C. Valley, J. Opt. Soc. Am. B **13**, 706 (1996).

[8] Y. Fainman, E. Klancnik and S. H. Lee, Opt. Eng. **25**, 228 (1986)

Chapter

5

Near-Transition Electro-Optics

Introduction

In this Chapter what is termed *phase-transition electro-optics*, is introduced. This unconventional configuration is based on the increased dielectric response close to the ferroelectric-paraelectric phase-transition that allows an increased, temperature tunable, electro-optic response in the higher symmetry phase.

Ferroelectricity and Electro-Optics

Ferroelectricity (a term introduced in formal analogy to ferromagnetism) was initially discovered in Rochelle Salt in 1921[1)] , but has since been observed in a limited, by very numerous family of crystals, and is today believed to be a quite natural configuration of a general class of dielectrics. In particular, most commonly used nonlinear optical crystals are ferroelectric. What is, therefore, a ferroelectric? A ferroelectric is a dielectric that in a certain temperature range manifests strong *reversible spontaneous polarization*. Generally, a dielectric is only very weakly susceptible to an external high frequency (optical) or low-frequency (static) electric field. The application of a field will induce a "very small" displacement in the structure of the crystal known as *electrostriction*. The rather small change will in turn induce an almost imperceptible change in the optical properties of the material. Some dielectrics, however, have a particular structure that, in certain temperature ranges, favors a thermodynamic relaxation into a *polarized* stated. That is, the basic crystal cell is stable in a noncentrosymmetric configuration. On a macroscopic level, this relaxation gives rise to what is termed *spontaneous polarization* (P_s) that can take on "huge" values ($\cong 10^{-6}$C/cm^2)[2)] . Crystals that have this polarized state are referred to as *pyroelectric*. A ferroelectric is a pyroelectric in which an external field of a given temperature-dependent strength E_c (*coercive field*) can **reverse** the spontaneous polarization. So, it comes natural to ask, what is the difference between a pyroelectric and a ferroelectric? The difference is that in the latter case we can obtain *macroscopic aligned samples*. Spontaneous

polarization engenders charge separation. This implies that a finite crystal relaxing into a noncentrosymmetric structure will tend to relax into a multidomain configuration, that is, a configuration formed by single macroscopic aligned regions (i.e. *domains*) each of which is mutually misaligned with the other. In this case no net charge separation is produced and the system is in a thermodynamic minimum. Consider now applying an external electric field in a given crystalline direction **x**: in a ferroelectric, if the electric field E is $E>E_c$, the domains will slowly coalesce into a single polarized domain: an anisotropic, yet homogeneous, noncentrosymmetric crystal. What happens if one should turn off the electric field? One might speculate that the finite sample has exposed surface charges, and thus the system should return to the nonpolarized disordered state. Ferroelectrics, however, manifest *hysteresis*: they have a "memory" of their initial state. Essentially the dipole-dipole interactions introduce a potential barrier, making the noncentrosymmetric state a local, although highly stable, thermodynamic configuration. Thus we have, in the end, a single, ordered crystal with an intense macroscopic P_s: all light-matter interaction mediated by a direct or indirect electric field (nonresonant interactions) in such a sample is strongly enhanced. The most relevant example, for our purposes, is the discussion contained in Chapter 2, concerning the Pockels Effect and electro-optics. In summary, electro-optics is essentially *optical propagation in ferroelectric crystals*.

Ferroelectric-Paraelectric Phase-Transition and Electro-Optics

"Standard" electro-optics in ferroelectrics has been extensively studied and routinely applied for the past three decades, and screening solitons described in previous Chapters are basically an application of this process. Electro-optics however can be extended to different phases and thermodynamic regimes. In this section we shall introduce what is referred to as *phase-transition* electro-optics, initially investigated by Agranat, Levya and Yariv, in 1989[3)] .

Spontaneous polarization occurs when, at a given T, a dielectric relaxes into a noncentrosymmetric polarized configuration. At a given higher temperature, referred to as the crystal Curie Temperature T_c, this relaxation is no longer possible, and the crystal does not manifest spontaneous polarization or ferroelectricity. In analogy to ferromagnetic phenomena, the crystal is said to be in a paraelectric state.

This circumstance can be interpreted in two complementary ways: i) the thermal oscillations have energy comparable to the potential barrier separating the counterpolarized states; ii) the stable crystal structure at the given T does not manifest a minimum in the noncentrosymmetric configuration. This last viewpoint is the easiest to adopt in a phenomenological thermodynamic interpretation of the transition. Thus at a given T_c the crystal suffers a transition from a polarized state to a nonpolarized state: a basic statistical phase-transition. Phase-transitions are an extremely interesting an important phenomena in general physics, and here we shall by no means attempt to discuss them thoroughly.

Transitions in ferroelectrics are essentially of dielectric nature, and are characterized by what is generally referred to as a *dielectric anomaly*. A dielectric anomaly is an increase of the small signal dielectric constant in proximity of the ferroelectric phase transition (divergence of linear response peculiar to all phase-transitions). Consider, for example, a paraelectric ferroelectric being slowly cooled towards the polar state ($T>T_c$). One way of microscopically interpreting "gentle" structural transitions (such as the ferroelectric-paraelectric one) is to look at the elastic restoring forces in the fundamental cell structure. Considering, intuitively, that the transition occurs as a central ion is displaced towards a more stable asymmetric position in the initially cubic lattice: these restoring forces become weaker and weaker as the transition is approached (*soft modes*). The centrosymmetric potential minimum becomes less "attractive" and other minima (polar ones) begin appearing. Finally at T_c these polar minima become more stable than the initial nonpolar one, and the system nonperturbatively "jumps" into one of these. *Weakening* of the restoring forces actually means that the linear response of the system to a small signal electric field *increases*: the dielectric constant increases. A simple phenomenological model, due to Curie and Weiss, allows a direct description of the dielectric anomaly when the mean field approach is valid, that is, in the paraelectric phase *before* the insurgence of long scale fluctuations (such as random noise induced domains). In this model, to a first approximation, the relative low-frequency (< 100Kc/s) dielectric constant ε_r is given by

$$\varepsilon = \frac{C}{T - T_0} \ , \tag{5.1}$$

where C and T_0 are phenomenological constants. T_0 is sometimes referred to as the *transition temperature*.

Equation (5.1) is generally valid for "gentle" displacive transitions[1)]. By this it is meant that the transition does not entail macroscopic phase-changes and is generally brought about by very small changes in the crystal structure: the spontaneous displacement is small compared to the crystal interatomic distances. Generally, such transitions are *theoretically* **second-order**, that is, they come about by a "continuos" growth from $P_s=0$ at T_c to actual finite values of P_s at higher values of T. In this case there is no direct "jump" from the nonpolar state to a polar one, but rather an intermediate regime in which the nonpolar minimum ceased to exist and the potential well becomes, literally, *flat*. In this case the linear response must diverge, and in fact for such a transition $T_0=T_c$, and $\varepsilon\rightarrow\infty$. In a finite sample this indeed cannot occur, and due to size effects, internal strains, inhomogeneities, etc. the transition occurs at a $T_0>T_c$, giving rise to what is termed a "gentle" first-order phase transition, to distinguish it from other first order wholly nonperturbative transitions such as the liquid-gas transition in H_2O. In this case, for a region of values of T close to T_c, the crystal thermodynamically manifest three potential minima: one central nonpolar one, and two polar ones (for a given crystal principal direction). Although the central minimum is somewhat loosened, it becomes unstable *before* disappearing. This is the common case for ferroelectrics, and in particular for KLTN.

What does eq.(5.1) imply for electro-optical phenomena? To address this question we should first realize that, as already mentioned in Chapter 2, electro-optics is not *peculiar* at all to the ferroelectric phase. It exists in the centrosymmetric nonpolar phase as well, and is routinely used in optical modulator components through the quadratic electro-optic effect. The effects is, however, quite weak, and strong external fields are needed for useful values of Δn. This is of course due to the "absence" of spontaneous polarization, as discussed in Chapter 2. In proximity of the dielectric anomaly, on the other hand, the polarization $P=\varepsilon E$ induced by an electric field drastically increases, as described by eq.(5.1), and extremely high values of Δn can be achieved with reasonably low applied electric fields. Thus phase-transition electro-optics is essentially the use of the dielectric divergence of the linear response in proximity of the phase-transition in the linear (i.e. when the mean field theory holds and $P=\varepsilon E$) paraelectric phase to drastically enhance the quadratic electro-optic effect.

Phase-transition electro-optics is at the basis of the nonlinear propagation effects described in Chapters 6 and 8. In the first case, the generally weak quadratic effect is shown to support screening solitons with relatively low applied external fields, leading to centrosymmetric screening solitons, first predicted by Segev and Agranat in 1997[4], and observed by DelRe et al. in 1998[5]. In the second case, the dielectric anomaly is shown to allow for completely new phenomena caused by spatial charge diffusion.

KLTN: a Composite Perovskite

Experiments described in the next Chapters are carried out in samples of potassium-lithium-tantalate-niobate (KLTN). The crystal is a composite of the known ferroelectric perovskites KTN and KLN, and is itself a perovskite[6]. It is formed, in the paraelectric phase, by a mixture of the two dioxide structures (each of which has the same structural properties of $BaTiO_3$). The fundamental cell is a cubic structure with either K^+ or Li^+ atoms at the eight vertexes, a central Ta^+ or Nb^+ atom, and O^- atoms on the six faces. The relative quantity of K/Li and Ta/Nb has certain major consequences on the stability and thermodynamic properties of the sample. In particular, and this is of central import in this treatise, they can drastically change T_c. Bulk samples of KLTN at any concentration are extremely difficult to grow, and the work of Agranat and coworkers on this material has allowed the realization of large optical quality crystals with room temperature Curie temperatures only recently[7]. In our studies we make use of two samples, described in the following Chapters, one with $T_c \approx 10°C$, and one with $T_c \approx 21°C$. Phase-transition electro-optics has become an accessible process with the successful growth of such specimens. Electro-optic crystals with near-room temperature Curie temperatures are indeed a rarity. This is essentially due to the fact that operation close to a transition needs temperature control, and near-transition operation is generally considered *out-of-control*. The studies carried out and described in successive Chapters prove that this is not the case: near transition operations offers a wealth of new and exciting, possibly useful, processes.

As most perovskites, KLTN in the paraelectric phase has a quadratic electro-optic tensor of m3m symmetry, manifests a structural displacive phase transition (with values of $C \approx 10^{5}°C$) and peak values of $\varepsilon_r \approx 3x10^4$, although higher values might be expected for small samples. KLTN can be described by a first order transition with $T_c < T_0$ by typically a few degrees, this

being due to inhomogeneities and growth induced strains. Since dielectric properties of the samples differ from sample to sample, we shall describe the single crystals in the description of the experiments discussed in successive Chapters. In order to exalt photorefractive properties, the samples are doped with small quantities of Va and Cu impurities, that act as donor sites. These impurities make the crystals photorefractively active from about 550 nm upwards (shorter wavelengths). In a typical configuration, the photorefractive response of KLTN is comparable with standard $LiNbO_3$ samples. The actual values of the relevant quadratic electro-optic coefficient range from $g_{xxxx}=g_{11}=0.10\div0.17\ m^4C^{-2}$.

All things considered, KLTN *does not appear singular*. By this, it is meant that the crystal does not represent a "mysteriously functional" crystal. It has all the characteristics that all other photorefractive ferroelectrics have, except that it is easy to use because it has a room temperature T_c. This basic fact, although not fundamental, is however extremely important in limiting the technological complexity of the experimental apparatuses that remain, as will be discussed later, simple and straightforward to build and use.

REFERENCES:

[1] *Ferroelectric crystals*, F.Jona and G.Shirane, (Dover, New York 1993)

[2] *Ferroelectric Materials*, Y.Xu (North Holland, Amsterdam 1991)

[3] A.Agranat, V.Leyva, and A.Yariv, Opt.Lett. 14, 1017 (1989)

[4] M.Segev and A.Agranat, Opt.Lett. 22, 1299 (1997)

[5] E.DelRe et al. Opt.Lett. 23, 421 (1998)

[6] A.Agranat, R.Hofmeister, and A.Yariv, Opt.Lett. 17, 713 (1992)

[7] B.Pesach, E.Refaeli, and A.Agranat, Opt.Lett. 23, 642 (1998)

Chapter

6

Centrosymmetric Spatial Screening Solitons

Introduction

In this Chapter we describe the experiments, carried out by DelRe et al. in 1998[1)], leading to the first observation of photorefractive screening centrosymmetric solitons. These spatial solitons, observed in KLTN, are supported by the dielectrically enhanced quadratic paraelectric screening photorefractive response in proximity of the ferroelectric phase transition. They are observed in both the 1+1D and 2+1D configuration[2)]. These particles were initially predicted, in the 1+1D case, by Segev and Agranat in 1997[3)], and their 1+1D theoretical treatment is briefly summarized.

Centrosymmetric 1+1D Spatial Screening Solitons

Centrosymmetric screening solitons stem from the same basic physical mechanism that supports ferroelectric screening solitons treated in Chapters 3 and 4. The main difference lies in the fact that they are due to the quadratic electro-optic response to charge separation and have a peculiar temperature dependence due to the vicinity of the phase-transition. The model here presented is simple and in all analogous to the one pertaining to "standard" screening solitons. In it, complicated, yet important, solid-state processes that come into play close to the transition are not taken into account. Experiments suggest that these processes *play a relevant role*, and, in Chapter 7, a model which takes into account one such process, the *material nonlinearity*, is discussed.

In steady-state and in the 1+1D case, the material equations and the nonlinear wave-propagation equation can be summarized as follows,

$$(s|A|^2 + sI_d + \beta)(N_d - N_d^+) - \gamma_r N N_d^+ = 0, \qquad (6.1)$$

$$\frac{dJ}{dx} = \frac{d}{dx}(q\mu NE + k_b T\mu \frac{d}{dx}N) = 0, \qquad (6.2)$$

$$\frac{d}{dx}E - \frac{q}{\varepsilon}(N_d^+ - N_a - N) = 0, \tag{6.3}$$

$$\left[\frac{\partial}{\partial z} - \frac{i}{2k}\frac{\partial^2}{\partial x^2}\right]A(x,z) = \frac{ik}{n}\Delta n(E)A(x,z), \tag{6.4}$$

$$V = -\int_{-l/2}^{l/2} E dx, \tag{6.5}$$

where

$$\Delta n(E) = \frac{1}{2}n^3 g_{eff}\varepsilon_0{}^2(\varepsilon_r - 1)^2 E^2 \tag{6.6}$$

is the index modulation due to the quadratic electro-optic response, assuming a linear polarization regime (*material linearity*), i.e. $P=\varepsilon_0(\varepsilon_r-1)E$, and g_{eff} is the effective quadratic electro-optic coefficient in the scalar configuration. The scalar treatment is valid if the initial polarization of the slab of light (confined along the x direction and propagating along the z direction) is polarized along a principal axis. The crystal m3m symmetry does not allow polarization coupling even in the presence of the external biasing voltage V giving rise to an x directed external field. For an x polarized beam ("extraordinary beam") $g_{eff}=g_{xxxx}=g_{11}$. A is the slowly varying amplitude of the optical field

$$E_{opt} = A(x,z)e^{ikz-i\omega t} + c.c. \tag{6.7}$$

and β is the dark generation rate. $I=|A|^2$ is the optical intensity and I_b is the artificial background illumination.

As done for ferroelectric screening solitons, we search *self-consistently* for self-guided solitary waves of the form

$$A(x,z) = u(x)e^{i\Gamma z}(I_d + I_b)^{1/2} \tag{6.8}$$

where Γ is the soliton propagation constant, and, searching solely for bright solitons, we limit the discussion to real u(x). In this self-consistent formulation I depends on x alone and we thus allow all the independent variables to only depend on x.

We transform the equations to dimensionless form through the transformations (identical to those implemented in Chapter 3)

$$\overline{N} = \frac{N}{N_d},\ \overline{E} = \frac{|E|}{V/l},\ \overline{N}_d^+ = \frac{N_d^+}{N_d},$$
$$r = \frac{N_d}{N_a},\ \overline{J} = \frac{|J|}{q\mu N_d V/l},\ \xi = \frac{x}{d}, \tag{6.9}$$

where

$$d = \frac{1}{(-2kb)^{1/2}}, \tag{6.10}$$

and

$$b = \frac{k}{n}\left[\frac{1}{2}n^3 g_{eff}\varepsilon_0{}^2(\varepsilon_r - 1)^2(V/l)^2\right] \tag{6.11}$$

characterizes the strength of the nonlinearity. We have assumed that $g_{eff}<0$ (leading to a self-focusing nonlinearity). The dimensionless equations are

$$N - a(1+|u|^2)\frac{(1-N_d^+)}{N_d^+} = 0,$$
$$J = NE + \varepsilon_1 N' = \text{const},$$
$$N_d^+ - 1/r - N - \varepsilon_2 E' = 0, \tag{6.12}$$
$$l/d + \int_{-l/2d}^{l/2d_s} d\xi E = 0,$$
$$u'' = -[\delta + E]u,$$

where $\delta=\Gamma/b$ and the prime stands for derivatives with respect to ξ, (dashed symbols are simplified) and

$$a = \frac{s(I_d + I_b)}{\gamma N_d},$$
$$\varepsilon_1 = \frac{k_b T l}{qdV}, \tag{6.13}$$
$$\varepsilon_2 = \frac{V\varepsilon}{lqdN_d}.$$

The nonlinear wave propagation problem, as it stands, is both *nonlocal* and *nonintegrable*. For particular experimental

conditions, however, as in the noncentrosymmetric case, nonlocality can be neglected and the interaction becomes local (screening nonlinearity). For typical experimental parameters relative to KLTN ($\lambda\approx0.5\mu m$, n=2.4, $\varepsilon\approx4000\varepsilon_0$, $V/l\approx2kV/cm$, $N_d\approx10^{18}cm^{-3}$, $r\approx20$), we obtain $d\approx2\mu m$, and $\varepsilon_{1,2}<<1$. Furthermore, for optical intensities of $\approx1W/cm^2$ (typical of screening configurations) $n\approx10^{-9}$. In view of these approximations $N_d^+=1/r$ as long as $E'<<(r\varepsilon_2)^{-1}\approx4$. Since $N_d^+<<1$, $N\propto ar(1+u^2)$. In a similar manner, if $\varepsilon_1 n'<<1$, nE=const=J, and

$$E=\frac{-\eta}{1+u^2}, \tag{6.14}$$

with

$$\eta=\frac{1}{\frac{d}{\ell}\int_{-l/2d}^{l/2d}\frac{d\xi}{1+u^2}}\ . \tag{6.15}$$

If $\Delta x/l<<1$ (as is always the case) this integration can be easily shown to give $\eta\cong1$.

The normalized nonlinear wave equation now becomes

$$\frac{d^2u(\xi)}{d\xi^2}=-\left[\delta-\frac{1}{\left(1+u(\xi)^2\right)^2}\right]u(\xi). \tag{6.16}$$

This equation has a first integral which can be found by quadrature

$$p^2-p_0^2=-\left\{\delta(u^2-u_0^2)+\frac{1}{1+u^2}-\frac{1}{1+u_0^2}\right\}, \tag{6.17}$$

where $p(\xi)=u'$, $p_0=p(0)$, and $u_0=u(0)$. Bright fundamental solitons (a single trapped light pulse) are found under conditions $u_\infty=u'(\infty)=u''(\infty)=0$, $u'(0)=p_0=0$, and $u''(0)/u_0<0$. Using this condition gives the final formal *local* nonintegrable saturable soliton wave-equation

$$\frac{d^2u(\xi)}{d\xi^2}=-\left[\frac{1}{1+u_0^2}-\frac{1}{\left(1+u(\xi)^2\right)^2}\right]u(\xi). \tag{6.18}$$

As in the noncentrosymmetric case, eq.(6.18) must be integrated numerically. The resultant profiles are somewhat similar to Gaussian pulses. A soliton existence curve can be found in the (u_0, $\Delta\xi$) parameter space that is qualitatively similar to the ferroelectric one. The actual curve will be used in the following section to compare experimental results with this simple local 1+1D theory.

Observation of 1+1D Centrosymmetric Screening Solitons in a Sample of Paraelectric KLTN

Experiments are performed in a sample of KLTN specifically treated so as to have a first order ferroelectric-paraelectric phase transition slightly below room temperature. Working at room temperature enables one to operate in a centrosymmetric phase close to the transition, thereby enhancing the electro-optic response (as discussed in Chapter 5), making centrosymmetric soliton observation possible with moderate (or low) electric fields.

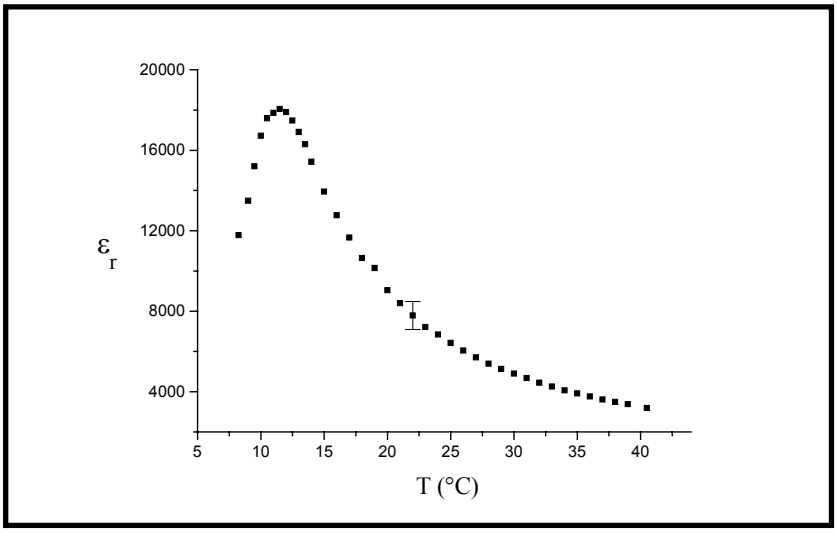

Fig.6.1: Measured values of low frequency ε_r as a function of temperature T in our KLTN sample. The error bar indicates experimental error.

In Fig. 6.1, we show measurements of ε_r as a function of temperature, and observe the large increase of ε_r in proximity of the ferroelectric-paraelectric phase transition (which occurs at ~12^o).

It should be noted that in these discussions we will frequently report bulk values of ε_r and discuss general thermodynamic properties of the samples giving relative values of crystal T.

Due to the "ever present" temperature gradient, these are only relevant to a specific *transverse* crystal region (the gradient is orthogonal to the propagation axis). This fact, avoidable with a more sophisticated apparatus, does however *not* influence perceptibly the observed nonlinear phenomena. Its main influence is tied to very-near-transition operation, where small gradients can drastically change the effective thermodynamic configuration of portions of the crystal at a given T. Thus, for example, whereas the *bulk* transition in this sample occurs at 12°C, in Chapter 8 we shall report observation relative to a linear polarization regime (absence of spontaneous polarization) at almost 10°C (relative to a region in the crystal far from the thermal contact).

Since Δn scales with $(\varepsilon_r\text{-}1)^2$, operation at temperatures slightly above the Curie temperature result in an increase of the quadratic electrooptic response. We also note that, in the specific case of KLTN, g_{eff} is negative, and bright solitons can be observed, i.e., in the screening regime KLTN becomes a self-focusing medium[4].

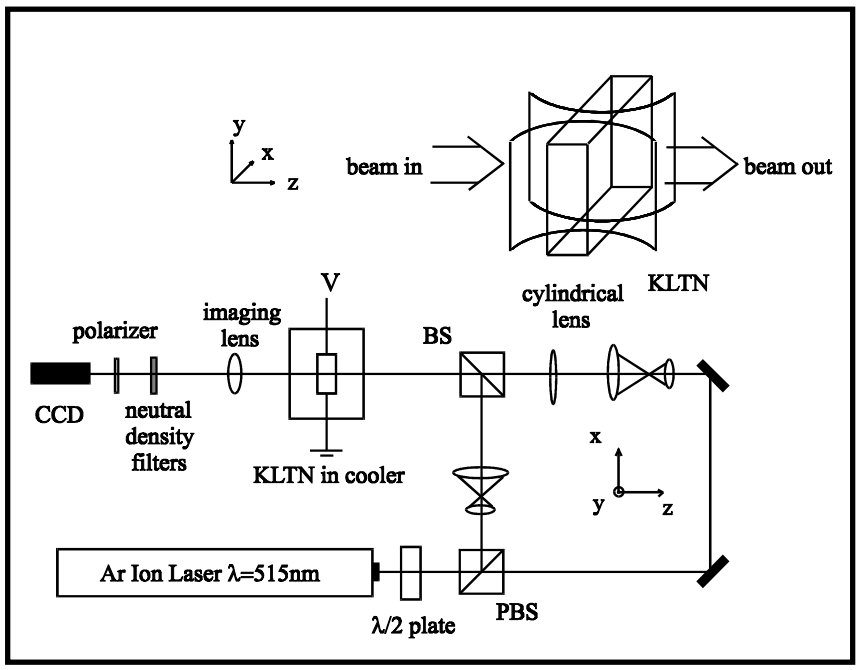

Fig.6.2: The experimental setup.

In Fig. 6.2 we illustrate the experimental setup. A CW Argon-ion laser beam is split into two orthogonal polarizations by a polarizing beam splitter (PBS). The transmitted beam, with

polarization parallel to the plane (x axis) of the figure, is focused by a cylindrical lens onto the input face of the KLTN crystal, with its narrow dimension parallel to x. The crystal is of dimensions 3.7 x 4.6 x 2.4 in the x, y, z directions, the latter being the direction of propagation. The sample is kept at a constant temperature by means of a current controlled Peltier junction (which allows fine temperature tuning). The effective quadratic electro-optic coefficient has been measured (via a separate standard electrooptic-interferometric experiment) and is $g_{eff} = -0.12\ m^2C^{-4}$, and the index of refraction is $n_b=2.2$. As shown in the figure, gold electrodes are sputtered on the x-axis faces, to which an external voltage V is applied. Finally, the input and output faces of the sample are imaged onto the sensitive area of a CCD camera. The y-axis polarized beam serves as the background beam: it is expanded, recombined with the soliton beam and made to illuminate the crystal uniformly while co-propagating with the soliton-forming beam.

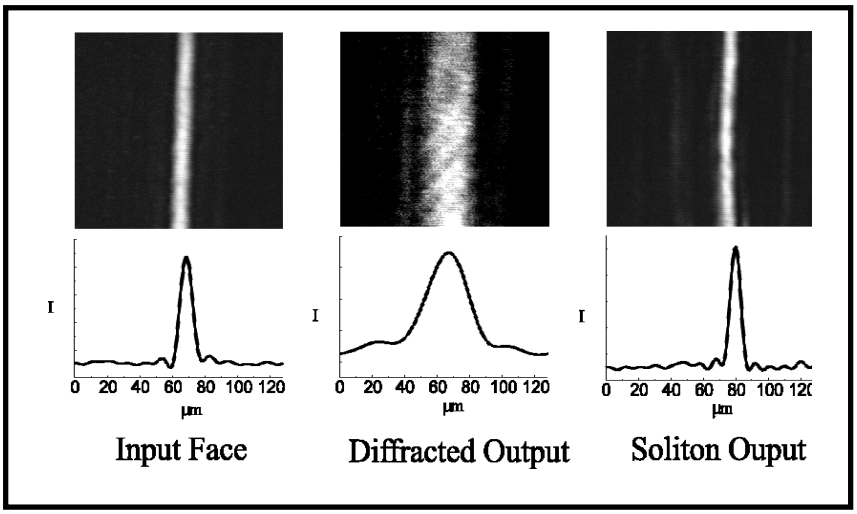

Fig.6.3: One dimensional photographs and profiles of the 9-μm wide FWHM input beam (left), diffracted output beam at V=0 (middle), and the self-trapped (soliton) output (right). The beam profiles are normalized to their maximum value in all cases.

In Fig. 6.3 we show typical experimental results: photographs and beam profiles at the input face of the crystal (left column) and at the output face in the normal diffraction regime (middle column, zero voltage). A 1D soliton forms with the application of a proper voltage V (right column). In the particular case shown in Fig. 6.3, the input beam is of 9 μm FWHM, and it diffracts to 29 μm with V=0. The self-trapped (soliton) beam

has the same width as the input beam: 9 μm, and it forms with intensity ratio $u_0^2 \cong 2.9$, V≅2kV and sample temperature of T=21°C.

Comparison to the Local 1+1D Screening Theory

In order to compare experimental results with the theory of solitons in photorefractive centrosymmetric media, a number of different experiments have been performed. Keeping the input beam fixed, the intensity ratio was varied and the applied voltage V allowing steady-state soliton observation was traced. Knowing the (measured) sample temperature T, we are able to predict, as previously stated, the values of V necessary to obtain soliton solutions given a value of u_0. By plotting the experimental set of existence points against the predicted existence curve we are able to asses the adherence of the 1D theory to experiments. Figure 6.4 shows a direct comparison between the theoretically-predicted existence curve and the experimentally measured values, for two different temperatures (at which ε attains different values). Several things are evident. First, for values of $u_0>1.5$ the normalized width ($\Delta\xi$), which is proportional to the applied voltage V, has a ***linear dependence on u_0***, which is observed in both the theoretical and the experimental results (although the slopes are somewhat different). This dependence is unique to this type of solitons, and stands in contradistinction with the dependence of V on u_0 for screening solitons that rely on the linear electrooptic effect (in that case $\Delta\xi \propto V^{1/2}$, and at high intensity ratios, $\Delta\xi \propto u_0$, as described in Ref. [5]) This observation confirms that these solitons indeed rely on the *quadratic* electrooptic effect. Another observation is that for both temperatures the existence curve "flattens" around $u_0=1$, which is consistent with the theoretical prediction.

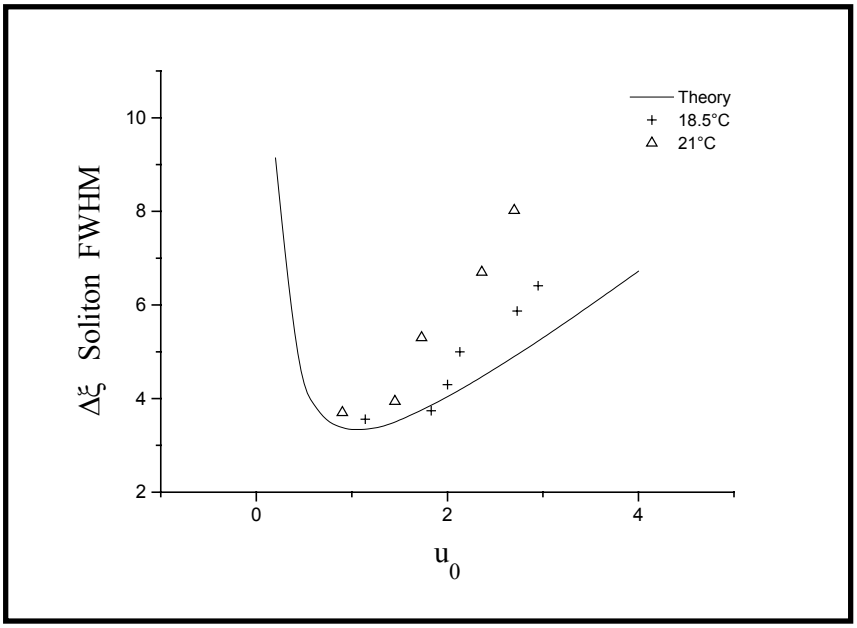

Fig.6.4: Soliton existence curves: theoretically predicted (solid curve) and experimentally measured points at 18.5^{o}C (crosses) and at 21^{o}C (triangles).

As apparent from Fig. 6.4, while there is good *qualitative* agreement between theory and experiments, the experimental values are shifted from the theoretical existence curve (for u_0>2) and the curves for both temperatures do not fully overlap (as expected from the theory). There are several plausible reasons for this discrepancy. The primary reason is that in the theory the background illumination is assumed to be uniform in x (and experiences the same absorption as the soliton beam), whereas in practice this beam is slightly guided "under" the soliton. In other words, the space charge field generated by the soliton beam gives rise to a change in the refractive index not only for the $\hat{x}$-polarized (soliton) beam (through $g_{iiii}=g_{xxxx}$) as it should, but also to an index change for the $\hat{y}$-polarized (background) beam (through $g_{jjii}=g_{yyxx}$), which is supposed to be uniform. This causes the background beam to be slightly guided in the region of the soliton, and is responsible for the deviation of the experimentally-measured existence curve from the theoretically-predicted one. Similar effects are observed in all experiments with screening solitons that rely on Pockels' effect, and they always lead to a shift of the experimentally-measured existence curve to higher values of $\Delta\xi$[6]. This effect can explain the deviation of the experimental existence curve from the theoretically predicted one, but ***cannot*** explain why the two data sets at the different

temperatures also deviate from each other. It is believed that, as often occurs in paraelectric materials at the proximity of the phase transition, ε_r ***depends on the local field***. This means that the "quadratic" electrooptic effect slightly deviates from quadratic dependence on the field E. The immediate implication of this argument and of the fact that the experimentally-measured existence curve at two different temperatures deviate from one another, is that along with the (known) mechanisms considered in the theory describing 1D solitons in these materials, other interesting phase-transition phenomena may play an important role (see Chapter 7). In particular, we expect that at sample temperatures that are even closer to the phase-transition, other phenomena, such as critical slowing, hysteresis, and fixing will become important, and the soliton itself can prove to be a very sensitive means of investigation. Finally we expect that, as far as applications are concerned, fixing (via cooling through the Curie temperature[7)]) will allow highly versatile imprinting of complicated soliton optical circuitry, making bulk optical reconfigurable waveguide components possible.

Observation of Centrosymmetric Circular-Symmetric 2+1D Screening Solitons in KLTN

In this section we shall describe the experimental observation of circular-symmetric photorefractive centrosymmetric screening solitons in a second sample of paraelectric KLTN. This observation supports claims as to the existence of circular-symmetric spatial particles supported by the screening nonlinearity in ferroelectrics, and is in itself quite a startling result. As discussed in previous sections, centrosymmetric screening solitons are only qualitatively described, even in the simple 1+1D case, by the local screening theory. They a fortiori involve a number of complicated phase-transition effects such as hysteresis, photoferroelectricity, and material nonlinearity. Furthermore, even neglecting these processes, a simple local theory in the 2+1D case has been proven to not allow stable circular-symmetric trapping, implying that 2+1D particles actually have a relevant nonlocal component. Notwithstanding this *two-fold* complexity, circular-symmetric particles exist. These phenomena, apart from being interesting in themselves as peculiar nonlinear objects in a complex system, can become a very important means of investigation of the actual nonlinear processes occurring in the crystal during the metastable regime close to the transition.

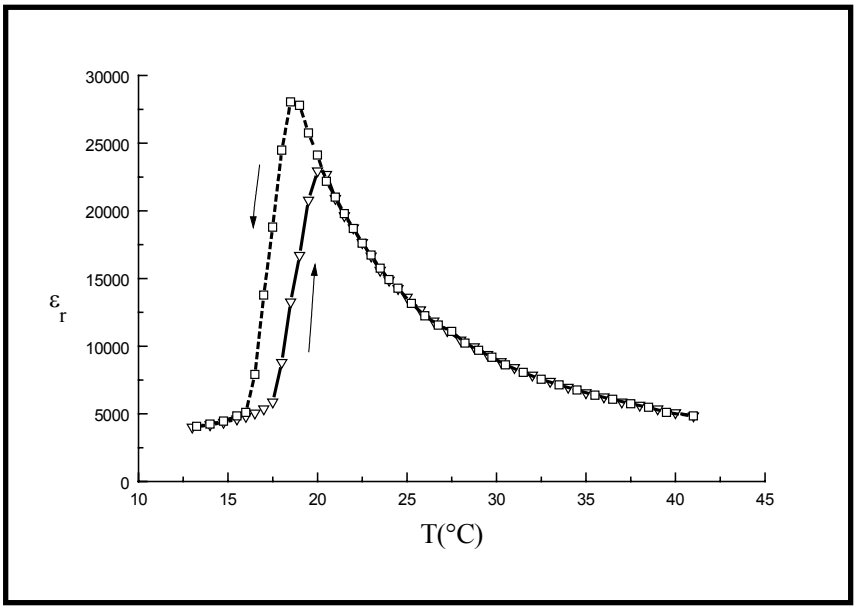

Fig.6.5: Measured values of ε_r as a function of temperature T. The two curves represent measured values for decreasing (squares) and increasing (triangles) temperatures.

Experiments are performed in a sample of 2.6 X 1.8 X 6.4 mm KLTN cut along the principal crystalline axes (which are all identical to each other, but we denote them here as x,y,z respectively). The crystal has a ferroelectric-paraelectric phase transition at $\cong$18.5°C as can be seen from measurements of ε_r as a function of temperature shown in Fig.6.5. This figure also shows the temperature hysteresis typical of first order phase transitions. The relevant quadratic electro-optic coefficient in the experimental configuration (shown in Fig. 6.6) is $g_{eff}=g_{xxxx}=-0.13\ C^{-2}m^{-4}$ as measured in a standard cross-polarizer experiment, and the index of refraction is $n_b=2.4$ (at λ=515nm).

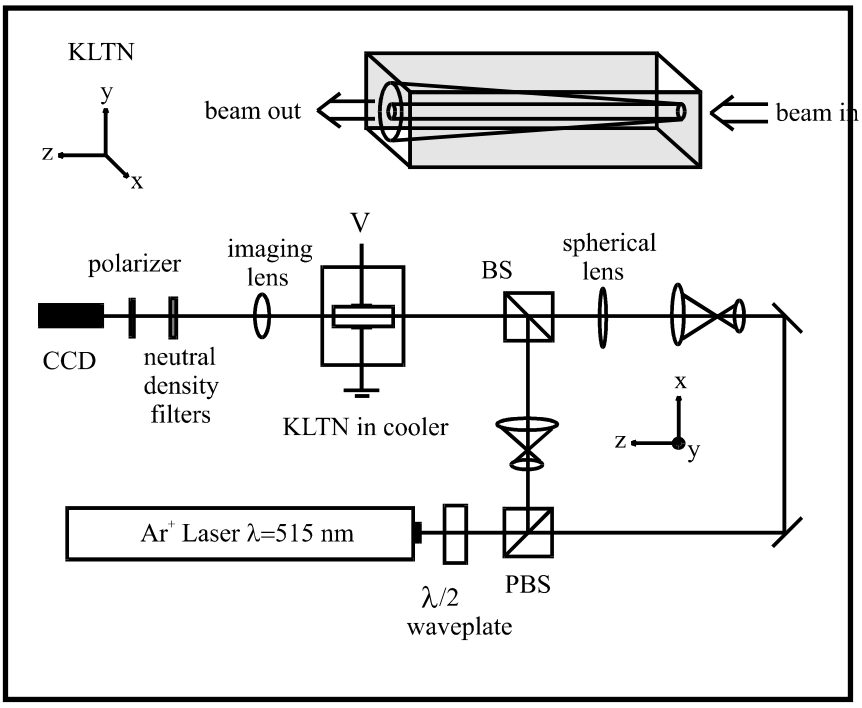

Fig.6.6: Experimental setup and configuration.

The basic setup is similar to previous experiments and is schematically illustrated in Fig.6.6. A single mode Argon ion laser operating at λ=515nm emits a y-polarized beam. This beam is sent through a $\lambda/2$ waveplate that rotates this polarization at an adjustable angle and is split into orthogonal polarized components by a polarizing beam splitter (PBS). The transmitted x-polarized beam (soliton beam) is first expanded and then focused by a 200 mm spherical lens onto the input face of the crystal. The reflected y-polarized beam serves as the background beam: it is first expanded and then recombined with the focused soliton beam (by means of a beamsplitter), so that these co-propagating beams experience the same absorption in the crystal (which makes stationary soliton-like propagation possible). The background beam is illuminating the crystal uniformly at all times. The beam at the input (with zero field applied) and the output (with and without field applied) faces of the crystal are imaged onto a CCD camera and recorded. The crystal is kept at a constant temperature T and a voltage V is applied between the x-faces of the crystal.

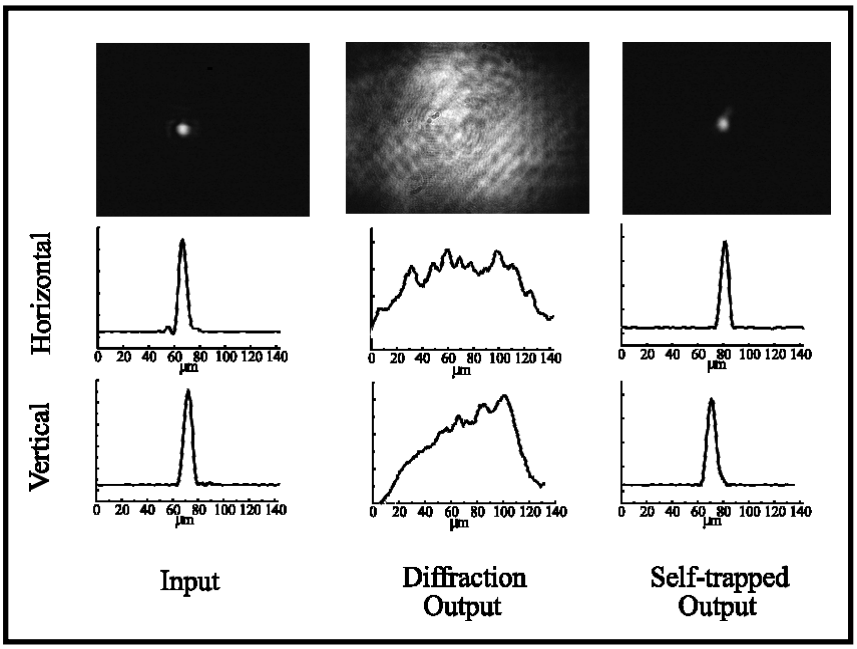

Fig.6.7: Photographs and profiles of input and output faces with and without applied voltage.

In Fig.6.7 we show typical experimental results. In this particular case, the intensity ratio (the ratio between the peak soliton intensity and the background intensity, u_0^2), is roughly 156 and a voltage of V≅1.15 kV has been applied, with T=29°C. The input beam, shown in the left column, has a intensity FWHM of 7 μm (equal in the horizontal and vertical directions) and, in absence of applied field, diffracts to approximately 90 μm (middle column, as expected from normal Gaussian beam propagation). When the appropriate field is applied, the beam self-focuses to 7 μm in the horizontal direction, and 8 μm in the vertical direction (right column). Note that the astigmatism is very small and is mostly in the tail of the vertical profile.

One dimensional spatial soliton formation occurs, as discussed previously, when the minimal set of soliton parameters satisfy a particular relationship, known as the soliton existence curve. Essentially, given a value of u_0^2, and an input beam width, at a fixed T, there is a restricted (rather narrow) range of values of applied voltage V that can give rise to solitary propagation solutions. Applied field values that are too low do not fully compensate for diffraction, whereas values that are too high try to transform the beam into a soliton that is much narrower than the incident beam, thereby leading to instability.

In analogy to the (1+1) D case, one can plot the soliton formation experiments on an existence curve that shows the soliton width (in normalized units) as a function of intensity ratio u_0^2. Since the theory of (2+1) D solitons in photorefractive centrosymmetric media is not available yet, we use the scaling of the existing (1+1) D theory. As in the (1+1) D case, ***two dimensional soliton formation is observed only for particular values of V, given a value of u_0 and a fixed input beam width***.

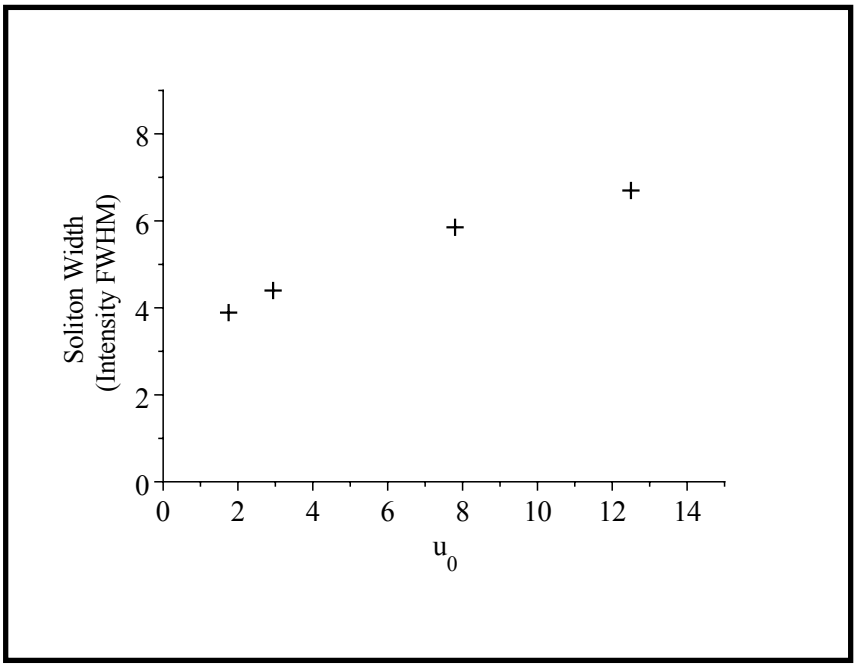

Fig.6.8: Experimental 2D soliton existence points. Solitons have been observed for T=29°C.

Figure 6.8 shows the experimental points in parameter space for which (2+1) D steady state solitons are observed. The vertical scale is the normalized soliton intensity FWHM (same in the x and y directions as circular self-trapping is observed) in units of $\Delta\xi = \Delta x/d$ where $d = (-2kb)^{-1/2}$, $b = (k/n_b)\left[(1/2)n_b^3 g_{eff}\varepsilon_0^2(\varepsilon_r - 1)^2(V/l)^2\right]$, and $k = 2\pi n_b/\lambda$, where λ is the wavelength, V is the applied voltage, and *l* the width of the crystal in the x direction. Existence points for low intensity ratios (u_0<1.5) are not available, as we were never able to get soliton formation in this range. ***This means that the nonlinearity must be***

saturated to support the formation of (2+1) D solitons. This is not too surprising, since at $u_0<<1$ the nonlinearity is in the Kerr limit, for which (2+1) D solitons are unstable (the beam undergoes catastrophic self focusing). This last issue resembles observations in SBN for which (2+1) D solitons are observed only for $u_0>1$, i.e., the nonlinear change in the refractive index must be in the saturation regime (albeit a different form of nonlinearity than in the present case) to support soliton propagation. This property is universal to all solitons in saturable nonlinearities, and is manifested here in an elegant way: the (2+1) D solitons can be observed only in the range at which they are truly stable. This is due to the inhomogeneities that are present in the crystal and introduce noise which can be "arrested" only when the nonlinearity is saturated and the waveguide induced by the soliton is multi-mode[8)].

REFERENCES:

[1] E.DelRe et al. Opt.Lett. 23, 421 (1998)

[2] E.DelRe et al. Appl.Phys.Lett. 73, 16 (1998)

[3] M.Segev and A.Agranat, Opt.Lett. 22, 1299 (1997)

[4] In contrast to ferroelectric screening solitons, in paraelectrics either bright or dark solitons can be observed, but not both.

[5] M. Segev, M. Shih and G. C. Valley, J. Opt. Soc. Am B **13**, 706 (1996).

[6] see, e.g., K. Kos, H. Ming, G. Salamo, M. Shih, M. Segev and G. C. Valley, Rapid Comm., Phys. Rev. E **53** , R4330 (1996)

[7] X. Tong, R. Hofmeister, M. Zhang, A. Yariv, A. Agranat and V. Leyva, Opt. Lett. 21, 1860 (1996).

[8] A.Snyder, D.Mitchell, and Y.Kivshar, Mod.Phys.Lett. B 9, 1479 (1995)

Chapter

7

Spatial Instability, Multisolitons, Speckle Self-Trapping, and Phase-Transition Nonlinear Material Effects

Introduction

In Chapters 4 and 6 spatial screening soliton formation was observed by fixing the relevant physical parameters so as to be close to the soliton existence curve. Here, experimental results are shown that clearly point out the onset of transverse spatial instability in centrosymmetric screening solitons, leading to the transition from a single 1+1D soliton particle to a regular array of 2+1D particles, for a given "nonsoliton" nonlinear regime. Furthermore, results showing a peculiar optical self-trapping of speckled beams are given. Finally, a brief summary of a possible explanation of the anomalies in the existence curve observed in centrosymmetric screening particles, discussed in Chapter 6, introducing in the screening model a first correction due to the material nonlinearity (nonlinear polarization), is discussed.

All three issues have, to date, *not* reached scientific maturity, and are thus only marginally discussed and no elaboration is provided. Attention is strictly concentrated on actual preliminary results.

Instability and Transition From a 1+1D Soliton to an Array of 2+1D Particles

Stability is a major issue in soliton science. In a purely mathematical perspective, it is *the* major issue. What is the use of finding a self-trapped solution to a more or less complicated nonlinear propagation equation if the solution is not stable, and thus not observable? From an experimental point of view, stability is a "self-solving" issue: if you observe self-trapped particles, they *must* be stable. This statement, however, should not lead to the absolutely incorrect idea that stability and instability analysis are not fundamental. Indeed, in order to get some hint as the nature of the complex nonlinear object we are observing, one type of analysis (analogous to a reductionist fission of a molecule) is to

destabilize it: study its instability. Furthermore, instability generally leads to the observation of very interesting phenomena, playing a role similar to highly dissipative boundary conditions that lead to actual manifestation of complexity. Spatial instability has been extensively studied by Zozulya, Mamaev and Saffman[1)] for noncentrosymmetric screening solitons based essentially on *local* numerical simulations. Here we show a similar result obtained in KLTN for a 1+1D spatial soliton simply by lowering the crystal temperature and "climbing" the dielectric anomaly.

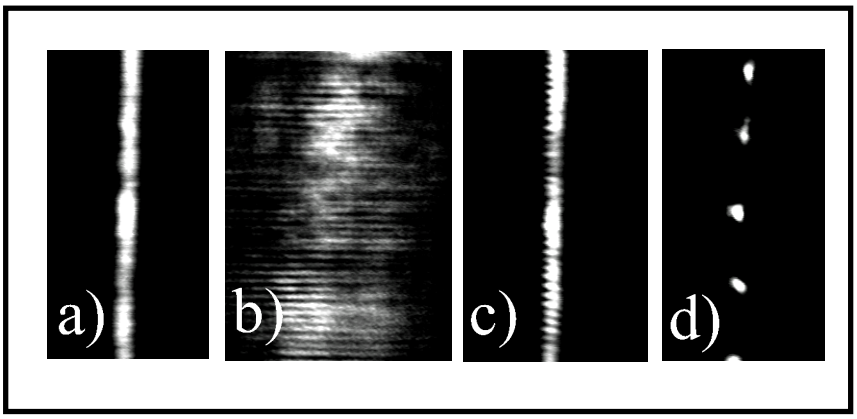

Fig.7.1: An initial 1+1D beam (a) diffracts for V=0 (b) and for V=360V forms a particle at T=28°C (c) that decays into a quasi-periodic array of 2+1D particles at T=23°C (d).

In Fig.7.1(a) is shown the input photograph of the 1+1D focused beam of 9μm Intensity FWHM. In the configuration described in Chapter 4, with the sample used in the 2+1D case, the beam diffracts (7.1(b)) with no applied field at T=28°C and for a u_0=4.2 it is self-trapped for an applied V=360V (7.1(c)). Decreasing the crystal temperature T to T=23.5°C, the final steady-state spatial output distribution is shown in Fig.7.1(d). The initial self-guided beam has split into a quasi-periodic array of self-trapped optical 2+1D pulses. The phenomenon has been explained in a local noncentrosymmetric numerical analysis as the spontaneous instability of the system with respect to a given transverse periodic spatial modulation (of period $\Lambda \approx 36\mu m$ in our case)[2)]. The onset of instability is believed to be caused by random noise present in the initial spatial distribution. The analogy with spatial structures observed in highly dissipative nonlinear systems is evident[2)].

Speckle Self-Trapping Phenomenology

In recent years much attention has been devoted to the investigation of so-called incoherent photorefractive screening solitons[3)]. The main qualitative feature that allows the trapping of light that randomly fluctuates in time for these phenomena is *temporal nonlocality*: the crystal response averages over fluctuations. The final soliton wave is not of course incoherent: it is a quite coherent wave that envelops this time averaged process. Essentially, the fluctuations and the nonlinear interaction occur at two separated temporal scales. Two questions arise naturally: 1) what happens when the scales are comparable? 2) what about spatial nonlocality?

The two questions are actually quite related in a particular situation which we shall briefly address. Most numerical and theoretical studies concerning spatial photorefractive screening solitons are based on local models (the screening model is in itself a local approximation). Photorefractive response, on the contrary, as discussed in Chapter 2, is also characterized by two transverse length scales. In particular, charge diffusion, much like diffusion in any other physical system, introduces a lower limit to the spatial components that can interact with the photorefractive charge separation. Thus, in analogy to temporal incoherent solitons, if we introduce a *spatial* modulation into the soliton beam with characteristic length scale L_f smaller than the diffusion length scale (Debye Length), that is $L_f << L_{Db}$, the nonlinear process should not *feel* this modulation. This is a mere rumination and further investigation will shed light on the process.

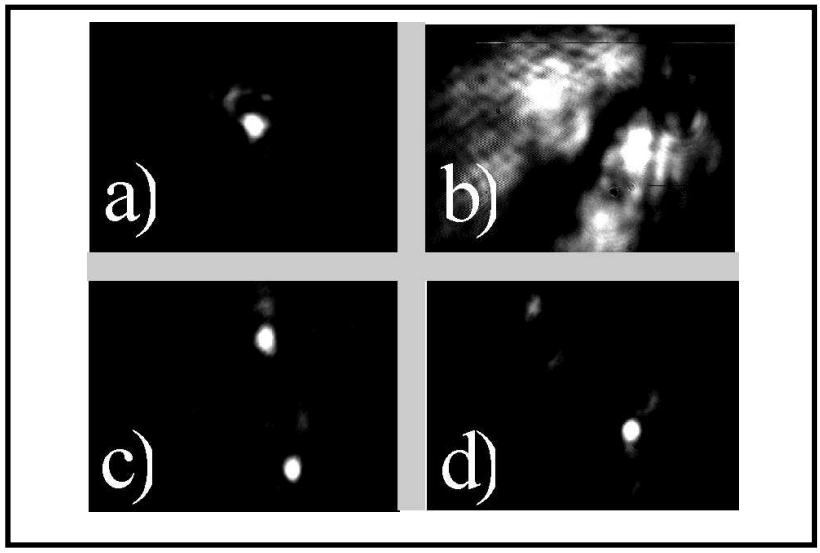

Fig.7.2: An initial 2+1D optical pulse (a) diffracts for V=0 (b) and for V=420V forms a two particle system (c) that traps into a single pulse at V=485V (d).

In Fig.7.2 are given preliminary results. The configuration is identical to that described in Chapter 6 in the 2+1D configuration, although now the focused beam is made to pass through a *speckled transparent glass plate*. The focused beam at the input is no longer a constant phase confined spatial pulse: it has a composite chirp. The actual structure of the phase profile depends on the size of the focusing lens, and can be imagined, approximately, as two different phase speckles imbedded in the one pulse. In slide 7.2(a) is shown the input pulse of 16μm intensity FWHM, and u_0=21, T=29°C. At V=0, the beam diffracts as shown in slide b). For an applied V=420V slide c) shows two distinct focused 2+1D particles. Finally at applied V=485V, slide d) shows that a single optical pulse has survived. These results seem to suggest, at least qualitatively, that trapping is occurring even in presence of the chirp, and that this may be due to spatial nonlocality. However, the observation of the intermediate steady-state regime of slide (c) might suggest that two single independent solitons form from the initial chirped pulse, and that these coalesce into one beam for a stronger nonlinearity.

Soliton Anomalies Induced by Material Nonlinearity

As described in Chapter 6, centrosymmetric screening solitons have been predicted in analogy to their noncentrosymmetric counterparts (see Chapter 3) observed

in SBN, $BaTiO_3$ and $KNbO_3$, substituting the linear Pockels effect present in noncentrosymmetric samples, with the quadratic electro-optic effect (dc Kerr effect). Experiments confirm their existence, and go further to demonstrate the stable existence of two-dimensional spatial self-trapping. Comparison to theory, however, reveals an anomalous behavior not contemplated in the initial model. Although agreement between theory and experiments for photorefractive screening solitons is hardly quantitative, yet one of the main qualitative characteristics, the fact that the soliton existence curve, that is, the set of points in the soliton peak amplitude-normalized width plane, is a "universal" single-valued curve, has always been confirmed. Centrosymmetric screening soliton experiments show that the existence curve manifests a peculiar dependence on crystal temperature not possibly contemplated in the standard model. Even more surprisingly, the experimental existence curve is more in disagreement with theoretical prediction the farther away the crystal is kept from the critical temperature, a circumstance that seems counterintuitive, as complicated material mechanisms are expected to come into play closer to the transition, not farther from it. Here we show how the nonlinear polarization response of the crystal in proximity of the phase-transition, complicating the Curie-Weiss dependence of the static crystal polarizability, allows soliton formation with a temperature dependent existence curve. This process breaks the existence curve "universality", enhancing the particular characteristics of the material in question, leaving a strong signature on soliton formation, represented by a new characteristic scale in the soliton nonlinear propagation equation.

Recalling that centrosymmetric screening solitons can be understood in the frame of the standard photorefractive model, also known as the Kukhtarev model, and the paraxial optical propagation wave equation, they can be intuitively thought of as stemming from diffraction compensation due to the electro-optical modulation of the crystal index of refraction induced by an internal space-charge field formed during the screening of an externally applied constant electric field on behalf of optically ionized impurity charges. In the ferroelectric 1+1D case, we have seen that when the optical beam is confined only in one transverse direction (for example the x direction) and propagates along the z direction, the nonlinear propagation problem leads to a saturated Kerr-like nonlinearity of the type $\Delta n \propto 1/(1+I/I_0)$, where I is the beam optical intensity and I_0 is the background crystal illumination. In the centrosymmetric case, this nonlinearity becomes, in the

standard model, $\Delta n \propto 1/(1+I/I_0)^2$, and qualitatively resembles the noncentrosymmetric screening soliton case.

The mechanism at the basis of screening solitons is the modulation of local crystal polarization induced by the light generated space-charge field. For temperatures deep in the ferroelectric phase, the relationship between polarization P and static electric field E is linear, that is $P=\varepsilon E$, where ε is the dielectric constant. Centrosymmetric solitons, on the other hand, make use of the enhanced dielectric response (dielectric anomaly) in proximity of the ferroelectric transition temperature. An external field can change the *thermodynamic equilibrium* of the crystal, effectively shifting the transition temperature. Since screening solitons stem from a point dependent internal electric field, the crystal will experience a different quasi-thermodynamic potential in different points, and thus will manifest a *local field induced change in the dielectric response*. This process inevitably breaks down the linear hypothesis and complicates the screening mechanism.

The free energy of the crystal A(P) can be approximated, in the stress-free case, as a function of the crystal polarization along a cubic direction (for example x direction) by

$$A(P) = (1/2)\chi P^2 + (1/4)\tilde{\xi} P^4 + (1/6)\zeta P^6 \ , \qquad (7.1)$$

where χ, $\tilde{\xi}$, and ζ are three material-dependent phenomenological, possibly temperature dependent, constants. The dielectric constant ε, as a function of the electric field $E=(\partial A/\partial P)$, defined as $\varepsilon=4\pi(\partial P/\partial E)$, can be approximated by

$$\varepsilon(E) = \varepsilon(0)(1 + 3\tilde{\xi} E^2 \varepsilon(0)^3 (4\pi)^{-3})^{-1} \quad , \qquad (7.2)$$

where

$$\varepsilon(0) = 4\pi/\chi = \varepsilon_0 C/(T - T_0) \qquad (7.3)$$

is the Curie-Weiss relationship discussed in Chapter 5, ε_0 is the vacuum dielectric constant, C and T_0 are phenomenological constants, and T is the crystal temperature. Thus, being the internal electric field dependent on the transverse variable x, i.e. E=E(x), we have that $\varepsilon=\varepsilon(x)$. Note that the constant $\tilde{\xi}$ is generally found to be a function of T, and that the above description is valid as long as the

spatial variations of E are such as to allow for a local thermodynamic description (through eq.(7.1)).

Limiting our analysis to the tractable 1+1D case, the quadratic electro-optic response of the crystal is

$$\Delta n(x) = -(1/2) n_b^{\ 3} g_{eff} \varepsilon_0^{\ 2} \varepsilon_r^{\ 2}(x) E^2(x) \qquad (7.4)$$

where n_b is the crystal background illumination, g_{eff} is the effective quadratic electro-optic coefficient and $\varepsilon=\varepsilon_0\varepsilon_r$.

The soliton self-consistent propagation problem is altogether identical to the known centrosymmetric screening problem described previously in Chapter 6 except that due to the spatial modulation of ε, the applied external field will generate, along with the normal separated charges $\rho_E = \varepsilon \nabla \cdot E$, polarization charges $\rho_P = E \cdot \nabla \varepsilon$. However, since in the standard description we are concerned with experimental configurations in which the direct influence of charge density can be neglected, the *screening theory still holds*. Assuming that the slowly varying amplitude A(x,z) of the optical field ($I = |A|^2$) be of the soliton form $A(x,z)=u(x)\exp(i\Gamma z)(I_d+I_b)^{1/2}$, where z is the direction of propagation, Γ is the soliton propagation constant, and I_d and I_b are respectively the dark and background irradiances, the internal normalized space-charge field is related to the normalized soliton amplitude u through

$$Y = -1/(1+u(\xi)^2) \qquad (7.5)$$

where $\xi=x/d$ is the transverse coordinate normalized to the quantity $d=(-2kb)^{-1/2}$, the characteristic length scale, and $b=(k/n_b)\Delta n_0$, the characteristic strength of the optical nonlinearity, where $\Delta n_0 = -(1/2) n_b^{\ 3} g_{eff} \varepsilon(0)^2 (V/L)^2$ (here g_{eff} is taken to be positive for a self-focusing medium such as KLTN) is the index of refraction change in the absence of light and without phase transition effects, being $k=2\pi n_b/\lambda$, λ the optical wavelength, V the applied voltage, L the width of the crystal in the direction of the electrodes (x direction), and $Y=E/(|V|/L)$.

The nonlinear propagation problem reduces in the 1+1D case to the following nonlinear propagation equation

$$\frac{d^2 u(\xi)}{d\xi^2} = -\left[\delta - \frac{(1+u(\xi)^2)^2}{((1+u(\xi)^2)^2+\alpha)^2}\right] u(\xi) \qquad (7.6)$$

where $\delta=\Gamma/b$ is determined by the boundary conditions, and $\alpha(V,T)=3\,\tilde{\xi}\,(\varepsilon(0)/4\pi)^3(V/L)^2$. The parameter α is dependent on temperature both through the dependence of $\varepsilon(0)$ (see eq.(7.3)) and through the dependence of $\tilde{\xi}$ on T. Physically, α is the relative change in dielectric constant induced by the applied constant field at a given T, since from eq.(7.2) we have $\Delta\varepsilon/\varepsilon\cong-\alpha$. It is important to note that through $\tilde{\xi}$ the whole problem becomes *material dependent*, it playing a role analogous to g_{eff}. In particular its sign is crucial, as its contribution can play a "focusing" role, or a "defocusing" one. Specifically, for first order phase transitions, $\alpha<0$ (being $\tilde{\xi}<0$) and the focusing is enhanced, whereas for second order ones, $\alpha>0$ (being $\tilde{\xi}>0$) and the interaction tends to have a defocusing effect. For $\alpha=0$ eq.(7.6) reduces to the centrosymmetric screening soliton equation.

In order to formally close the self-consistent approach, we must relate the value of δ in eq.(7.6) to the boundary conditions, integrating eq.(7.6) by quadrature and imposing the conditions $u'(0)=u(\infty)=u'(\infty)=u''(\infty)=0$ pertaining to bright solitons, and defining $u_0=u(0)$, we obtain the final expression for δ

$$\delta=\frac{1}{2u_0^{\,2}}\left[\frac{1}{\alpha+1}-\frac{1+u_0^{\,2}}{\alpha+(1+u_0^{\,2})^2}+\frac{1}{\sqrt{\alpha}}\,\mathrm{ArcTan}\left(\frac{1+u_0^{\,2}}{\sqrt{\alpha}}\right)-\frac{1}{\sqrt{\alpha}}\,\mathrm{ArcTan}\left(\frac{1}{\sqrt{\alpha}}\right)\right] \tag{7.7}$$

which is valid for $\alpha>0$, but formally holds also for $\alpha<0$. Explicitly, the $\alpha<0$ case gives

$$\delta=\frac{1}{2u_0^{\,2}}\left[\frac{1}{\alpha+1}-\frac{1+u_0^{\,2}}{\alpha+(1+u_0^{\,2})^2}+-\frac{1}{\sqrt{-\alpha}}\,\mathrm{ArcTanh}\left(\frac{1+u_0^{\,2}}{\sqrt{-\alpha}}\right)+\frac{1}{\sqrt{-\alpha}}\,\mathrm{ArcTanh}\left(\frac{1}{\sqrt{-\alpha}}\right)\right]. \tag{7.8}$$

This formally closes the self-consistent propagation problem.

Numerical integration of eq.(7.6) with eq.(7.7) (or 7.8) gives trapped soliton particles with an existence "point" in the (u_0, $\Delta\xi$, α) space, i.e. a temperature dependent existence curve. This model has yet to be pitted against experimental observations, but is has the advantage of showing how a nonlinear phase-transition process can easily modify even the basic qualitative foundations of screening solitons.

REFERENCES:

[1] A.Mamaev, M.Saffman, and A.Zozulya, Phys.Rev.Lett. 76, 2262 (1996)

[2] *Exploring Complexity. An Introduction*, I.Prigogine and G.Nicolis (R.Piper GmbH & Co. KG, Monaco 1987)

[3] see refs. [90]-[93] in Crosignani et al. , Riv.Nuov.Cim. 21, 6.

Chapter

8

Nonlinear Diffraction Effects and Solitons due to Anisotropic Charge-Diffusion based Self-Interaction

Introduction

In Chapters 4,6, and 7 solitons supported by the screening interaction have been amply discussed and clarified. This Chapter is dedicated to the description of an entirely different class of nonlinear phenomena connected to optical self-interaction mediated by the *charge-diffusion* process in nonpolar ferroelectrics in *close* proximity of the dielectric anomaly, first predicted and experimentally demonstrated in 1998 by Crosignani, Degasperis, DelRe and DiPorto.[1)]

Physical Model and 1+1D Case

In the screening mechanism, the inherently asymmetric internal space-charge diffusion field (see Chapter 2) $\mathbf{E}_{SC}=-(K_BT/e)\nabla[\ln(I+I_d)/I_d]$, where I is the optical intensity and I_d is the dark irradiance of the crystal, plays a *negligible role*, leading to self-bending[2)].

In Chapters 5 and 6 we discussed propagation in centrosymmetric photorefractive crystals with quadratic (but not linear) electro-optic effect. In this case, since the nonlinear refractive index contribution for unbiased centrosymmetric crystals is proportional to the square of $\mathbf{E}_{SC}$, *its asymmetry is no more relevant* and it is natural to look for the existence of self-confined propagating beams with no self-bending. Here, we discuss the general 1+1D propagation equation in unbiased centrosymmetric PR crystals and demonstrate the existence of such solutions, in the form of both self-confined and self-focused beams.

In centrosymmetric media the photoinduced change of refractive index is given by $\Delta n=-(1/2)n^3 g\varepsilon_0^2(\varepsilon_r - 1)^2 E_{sc}^2$, where n is the unperturbed refractive index of the crystal, g the effective quadratic electro-optic coefficient and ε_r the low-frequency dielectric constant. As done in Chapter 6, this

expression can be inserted into the parabolic wave equation (see Chapter 2)

$$[\mathrm{i}\frac{\partial}{\partial z}+\frac{1}{2k}\frac{\partial^2}{\partial x^2}]A+\frac{k}{n}\Delta nA=0 \quad , \tag{8.1}$$

describing the evolution of the slowly-varying amplitude A of the propagating optical field $E_{opt}=A(x,z)\exp(ikz-i\omega t)+c.c.$, where $k=n\omega/c$. Proceeding in this way we obtain

$$(\mathrm{i}\frac{\partial}{\partial \zeta}+\frac{\partial^2}{\partial \xi^2})A+\gamma\frac{(\partial|A|^2/\partial\xi)^2}{|A|^4}A=0 \quad , \tag{8.2}$$

where $\zeta=kz$, $\xi=\sqrt{2}kx$, and $\gamma=-n^2k^2g\varepsilon_0^2(\varepsilon_r-1)^2(K_BT/e)^2$. This model equation applies if we neglect the dark irradiance I_d with respect to the intensity $I=|A|^2$, a condition which obviously requires the peak intensity I_0 to be much larger than I_d. We note that, because of the structure of Eq.(8.2), the influence of the loss term $i\alpha A$, which has been omitted, can always be accounted for by multiplying its solutions by $\exp(-\alpha\zeta)$. Moreover, if $A(\xi,\zeta)$ is a solution, then also $aA[p(\xi-\xi_0),p^2(\zeta-\zeta_0)]$ solves Eq.(8.2) for arbitrary real p, ξ_0, and ζ_0 and complex a. This property, which is valid, as far as the relative scaling between longitudinal and transverse coordinates is concerned, also if I_d is not neglected, implies that localized solutions corresponding to self-guided propagation (when they exist, see below) **cannot possibly obey a peak amplitude-width relation** (the so-called *existence curve*) as in the case of Kerr-type or ordinary photorefractive solitons described in previous Chapters.

Self-Focusing and Diffusion-Driven 1+1D Solitons

In order to solve Eq.(8.2), it is expedient to introduce the new independent variable B through the transformation $A=B^{\mu}$, where $\mu=1/(1+4\gamma)$. Different types of solutions of Eq.(8.2) can then be associated with the sign of the parameter μ. Let us first consider the case $\mu>0$, i.e., $\gamma>-1/4$. A particular solution of Eq.(8.2) reads

$$A(\xi,\zeta)=\frac{A_0\exp[i\phi(\xi,\zeta)]}{(1+16\zeta^2/\mu\delta^4)^{1/4}}\exp[-\frac{\xi^2}{\delta^2(1+16\zeta^2/\mu\delta^4)}]$$

$$x(H_n[(2/\mu)^{1/2}\frac{\xi}{\delta(1+16\zeta^2/\mu\delta^4)^{1/2}}])^{\mu} \quad , \qquad (8.3)$$

where A_0 and δ are arbitrary parameters fixed by the $\zeta=0$ boundary beam-profile, H_n are the Hermite polynomials and

$$\phi(\xi,\zeta)=\frac{4\zeta\xi^2}{\mu\delta^4(1+16\zeta^2/\mu\delta^4)}+$$
$$-\mu^{1/2}(n+1/2)\,\mathrm{arctg}(4\zeta/\mu^{1/2}\delta^2) \quad . \qquad (8.4)$$

Solution (8.3)-(8.4) describes nonlinear diffraction leading to Gaussian self-focusing. In the limiting case $\mu\to\infty$, that is for $\gamma=-1/4$, for all even values of n there is *no diffraction* since these solutions take all the same Gaussian expression (*Gaussian Solitons*)

$$A(\xi,\zeta)=A_0\exp[-2i(1+2n)\zeta/\delta^2]\cdot$$
$$\exp[-(1+2n)\xi^2/\delta^2)] \quad . \qquad (8.5)$$

From an experimental point of view, the most relevant solution of the kind given in Eq.(8.3) corresponds to n=0 (i.e., H_0=1); in fact, in this case the boundary condition has a Gaussian form and can be easily imposed. Referring to this situation, it is important to note that μ larger than unity (i.e., -1/4<γ<0) gives rise to *nonlinear self-focusing* while μ smaller than unity (i.e., γ>0) leads to *defocusing* with respect to linear diffraction corresponding to μ=1 (γ=0). For the very special value γ=-1/4, the solution has the expression given by Eq.(8.5) with n=0.

For comparison, we note that nondiffracting nonstationary solutions, analogous to those found in ref.[2] for noncentrosymmetric crystals, exist also in our case and read

$$A(\xi,\zeta) = A_0 \exp\{-i[\eta\zeta(\xi + 2\eta\zeta^2/3)]\} \cdot [\mathrm{Ai}\left((\eta/\mu)^{1/3}(\xi + \eta\zeta^2)\right)]^{\mu} \tag{8.6}$$

where Ai(x) is the Airy function and η is a free parameter that is related to its main width .

Let us now consider the case μ<0 (i.e., γ<-1/4). In this case, particular solutions in the form of solitary waves (*Diffusion-Driven Solitons*) are

$$A(\xi,\zeta) = A_0 \exp[i(\chi\xi - \beta\zeta)] \cdot \left[\frac{1}{\cosh[(\beta/|\mu|)^{1/2}(\xi - 2\chi\zeta)]}\right]^{|\mu|}, \tag{8.7}$$

where χ is a constant that depends on the phase modulation at the boundary ζ=0 and is responsible for the beam transverse displacement at a constant rate 2χ, and β relates to signal width.

A class of solutions can also be obtained by Eq.(8.3) through the substitution $\mu \rightarrow -\mu$. However, because of the negative value of μ, the Hermite polynomials in Eq.(8.3) now appear in the denominator and, therefore, their zeros are singularities in the variable ξ of the solution. This implies that the only physically acceptable solutions are obtained for *even* degree polynomials, i.e., for n=2m. For instance, the one associated with H_0 is

$$A(\xi,\zeta) = \frac{A_0 \exp[-i\phi(\xi,\zeta)]}{(1-16\zeta^2/|\mu|\delta^4)^{1/4}} \cdot \exp[-\xi^2/\delta^2(1-16\zeta^2/|\mu|\delta^4)], \quad (8.8)$$

where

$$\phi(\xi,\zeta) = \frac{4\zeta\xi^2}{|\mu|\delta^4(1-16\zeta^2/|\mu|\delta^4)} + \frac{|\mu|^{1/2}}{4}\ln\left[\frac{\delta^2|\mu|^{1/2}+4\zeta}{\delta^2|\mu|^{1/2}-4\zeta}\right]. \quad (8.9)$$

This solution corresponds to a self-focusing process leading to *catastrophic collapse*, unless the propagation distance is limited to values such that $\zeta < \delta^2|\mu|^{1/2}/4$.

The possibility of explicitly finding the above analytic solutions is based on the neglecting of the dark irradiance I_d (as, for example, done in Ref.[2]). Actually, if I_d is not neglected, it is possible to show that, strictly speaking, *no localized solitary wave solutions exist*. In order to evaluate the influence of the beam tails, where I is inevitably comparable with I_d, we have performed a numerical 1+1D propagation. For the typically large values of I_0/I_d usually present in most experimental situations, the solutions are by all practical means indistinguishable from the ones pertaining to the exact model

over the transverse width of the crystal and for typical crystal lengths.

Let us now discuss the possibility of experimentally observing the nonlinear propagation effects predicted by the above analytical results. In a standard experimental configuration, a polarized argon ion laser beam operating at, for example, $\lambda=\omega/c=515nm$ is focused by means of a cylindrical lens onto the input face of a zero-cut sample, so as to propagate parallel to it. The beam is polarized in a plane orthogonal to the lens axis (along the confined direction). In order to evaluate the feasibility of observing self-focusing and eventually self-trapping, we have to evaluate the order of magnitude of Δn (see Eq.(8.1)), which has to be large enough to provide beam guidance. In our case, the nonlinear index modulation is determined, for a given crystal temperature T, only by the size (and eventually shape) of the input beam. No external parameters, such as intensity ratio (as long as $I_0>>I_b$) or external voltage, are present. In particular, the index modulation, for a fixed T, is given by $\Delta n = |\gamma| n/(2k^2)[d(lnI)/dx]^2= |\gamma| n/(2k^2)4x^2/w^4$, where we have assumed $I=I_0exp(-x^2/w^4)$ (see Eq.(8.5)) . The index change between x=0 and x=2w gives thus rise to an effective $\Delta n = 16|\gamma| n/2k^2w^2$. For the special value $|\gamma|=1/4$ we have, for $w=6\mu m$ (corresponding to a $10\mu m$ intensity full-width half-maximum), $\Delta n=1.6x10^{-4}$ which is in the range of values able to provide *linear* waveguiding. We underline, as already mentioned, *that no existence curve is present* but rather the crystal parameters have to be such as to produce the appropriate values of γ. Considering typical parameter values, such as $n \cong 2.4$, $g \cong 0.15m^4C^{-2}$, and $(K_BT/e) \cong 26mV$ at room temperature, we need very high values of ε_r in order to reach the necessary order of magnitude. Such values are only attainable in particular paraelectric materials *close to the ferroelectric phase transition* (see Chapter 5). For example, samples of SBN[3)] can have values of $\varepsilon_r \cong 2x10^4 \div 8x10^4$ for $T\cong125 \div 140°C$ and one can expect to be able to observe significant diffusion-driven nonlinear diffraction compensation (the effective Δn ranges in this case between $1.8x10^{-5}$ and $2.7x10^{-4}$). In the next section we shall discuss experiments carried out in a sample of paraelectric KLTN, in which actual trapping is **not** obtained, but significant nonlinear dynamics are observed (as described below).

Returning to Eq.(8.2), the predicted nonlinear behavior depends on the light input conditions and the value of the parameter μ. For the above mentioned configuration, the input beam is an unchirped focused 1D Gaussian beam. For the mentioned case of paraelectric SBN, γ takes values from approximately -0.03 to -0.5, so that positive values of μ larger than approximately 1.1 and negative values less than -1 are possible. This means that, in principle, *self-focusing* described by Eq.(8.3) (with n=0), *Gaussian solitons* described by Eq.(8.5) (again with n=0) and *hyperbolic solitons* described by Eq.(8.7) (with χ=0) can be observed (although no such measurement has to date been reported).

Full 2+1D model: Noncircular Diffusion-Driven Solitons and Anisotropy-Induced Beam Aspect-Ratio Locking

Here, we investigate theoretically nonlinear propagation of a localized optical beam in a ferroelectric heated above the Curie temperature, as described in the previous section, but extended to the general 2+1D configuration, predicting anisotropic diffraction and trapping. The basic relevant physical model, introduced in the previous section in the 1+1D case, common to all standard doped ferroelectrics, produces in the extended 2+1D case *the first natural realization of a higher-order anisotropic nonlocal logarithmic-type nonlinearity which remarkably allows a direct nonperturbative analytical treatment*. The model equation allows the interpretation of the phenomena observed (and reported on below) and furthermore supports what is the first class of two-dimensional solitary waves, in the form of noncircular spatial solitons, *without characteristic transverse length scale*.

The full 2+1D parabolic paraxial equation describing monochromatic propagation is

$$[\mathrm{i}\frac{\partial}{\partial z} + \frac{1}{2k}(\frac{\partial^2}{\partial x^2} + \frac{\partial^2}{\partial y^2})]A_i(x,y,z) + \frac{k}{n}\Delta n_{ij}A_j(x,y,z) = 0 \qquad (8.10)$$

where **A**(x,y,z) is the slowly varying amplitude of the optical field $\mathbf{E}_{opt}=\mathbf{A}(x,y,z)\exp(ikz-i\omega t)$ + c.c., and $k=n\omega/c$. Equation (8.10) assumes a *scalar form* for a large class of ferroelectrics above the Curie temperature. For example, for perovskite-type compounds (like KLTN), the symmetry is m3m[3] and only two relevant independent electro-optic coefficients, that is $g_{xxxx}=g_{11}$ and $g_{xxyy}=g_{12}$, are nonzero.[4] This is equally true for symmetry classes 2m, 222, mmm, 422, 4mm, $\bar{4}$2m, 4/mm, 23, m3, 432, and $\bar{4}$3m, if polarization coupling through the g_{xyxy} term is again negligible. We limit our analysis to positive values of g_{11} and g_{12} occurring in perovskites (like KLTN), although the treatment can be extended to negative values, in which case defocusing plays an important role. Hence, for an input x-polarized beam, Eq.(8.10) is reduced to the scalar form

$$[i\frac{\partial}{\partial\zeta}+(\frac{\partial^2}{\partial\xi^2}+\frac{\partial^2}{\partial\eta^2})]A+[\gamma_1(\frac{\partial|A|^2/\partial\xi}{|A|^2})^2+\gamma_2(\frac{\partial|A|^2/\partial\eta}{|A|^2})^2]A=0 \tag{8.11}$$

where $A=A_x$, $\gamma_1=-k^2n^2\varepsilon_0^2(\varepsilon_r-1)^2g_{11}(K_bT/e)^2$, $\gamma_2=-k^2n^2\varepsilon_0^2(\varepsilon_r-1)^2g_{12}(K_bT/e)^2$, and we have introduced the dimensionless variables $(\xi,\eta)=\sqrt{2}\,(kx,ky)$, $\zeta=kz$. Equation (8.11) represents the scalar anisotropic diffusion-driven nonlinear propagation equation, an extension of eq.(8.2). *Anisotropy* is contained in the fact that in general $\gamma_1\neq\gamma_2$, whereas nonlocality is contained in the derivative in the nonlinear source, typical of any diffusion-based process. The form of the nonlinear term, the square of a logarithmic derivative, allows for a number of explicit solutions, all independent of the beam peak intensity I_0, already discussed in the 1+1D case. We limit our investigation to two classes corresponding, respectively, to nonlinear diffraction and self-trapping. The first one reads

$$A(\xi,\eta,\zeta)=\frac{A_0}{(p_1p_2)^{1/4}}\exp(-\xi^2/d_1^2p_1-\eta^2/d_2^2p_2)\exp[i\phi(\xi,\eta,\zeta)] \tag{8.12}$$

where $d_{1,2}$ are the input (normalized) widths in the x,y directions, $p_{1,2}=[1+b_{1,2}(\zeta-\zeta_{1,2})^2]$ with $b_{1,2}=16(1+4\gamma_{1,2})/d_{1,2}^4$ and $\phi(\xi, \eta, \zeta)= (p'_1\, \xi^2/ p_1 + p'_2\, \eta^2/ p_2) / 8 -(2 / d_1^2\, b_1^{1/2}) \arctan[b_1^{1/2}(\zeta - \zeta_1)]-(2 /d_2^2\, b_2^{1/2}) \arctan[b_2^{1/2}(\zeta - \zeta_2)]$ (the prime standing for derivative with respect to ζ). It is valid for values of $0>\gamma_{1,2}>-1/4$ and describes nonlinear anisotropic self-focusing in the two transverse dimensions x and y. When a Gaussian beam is focused onto the z=0 plane, we deduce from Eq.(8.12) that its ellipticity Λ, evolves as

$$\Lambda(\zeta) = \frac{d_2}{d_1}\frac{\left[1 + b_2(\zeta - \zeta_2)^2\right]^{1/2}}{\left[1 + b_1(\zeta - \zeta_1)^2\right]^{1/2}} \quad . \qquad (8.13)$$

For $(\zeta-\zeta_{1,2})^2>>1/b_{1,2}$, $\Lambda(\zeta)$ tends to the asymptotic value $\Lambda_\infty=[1/\Lambda(0)][(1+ 4\gamma_2)/(1+ 4\gamma_1)]^{1/2}[(1+ b_2\zeta_2^2)/(1+ b_1\zeta_1^2)]^{1/2}$, that depends on the input ellipticity (and eventually astigmatism) and the crystal temperature T. Whenever $[(1+ b_2\zeta_2^2)/(1+ b_1\zeta_1^2)]^{1/4}[(1+ 4\gamma_2)/(1+4\gamma_1)]^{1/4}=\Lambda(0)$, the input ellipticity is recovered and maintained as a result of the nonlinear interaction. From Eq.(8.12), it also obvious that 2+1D Gaussian diffusion-driven solitons (both cylindrical and elliptical) would only be possible when diffraction is isotropically compensated both in the x and y direction, that is when both $\gamma_1=-1/4$ and $\gamma_2=-1/4$, a circumstance that requires $g_{11}=g_{12}$ (while, in general, $g_{11}>g_{12}$). Therefore, unlike the 1+1D case, treated in the previous section, diffusion-driven scalar Gaussian solitons are *not* generally possible. Note that when $d_1=d_2$, the model predicts (see Eq.(8.13) and the expressions of $b_{1,2}$ after Eq.(8.12)) beam evolution toward an asymmetric Gaussian profile with ellipticity $\Lambda_\infty= [(1+ 4\gamma_2)/(1+ 4\gamma_1)]^{1/2}$, a signature of the strong anisotropy of the physical system.

Thus the first class of solutions describes analytically anomalous anisotropic self-induced diffraction and, in

particular, allows for the description of the observed beam aspect ratio evolution, described in the next section.

The second class of solutions of Eq.(8.11) , valid for $\gamma_1 < -1/4$ and $\gamma_2 < -1/4$, reads

$$A(\xi,\eta,\zeta) = A_0 \exp(-i(\alpha_1^2\beta_1^2 + \alpha_2^2\beta_2^2)\zeta)\left(\frac{1}{\cosh(\beta_1\xi)}\right)^{\alpha_1^2}\left(\frac{1}{\cosh(\beta_2\eta)}\right)^{\alpha_2^2} \tag{8.14}$$

where $\alpha_1^2 = -1/(1+4\gamma_1)$, $\alpha_2^2 = -1/(1+4\gamma_2)$ and β_1 and β_2 are arbitrary parameters. This represents a class of nongaussian self-trapped solutions in the form of *noncircular 2+1D spatial solitons*. These solutions, although feasible (unlike Gaussian solitons), have not been observed in KLTN (see discussion below). They are singular in that they do not obey any sort of light-dependent existence curve: they exist for arbitrary values of β_1 and β_2, and are determined solely by the actual proximity to the dielectric anomaly. *They have no characteristic length scale*, as their 1+1D counterparts. Stability analysis can be carried out along the lines introduced in Ref.[4], extending the 1D treatment to the 2D case considering the separability of eq.(8.11). Thus, if l_p is the characteristic length scale of the perturbation, and l_x and l_y are those of the soliton, stability can be demonstrated when $l_{x,y} >> l_p$. Solitons exist **only** when self-trapping is present in **both** transverse directions. Given β_1 and β_2 , the trapped ellipticity reflects the ratio of the strength of the nonlinearity in the two directions.

Experimental Observation of Intensity Independent Self-Focusing and Beam-Aspect Ratio Recovery and Conservation in Near-Transition Unbiased KLTN

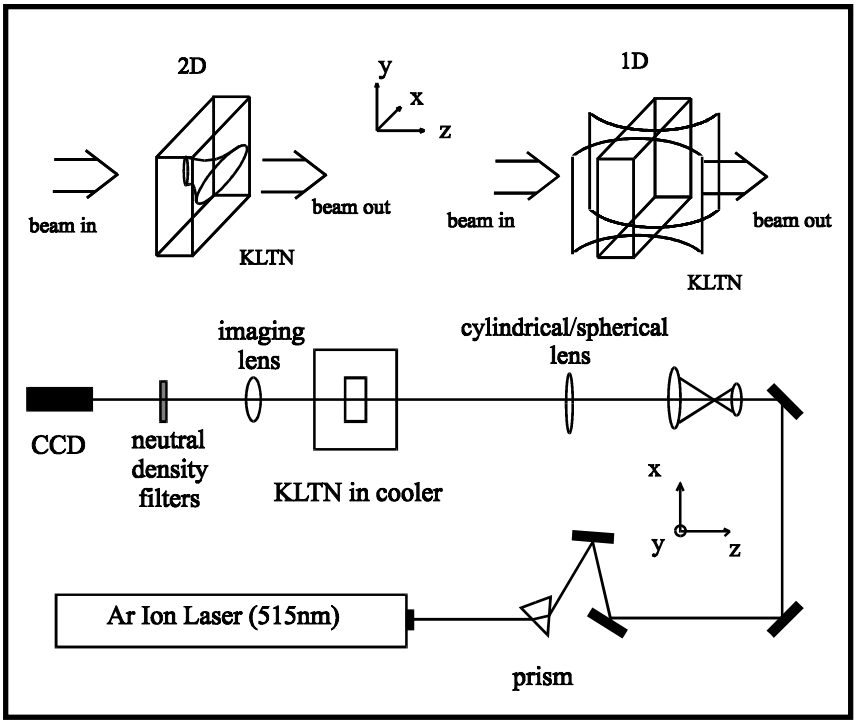

Fig.8.1: Experimental setup.

Experiments are carried out making use of the setup schematically illustrated in Fig.8.1, similar to those discussed in Chapters 4 and 6. The first experiment performed consisted in launching into a sample of KLTN a 1D Gaussian beam and observing its diffraction at the output facet. The input beam, a TEM_{00} λ=515nm polarized (along the x direction) beam from a CW Argon ion laser, is focused onto the input facet of the sample by means of a cylindrical lens with f=150mm (and axis parallel to the y direction). The sample of KLTN (already used in Chapter 6) measures $3.7^{(x)}x4.6^{(y)}x2.4^{(z)}$ mm, being zero-cut and polished along its cubic axes. The crystal is doped with Cu and V impurities and manifests its dielectric anomaly at T_c=9.8°C (decreasing temperature loop) passing from the room temperature cubic

paraelectric phase to the noncentrosymmetric ferroelectric phase. Input beam profile and output diffraction along the z-direction (direction of propagation) was monitored by means of an imaging lens (f=60mm) and a CCD camera. The crystal temperature was controlled via a Peltier junction in thermal contact with the crystal. In this configuration the input light distribution (a slab of light) has an input full-width-half-maximum (FWHM) of 13μm (in the confined x direction). When the crystal is kept at room temperature (T=20°C) the beam diffracts to 22μm, as expected from linear Gaussian diffraction with a crystal index of refraction n=2.4. Lowering the crystal temperature towards T_c considerable self-focusing was observed, as shown in Fig.8.2, from 22μm to 17μm.

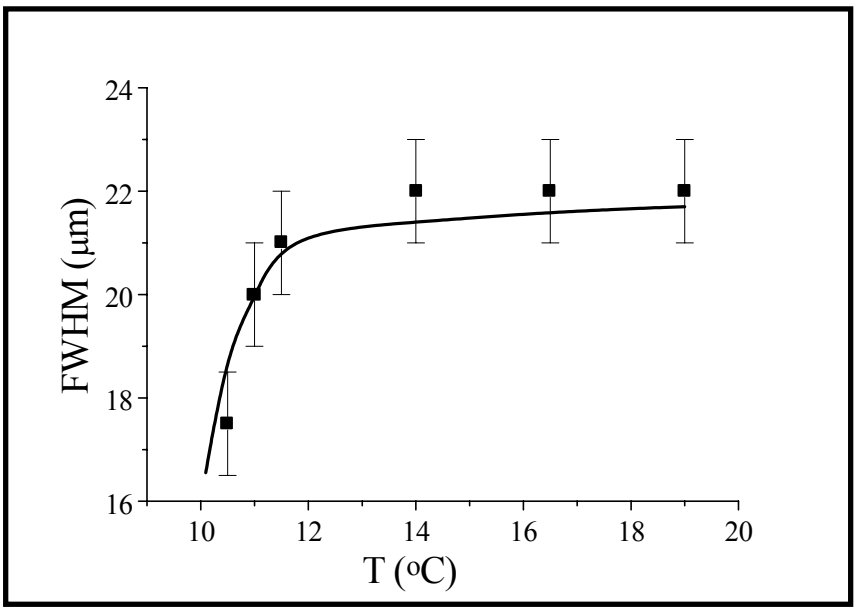

Fig.8.2: Values of output beam FWHM in the 1+1D configuration compared to diffusion-driven self-focusing theory.

At even lower temperatures, as the critical regime was reached, domain formation and strong beam distortion was observed (first domain enucleation in the investigated crystal region was observed at 10.0-10.2°C). Heat transfer occurred only through the bottom facet of the crystal which was therefore not uniformly thermalized during the experiment, presenting a transverse temperature gradient (especially at low values of T). Our observations refer to a limited transverse (in the xy plane) region of the crystal (about 200x200 μm) where the effect of the gradient was negligible. The peak beam intensity used was of the order of $I_0 \approx 10^2$

W/cm^2 , at the crystal input face (spurious background illumination was at least four orders of magnitude less intense). The experiment was repeated for higher values of I_0 (up to ten times more intense), but no appreciable difference was observed, other than in the duration of the transient build-up regime. Next, 2+1D propagation in this same configuration was investigated. The cylindrical lens was substituted with a spherical one and, at the input facet of the crystal, a highly confined circular Gaussian beam was launched. At the output, Gaussian linear propagation was observed for room temperature, but as the crystal was cooled into the near-transition regime, a peculiar beam deformation leading to a beam with *elliptical* transverse intensity profile was observed. The beam manifested self-focusing in the x direction, parallel to the beam polarization (which did not suffer any rotation). Thus, introducing a prism (as shown in Fig.8.1) before the beam expander, an asymmetric elliptical, approximately stigmatic, Gaussian beam was launched into the crystal and diffraction as a function of temperature was investigated. Results are shown in Fig.8.3.

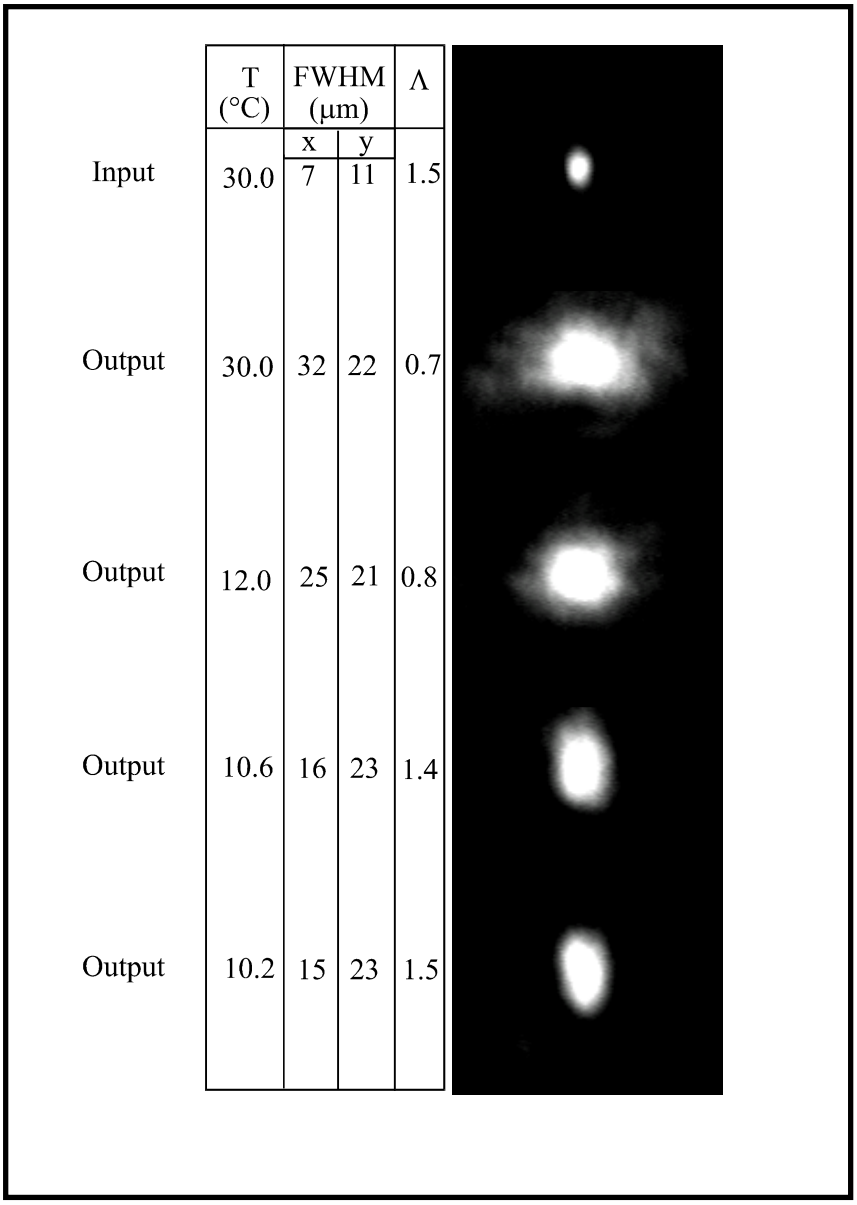

Fig.8.3: Photographs of the beam at input and output facets of the crystal. Decreasing the crystal temperature the input ellipticity is recovered.

The input beam, with intensity $FWHM_x$=7μm and $FWHM_y$=11μm, has an input ellipticity $\Lambda=(FWHM_y/FWHM_x)$=1.5. For high values of temperature, at which beam propagation is linear (from approximately 15°C **upwards** diffusion has a negligible effect), the typical "inversion" of ellipticity at the output of the crystal, from 1.5 to 0.7, was observed, this being a consequence of standard diffraction (stronger confinement, stronger diffraction). As the crystal temperature was lowered, an evolution of the output

ellipticity towards a *higher value* was observed. At approximately T=10.2°C the input ellipticity was recovered, as shown in Fig.8.3, the beam maintaining its Gaussian transverse profile. Input laser power was adjusted in order to have a peak intensity comparable to the 1+1D case and again the experiment was repeated for various values of I_0 observing no appreciable difference in the final stationary configuration.

Discussion

In order to test the quantitative agreement between theory and experiment we must evaluate the values of γ_1 and γ_2 as a function of T. The beam astigmatism was negligible in the 2+1D configuration ($\zeta_1=\zeta_2=0$). The principal dependence of the γ_i (i=1,2) on temperature is through ε_r , that is greatly enhanced as the temperature is lowered towards T_c . In proximity of the phase-transition the bulk dielectric crystal response is smeared-out by the temperature gradient and other large-scale crystal inhomogeneities and values of ε_r will in general be far lower than actual "local" crystal values. For temperatures where these effects have a negligible effect (T>12°C with the setup) we are able to fit bulk ε_r values with the Curie-Weiss law, with $C=1.3\text{x}10^5$(°C) and T_0=6.2°C. The peak value of ε_r actually measured directly (in the capacitance experiment) was approximately $3\text{x}10^4$. For values of T closer to T_c we measured directly the local (for the transverse regions of about 200x200 μm^2) electro-optic index modulation by inserting the sample in one arm of a Mach-Zehnder interferometer. With the polarization parallel to the applied external field, the measurements allowed the evaluation of γ_1 : with the polarization orthogonal to the applied field we determined the value of γ_2 . In the out-of-transition range, this allows also a measurement of $g_{11}=0.12 m^4C^{-2}$ and $g_{12}=0.02 m^4C^{-2}$ (taking g>0 in KLTN, having independently measured ε_r). Measured values of γ_1 are listed in Tab.8.1 for near-transition temperatures. The listed values are higher than those expected from the Curie-Weiss relationship, and this can be phenomenologically attributed to an increase in the value of g_{11}, as the quadratic dependence of Δn still held for low applied voltages (V<250V). Values of γ_2 where such as to induce no appreciable diffusion-driven effects, remaining its value always more than five times smaller (in absolute value) than the corresponding values of γ_1 for the temperatures investigated. In Fig.8.2 the solid curve represents the theoretical curve obtained from Tab.8.1 for the

1+1D case (i.e. Eq.(8.3) with n=0). The quantitative agreement is satisfactory, although the strong focusing for temperatures very near T_c may indicate that here some different mechanism is playing an important role. For ellipticity recovery in the 2+1D case we recover the input ellipticity $\Lambda(0)=1.5$ at T=10.2°C (see Fig.8.3). The 2+1D theory predicts that the "recoverable" ellipticity at this temperature is $\Lambda_{theor}=1.3$, being $\gamma_1=-0.17$ (see Tab.8.1) and $|\gamma_2|<<1$. Thus again, as in the 1+1D case, the nonlinear response is stronger than expected.

Regarding the possibility of observing noncircular diffusion-driven solitons, our samples of KLTN do not support a sufficiently strong dielectric anomaly. The mechanism is however not peculiar to KLTN and stronger anomalies have been reported in different ferroelectrics, as mentioned in the previous section, such as SBN (strontium-barium-niobate) and SbSI (antimony sulphoiode)[3]. In these materials at least 1+1D solitons should be attainable.

Tab.8.1: Interferometrically measured values of γ_1.

T(°C)±0.2°C	**γ_1 ±0.02**
10.2	-0.17
10.5	-0.09
11.0	-0.06
11.5	-0.04
12.0	-0.03

REFERENCES:

[1] B.Crosignani, E.DelRe, P.DiPorto, A.Degasperis, Opt.Lett. 23, 912 (1998)

B.Crosignani, A.Degasperis, E.DelRe, and P.DiPorto, *Nonlinear optical diffraction effects and solitons due to anisotropic charge-diffusion based self-action*, to appear Physical Review Letters (Febbraio 1999)

[2] D.N. Christodoulides and T.H. Coskun, Opt.Lett. **21**, 1460 (1996)

[3] Y. Xu, "Ferroelectric Materials and their Applications", (North-Holland, Amsterdam 1991).

[4] A.Yariv and P.Yeh, *Optical Waves in Crystals* (Wiley, New York 1984).

Chapter

9

Spontaneous Self-Trapping of Optical Beams in a Metastable Crystal

Introduction

In a general context, solitons in Optics stem from a nonlinear optical interaction with the medium that hosts propagation. The “classical” integrable nonlinear equations describe soliton formation for *small* nonlinear corrections to dispersive continuos propagation, valid for a large number of different systems, and are therefore rightly considered “universal”. In Chapters 3-8 we described a different class of solitons supported by a nonintegrable nonlinear interaction. Such manifestations derive from a generally non-perturbative indirect interaction. Characterized by a richer phenomenology than "classical” particles, they have in common with these the fact that they are caused by a precise (“deterministic”) light induced change in the characteristics of the medium.

In this Chapter we describe the observation, accomplished by DelRe, Tamburrini, Segev and Agranat in 1998[1)], of a new mechanism capable of self-trapping optical beams: **soliton formation that stems from spontaneous crystalline ferroelectric domain-ordering**, *seeded* by a weak photorefractive diffusion field. These solitons, in contrast with all other solitons described here or previously observed in Optics, are *not caused* by the light induced interaction. The host system is *a priori* in a metastable critical regime that is appreciably far from equilibrium. The arbitrary coupling to the propagating wave seeds a spontaneous transition that, due to the highly unstable configuration, allows the initial seed to induce a strong control on the ensuing spontaneous structure: the spontaneous soliton. This new particle is fundamentally different from other solitons: it has no functional or energetic relationship with supporting mechanisms. The phenomenon finds a natural analogy in the context of complex phenomena in strongly dissipative systems, shifting our standard perspective of soliton manifestations. Thus, we have passed from integrable perturbative systems to nonintegrable interacting systems, and finally to highly nonlinear, wholly out of equilibirum systems: remarkably all manifest soliton particles.

Critical Propagation

Spontaneous symmetry breaking in systems undergoing a phase-transition represents one of the most intriguing subjects of statistical physics. In this regime, fluctuations are exhalted and ultimately allow for a macroscopic dynamical change in the properties of a system. Here, the investigation of light propagation in such a metastable configuration is described and it is experimentally shown that, when some form of coupling exists between the propagating entity and the out-of-equilibrium host, the spontaneous material response can lead to considerable nonlinear propagation effects. More specifically, we launch a very narrow optical beam into a photorefractively-nonlinear sample of KLTN and examine its diffraction. When the crystal is at a temperature slightly above the paraelectric-ferroelectric transition (in the paraelectric phase), the beam is strongly distorted. After a temporal transient, the initially diffracting and heavily distorted beam self-focuses and eventually self-traps: exhibiting stationary (non-diffracting) propagation, resembling a spatial soliton. This occurs in both one (1+1D) and two (2+1D) transverse dimensions. The resultant "solitons" are extremely **insensitive** to the parameters of the light beam, and are formed by spontaneous crystalline ferroelectric domain ordering seeded by the weak photorefractive diffusion field. We refer to this self-trapping mechanism as "spontaneous self-trapping" to underline the fact that the interaction is a seeded thermodynamic relaxation, entirely different from all other phenomena described in previous Chapters.

Optical beam propagation at the vicinity of the Curie temperature in media undergoing a phase-transition has been addressed in Chapters 5-8[2)]. However, no observation has been described in the highly-nonlinear metastable critical regime itself. Typically, the medium is optically *opaque* at the Curie temperature (*critical opacity*), as the strong density fluctuations severely scatter light. Numerous other effects were observed in such systems. For example, in supersaturated aqueous urea solutions, light induces crystallization and prenucleation[3)]. In some atomic / molecular systems laser induces clustering[4)]. In paraelectric KLTN, the screening of space-charge separation induces metastable ferroelectric clustering[5)]. In nematic liquid crystals, laser-heating generates isotropic "holes" giving rise to strong self-phase modulation[6)], and in metals at the melting point, an enhanced cubic nonlinearity has been reported[7)]. Thus far, optical *propagation* effects have been studied only in critical

binary liquid mixtures[8], and even there only theoretically. Here we study nonlinear beam propagation *at the crystalline phase transition itself*.

Apparatus

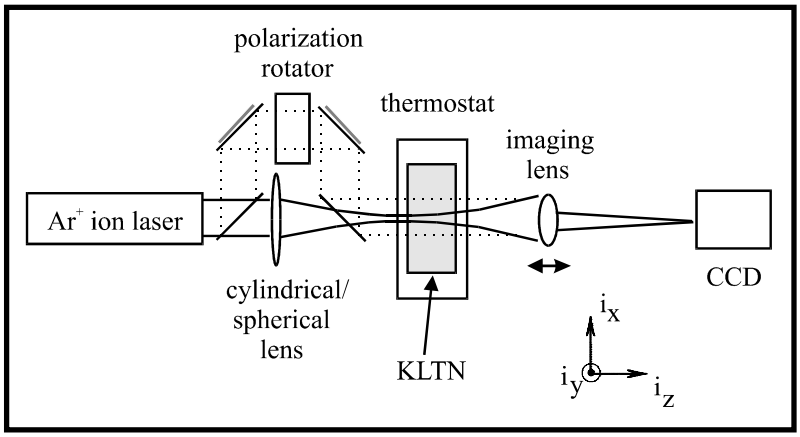

Fig.9.1: Experimental setup.

Experiments are carried out with the setup shown in Fig. 9.1, again wholly similar to the apparatuses described in previous Chapters[9]. A λ=514nm linearly polarized (||x) laser beam is focused onto the input face of a zero-cut KLTN sample, oriented with one principal axis (call it the z axis) parallel to the propagation direction. Initially a 1D beam (narrow in the x-direction) is launched by means of a cylindrical lens, and spatial effects are investigated. Then, the experiment is repeated with a *circular* beam. The beam is imaged onto a CCD camera by a lens placed after the sample. The sample is kept at a temperature T by means of a current-controlled Peltier junction and a feedback stabilizing driver. A second beam is split after the laser, illuminating the crystal uniformly while co-propagating with the (first) focused beam. In contradistinction with all other experiments with photorefractive screening solitons[2)9)], here this beam is used to investigate the physical process, and *does not* participate in the nonlinear interaction. It is blocked during "soliton formation".

The sample of KLTN (the same as that used in Chapters 6 and 8) measures $3.7^{(x)}$x$4.6^{(y)}$x$2.4^{(z)}$ mm and has a pale green

color. It is doped with Vanadium and Copper and exhibits strong photorefractive response in the visible spectrum[10]. It has a refractive index of n=2.4 (at λ=514nm) and quadratic electro-optic coefficients of $g_{11}=0.12m^4C^{-2}$ and $g_{12}=0.02m^4C^{-2}$ [2]. Measurements of the low frequency dielectric constant ε_r reveal a dielectric anomaly at T_c=10°C (decreasing loop), that indicates a first-order (from paraelectric to ferroelectric) phase-transition. In the absence of external elements, the onset of the noncentrosymmetric phase and macroscopic domain formation are seeded by imperfections and local strain, and can be viewed, due to the electro-optic response to the spontaneous polarization, by visual inspection. Fitting the values of ε_r in the paraelectric region with the Curie-Weiss law $\varepsilon_r=C/(T-T_0)$ described in Chapter 5 gives $C=1.5x10^5$ °C and T_0=6.2 °C . The transition manifests temperature hysteresis[11] for T<14°C characteristic of first-order transitions, indicating that the nucleation is affected by the presence of long range dipolar domain forces (domain-nucleation interaction). Our measurements refer to the decreasing temperature branch.

1+1D Particles

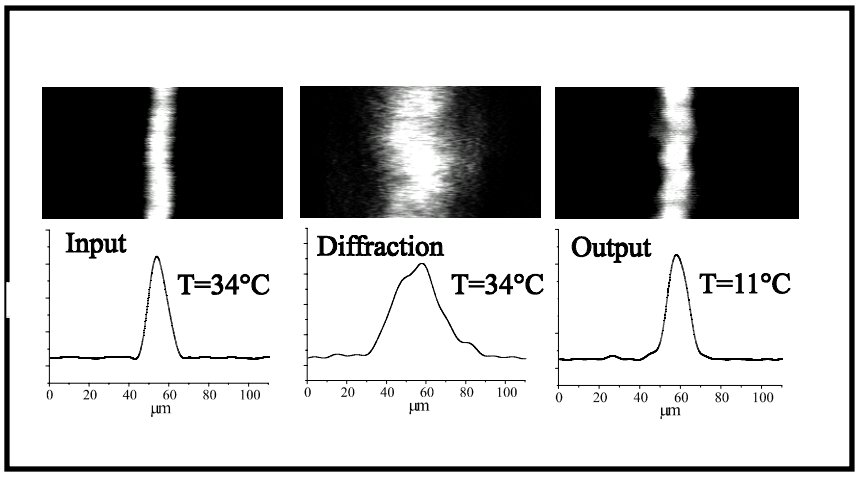

Fig.9.2: Typical (1+1) D self-trapping results: the 11μm FWHM input beam (left), the diffracted 26μm output beam (middle), and the self-trapped output at T=11°C (right).

In the 1+1D configuration, a cylindrical lens of f=150 mm generates a 1D Gaussian "sheet of light" at the input, as shown in Fig.9.2. The left column shows the image and profile of the input beam, for T=34°C (deep in the paraelectric

phase). The confined direction has an input full-width-half-maximum (FWHM) of 11 μm. At the crystal output, after the 2.4 mm in-crystal propagation, the beam has diffracted to 26 μm (central column), as approximately expected from linear Gaussian propagation. When the temperature is lowered into the metastable regime at T=11°C, after some transient characterized by strong "spike-like" beam displacement (characteristic times <<1s), the output beam resembles the input, and no diffraction is observed (right column in Fig.9.2). This result is fully reproducible in a whole range of peak beam intensities, from 0.1 to about 10 Wm^{-2} ***without*** any observable changes, apart from the duration of the initial transient regime (typically a few seconds in this range of intensities).

2+1D Particles

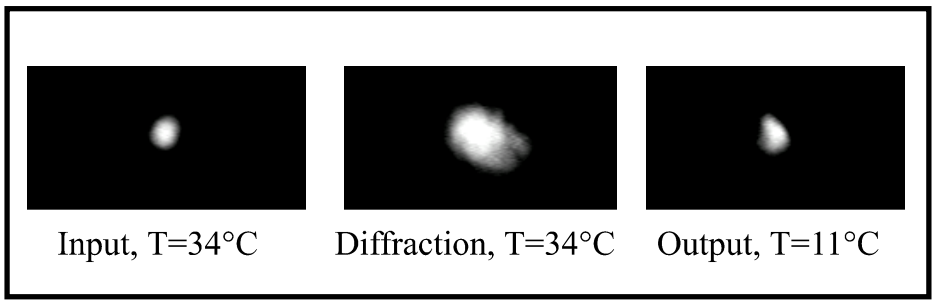

Fig.9.3: Typical (2+1)D self-trapping results: the 11μm FWHM input beam (left), the diffracted 24μm output beam (middle), and the self-trapped output beam at T=11°C (right).

In the (2+1)D configuration, the focusing lens is spherical (f=150mm). Typical results are shown in Fig. 9.3: the circular 11 μm FWHM input beam (left), the diffracted 24 μm output beam when the crystal is deep in the paraelectric phase (middle), and the self-trapped output beam at T=11°C (right), when diffraction is compensated and the beam intensity is concentrated in a 11 μm spot. The final nondiffracting "needle" beam is observed after a transient dominated by strong beam deformation and rapid sideways switching. We repeated this experiment under beam intensities varying through the range investigated in the (1+1)D configuration, and again, apart from the duration of the transient, no observable difference in the steady-state results was observed.

Domain Structure

We investigated the decay dynamics of these "spontaneous solitons", by first observing self-trapping (as in Fig.9.3), then blocking the focused beam and allowing the collimated beam to illuminate uniformly the crystal, keeping the crystal temperature constant. Adjusting the uniform beam intensity so as to make it comparable to the soliton peak intensity, and allowing the space-charge field to relax (erasure occurs in a few seconds, for the intensities used, see τ_d in Chapter 2), the collimated beam was blocked and the focused beam was again launched. Diffractionless propagation ***without observable transient dynamics*** was observed (note that mere photorefraction is a reversible process, see Chapter 2). Repeating the same procedure increasing the crystal T from the initial 11°C to approximately 14°C, no noticeable effects were observed. Only at T>14°C, the trapping disappeared. Separate ε_r measurements show that this temperature approximately coincides with the high temperature of the hysteresis loop.

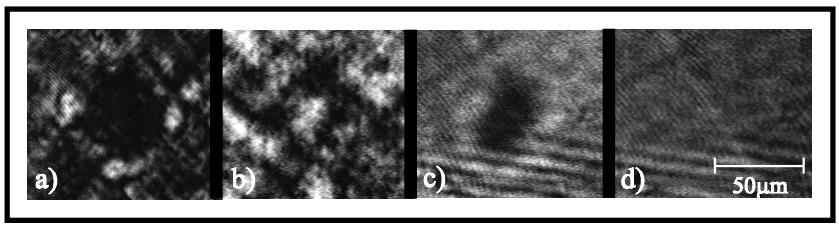

Fig.9.4: The output face of the crystal at T=11°C illuminated by plane wave polarized at 90° with respect to the previously formed soliton polarization (a); at 45° (b); at 90° after heating the sample to T=13°C (c); and at 90° heating it to T=15°C (d).

The refractive index pattern that supports the "soliton" was then investigated at T=11°C. In the 1+1D configuration a microphotograph was taken of the crystal output face with soliton beam blocked and the uniform beam (polarized along the y axis, at 90° with respect to the x axis) illuminating the sample. *The uniform illumination "repels" from the region in which the soliton has formed*. Repeating the procedure in the more complicated 2+1D configuration gave the results shown in Fig.9.4. In 9.4(a), is shown the output face of the crystal with the soliton beam blocked and the uniform beam polarized along the y axis. As in the 1+1D case, *light is*

repelled from the region that gives rise to the soliton. In 9.4(b) the polarization of the uniform beam was rotated by 45°. Here, some of the light is trapped in the region where the soliton has formed (central intensity hump). Figures 9.4(a) and 9.4(b) indicate that domains have formed with a prevalent domain-wall orientation at 45° with respect to the cubic axes. Heating the crystal (in absence of illumination) to 13°C (just below the hysteresis loop high temperature) and returning to a y-polarized uniform beam reveals that a structure persists even though the characteristic domain walls are no longer observable (9.4(c)). The domains have diminished in size and the crystal response is due to a less ordered clusterization (outside the central hump). Finally, in Fig. 9.4(d) the crystal was heated to 15°C. Effects due to the initial "soliton" are no longer observable. Note that without first forming the soliton, the crystal does not exhibit any domain structures at T=11°C, and the microphotograph is almost identical to that of 9.4(d) (which was taken at T=15°C).

Symmetry Breaking

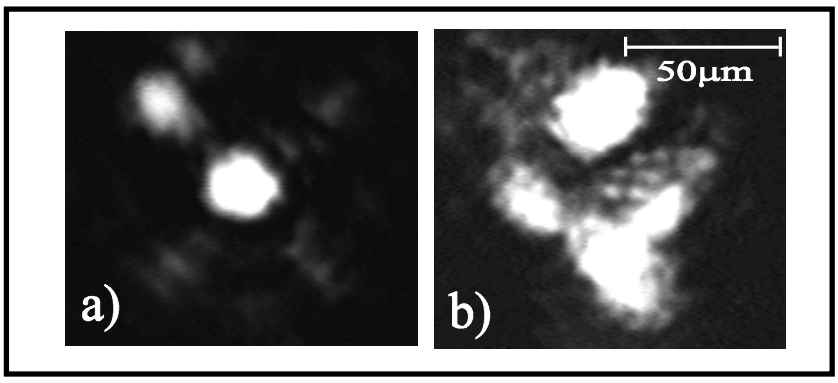

Fig.9.5: Nonlinear "splitting" of the input circular polarized beam into a trapped linearly polarized beam (a) and a diffracted orthogonally polarized one (b) Pictures are taken with a polarizer before the CCD camera.

To investigate the preference of this soliton-forming mechanism to the optical polarization, a *circularly-polarized* circular beam was launched (by simply inserting a $\lambda/4$ plate in the beam path before the sample, in the (2+1)D configuration). The circularly-polarized beam *never self-traps* as a whole, for any value of near-transition T. At T=11°C, the beam always splits into two distinct parts. The first part is trapped (as in the linearly polarized case) and is itself linearly polarized either in the x or y direction. The second part, polarized orthogonal to the trapped beam, is always distorted and appears to be repelled from the central beam region, as

shown in Fig.9.5. *The actual direction of the linear polarization of the guided portion of the beam was random, with probability of having a self-trapped x-polarized beam almost identical to that of having a y-polarized one.* That is, the choice of the actual polarization of the self-trapped component is made in tandem with the growth of crystalline (ferroelectric) domains, which are themselves affected by the optical polarization. This noise-induced symmetry breaking is a clear sign of complex behaviour.

Physical Mechanism

The self-trapping mechanism is not based on thermal effects or on strain-induced photovoltaic processes[12] as, like in the previously described diffusion-driven phenomena, intensity does not play any significant role, i.e., ***self-trapping is not affected under intensity variations over a large intensity range***. The fast dynamics during the transient phase indicates that spontaneous domain formation in the undercooled system is involved[13]. The underlying mechanism is believed to be based on light-induced diffusion space-charge fields, which are approximately intensity-independent. Such diffusion fields, in a periodic structure, can induce ***periodic*** ferroelectric domain reversal[14]. In what follows, we provide an explanation of this optical self-trapping that is driven by a light-seeded guiding domain-pattern.

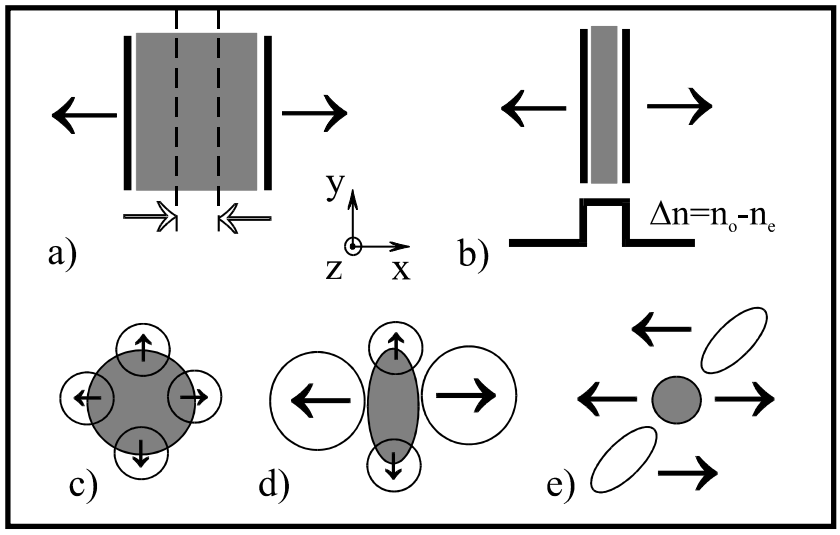

Fig.9.6: The spontaneous self-trapping mechanism: (a) The diffracting 1+1D beam (shaded region) seeds two counter-polarized domains with spontaneous polarization. Light is concentrated on a smaller area, thus moving the maxima of the diffusion fields inwards, which make the walls drift inwards. (b) The stationary index structure that traps the beam. (c) The initial diffusion-induced domains in the 2+1D case. (d) The prevailing domains for an x-polarized beam (shaded). (e) The final domain structure with prevalent x directed domains and residual screening regions with 45° walls.

In the 1+1D case, the initially-highly diffracting beam propagating in the crystal is exciting electrons from impurities into the conduction band, where they diffuse to less illuminated regions, being re-trapped there by other ionized donors or acceptors. Since the donors left behind are positively-charged, this process leads to charge separation and to a space charge diffusion field in the x direction (the direction of beam confinement) (see Chapter 2). Near the critical regime, the non-centrosymmetric ferroelectric configuration begins competing with the unpolarized (paraelectric) phase and any electric field larger than the coercive field E_c (at T) can seed domain formation (see discussion in Chapter 5). The diffusion field is given by $\mathbf{E_d}=-(K_bT/q)\nabla I/(I+I_d)$, [$K_b$ is the Boltzmann constant, q the electron charge, I the intensity distribution, I_d the dark irradiance, and the gradient is over spatial coordinates] (see Chapters 2 and 8). For an input Gaussian beam, E_d is very small in the central region (where the gradient is zero) and far from the beam, whereas in the region surrounding the beam (at a distance of the order of the beam radius σ from the beam's center) it reaches $E_d \approx (K_bT/q)2/\sigma \approx 50V/cm$. Near the phase transition, E_c is smaller than E_d, and E_d can induce domain formation. Thus, on both sides of the propagating "1D sheet of light" two counter-polarized domains start to form, leaving the central region in the paraelectric phase (Fig. 9.6a). In the center, the refractive index remains unaffected ($n_p=2.42\pm0.06$) as this region always remains in the paraelectric phase, whereas at the ferroelectric region the crystal is birefringent with $n_e<n_p<n_o$. Thus, when the beam is x-polarized, it corresponds to extraordinary polarization in the ferroelectric region, which has a lower refractive index [$n_e \cong (2.29\pm0.06)$] than that of the central paraelectric region (n_p). Thus, this beam "sees" a waveguiding structure (Fig. 9.6b), and is guided in the central region. This causes the intensity to be distributed over a

smaller area and moves the region in which E_d is large inward towards the center of the beam. This process of domain propagation stops at the inner-most region upon the beam where E_d cannot surpass E_c. If the input beam is approximately the fundamental mode of this waveguide pattern, a condition which depends on the value of E_c at the given T (E_c=0 at T=T_c), self-trapping occurs (Fig. 9.6b). On the other hand, if the beam is y-polarized, it experiences a lower index of refraction in the central paraelectric region, because n_o is slightly larger than n_p (n_o=2.45$\pm$0.06), and is anti-guided (repelled) from the central region, as observed in the experiments.

In the 2+1D case, the situation is more complex. Figures 9.4a and 9.4b indicate that, as in the 1+1D case, at the center of the beam the crystal remains in a paraelectric state, whereas outside the beam domains form and are prevalently polarized along the direction of the polarization of the writing beam. Figure 9.5 indicates that the prevailing domain structure is selected *during* the nonlinear process. Consider first a beam polarized linearly along the x axis. Initially the diffusion field induces ferroelectric domains at the margins of the diffracting beam oriented approximately in parallel with the direction of the electric field. Each single domain can only be polarized along a principal axis, as shown in Fig. 9.6c. The optical confinement (waveguiding), however, is efficient only for the domains that are polarized parallel to the beam polarization. Thus, of the various domain structures initially seeded, only the counter-polarized domains parallel (and anti-parallel) to the x axis “grow” (Fig. 9.6d). Due to the strong dipolar interactions, these two domains prevail, giving rise to intermediate screening of y-polarized domains with walls at 45°, which is the final domain structure observed in Fig. 9.4 and illustrated in Fig. 9.6e. This interpretation is supported by the results with the circular polarized beam: in this case diffraction compensation is efficient for both polarizations; however at the end only one type of domain prevails. The prevailing spontaneous polarization coincides with the polarization of the guided beam. The other component is repelled from the guiding central region and diffracts, distorted by the complex domain structure.

Discussion

It should be underlined that this mechanism of spontaneous self-trapping is unique in that the index modulation Δn is not functionally related to the propagating optical beam.

Secondly, the hysteric behavior implies that the soliton is *not self-supported*: once a stable domain pattern has formed, the dynamics of the interaction passes from a transient statistical nonlinear evolution to a linear propagation regime that is identical to that of a fabricated waveguide. In this respect, the only related system in Optics is the self-induced permanent waveguides in photosensitive polymers[15]**.** However, observations leave several questions unanswered, as the microscopic details of this complicated soliton formation via spontaneous formation of domain structures are not clear, and no rigourous theoretical formulation is, as of yet, available. Certainly, further investigation into the statistical nature of the phenomena, interactions between two spontaneous solitons, and self-induced ordering characterization will lead to even more interesting observations and prove to be a powerful tool in investigating phase-transition phenomena. For example the very fact that *spontaneous solitons allow transmission through an otherwise opaque medium is unique, and has few equivalents in Optics*.

REFERENCES:

[1] E.DelRe, M.Tamburrini, M.Segev, and A.Agranat, *Spontaneous self-trapping of optical beams in metastable paraelectric crystals*, submitted to Physical Review Letters (November 1998)

[2] M. Segev and A. Agranat, Opt. Lett. **22**, 1299 (1997); E. DelRe et al., ibid **23**, 421 (1998); Appl. Phys. Lett. **73**, 16 (1998); B. Crosignani et al., Opt. Lett. **23**, 912 (1998).

[3] B. Garetz, et al., Phys. Rev. Lett, **77**, 3475 (1996).

[4] A. Tam, G. Moe, and W. Happer, Phys. Rev. Lett. **35**, 1630 (1975).

[5] G. Bitton, M. Razvag, and A. Agranat, Phys. Rev. B **58**, 5282 (1998).

[6] P. Wang, H. Zhang, and J. Dai, Opt. Lett. **13**, 479 (1988).

[7] S. Dhanjal et al., Opt. Lett. **22**,1879 (1997).

[8] B. Jean-Jean et al., Phys. Rev. A **39** 5268 (1989).

[9] M. Shih, M. Segev, G. Valley, G. Salamo, B. Crosignani, and P. DiPorto, Electron. Lett. **31**, 826 (1995).

[10] B. Pesach, E. Refaeli, and A. Agranat, Opt. Lett. **23**, 642 (1998).

[11] F. Jona and G. Shirane, *Ferroelectric Crystals*, (Dover, New York, 1992).

[12] D. Kip, E. Kratzig, V. Shandarov and P. Moretti, Opt. Lett. **23**, 343 (1998).

[13] X. Tong et al., Opt. Lett. **21** 1860 (1996).

[14] A. S. Kewitsch, M. Segev, A. Yariv, G. Salamo, T. Towe, E. Sharp, and R. Neurgaonkar, Phys. Rev. Lett. **73**, 1174 (1994).

[15] A. S. Kewitsch and A. Yariv, Opt. Lett. **21**, 24 (1996).

Al Collegio dei Docenti del Dottorato di Fisica, Università dell'Aquila

Al Coordinatore del Dottorato di Ricerca in Fisica, Università dell'Aquila

Con riferimento alla vostra richiesta di valutazione della tesi di dottorato del Dott.Eugenio Del Re, allego la mia relazione scientifica.

Roma,

Prof.Antonio Degasperis
Università di Roma "La Sapienza"

Relazione Scientifica Sulla Tesi di Dottorato del Dott.Eugenio Del Re, intitolata "Solitons and Nonlinear Optical Propagation in Ferroelectric and Near-Critical Paraelectric Photorefractive Crystals"

La tesi presentata dal candidato descrive ricerca originale ed innovativa in un campo che recentemente ha attratto forte interesse da parte della comunità scientifica che si occupa di ottica non lineare e fisica dei solitoni: la propagazione di luce in cristalli fotorifrattivi. In particolare, egli affronta il problema in maniera del tutto orginale, estendo la fenomenologia solitonica spaziale dalla configurazione tradizionale, detta "screening", ad una serie di nuovi processi presenti nei cristalli fotorifrattivi in prossimità di una transizione strutturale. In questo modo, egli dimostra come sia possibile innescare una serie di fenomeni fortemente non lineari anche in condizioni sperimentali relativamente semplici ed accessibili.
In particolare, nella fase paraelettrica, la divergenza dielettrica ha consentito al candidato la prima osservazione dei solitoni screening in un mezzo centrosimmetrico, prevista teoricamente alla fine del 1997. Questa osservazione consente, in generale, di riprodurre gran parte della fenomenologia non lineare osservata in fase noncentrosimmetrica. Avvicinandosi alla transizione, il candidato ha osservato un fenomeno del tutto nuovo, innescato dalla diffusione di cariche fotogenerate nel material, che, sia teoricamente che sperimentalmente, ha aperto un nuovo campo di indagine, denominato "diffusion-driven phenomena". Infine, il candidato ha osservato per la prima volta solitoni spaziali determinati dalla instabilità termodinamica del cristallo, un fenomeno che suscita interesse anche nel campo della ricerca fondamentale della materia.
Le ricerce svolte hanno un filo conduttore unico: lo studio della propagazione non lineare in un mezzo in prossimità di una transizione. Esse sono state pubblicate sulle più prestigiose riviste internazionali di fisica e ottica, quali Physical Review Letters, Optics Letters, Applied Physics Letters, e The Journal of the Optical Society of America B; sono state presentate a diversi convegni internazionale e costituiscono, a mio parere, un contributo rilevante alla ricerca nel campo dell'ottica.
La monografia è chiara e ben strutturata, descrive in maniera concisa la sperimentazione, ed è ben corredata di bibliografia.
Il mio giudizio globale, frutto della lettura della monografia e della letteratura scientifica prodotta, è favorevole alla concessione al candidato del titolo di Dottore di Ricerca.

In fede,

Prof.Antonio Degasperis Roma,